AUTOMATIC MID-WATER TARGET DETECTION USING MULTIBEAM WATER COLUMN
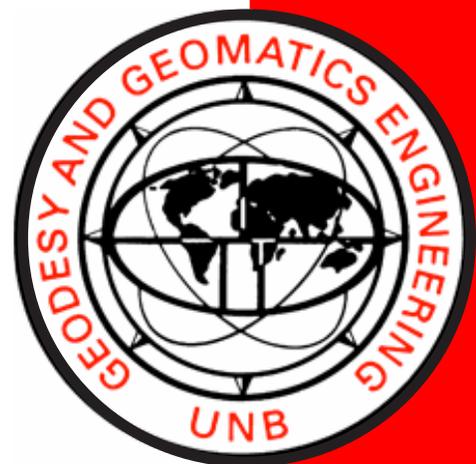
CARLOS RUBRIO VIDEIRA MARQUES

August 2012

AUTOMATIC MID-WATER TARGET DETECTION USING MULTIBEAM WATER COLUMN

Carlos Rubrio Videira Marques

Department of Geodesy and Geomatics Engineering
University of New Brunswick
P.O. Box 4400
Fredericton, N.B.
Canada
E3B 5A3

August, 2012

PREFACE

This technical report is a reproduction of a thesis submitted in partial fulfillment of the requirements for the degree of Master of Science in Engineering in the Department of Geodesy and Geomatics Engineering, August 2012. The research was supervised by Dr. John Hughes Clarke and the Portuguese Naval Academy.

As with any copyrighted material, permission to reprint or quote extensively from this report must be received from the author. The citation to this work should appear as follows:

Rubrio Videira Marques, Carlos (2012). *Automatic Mid-Water Target Detection Using Multibeam Water Column.* M.Sc.E. thesis, Department of Geodesy and Geomatics Engineering Technical Report No. 280, University of New Brunswick, Fredericton, New Brunswick, Canada, 176 pp.

DEDICATION

For my love and eternal girlfriend Mileta, and to Tome Rubrio our son.
I would also like to dedicate this to my parents and brother for their continuing support
and encouragement.

ABSTRACT

A potential new automatic application in multibeam water column is the recognition and precise location of suspended mid-water targets. This is already being applied manually in the ArcticNet program for searching for lost under-ice mooring hardware.

The pattern of the scattering field around a suspended point mid-water target is directly related to the multibeam imaging geometry, including pulse length, transmission and reception main lobe beam-widths as well as side lobe spacing and suppression. Knowing this geometry-specific scattering pattern, optimal 3D matched filters can be designed to pick out faint targets from noise. Having picked an object in this manner, its location can be derived with the same positioning uncertainty that we already associate with depth.

Equivalent detection of objects can be achieved manually by the trained operator when carefully inspecting all the data, but is a very long and tedious task. An automatic algorithm developed as the main component of this thesis can be used to perform this task more rapidly and reliably, as well as tracking the object's movement. These new capabilities can be used in oceanographic research, in search and rescue, also for military purposes, and to track geological activity. A specific case study used as an example is the monitoring of suspended targets over seabed markers that are progressively displaced by landslides.

ACKNOWLEDGEMENTS

I would like to express my most sincere gratitude to everyone that made this amazing experience at the University of New Brunswick the most interesting and challenging experience. I particularly want to thank my supervisor Dr. John Hughes Clarke for his contagious excitement and keen interest in all Multibeam, Oceanography and Geology issues, for providing invaluable information and continuously motivating my studies and research. His continuous incentive to always look for more made me try new approaches to the problem and expand my knowledge.

I would also like to thank Dr. Yun Zhang and Dr. Jonathan Beaudoin for being my supervisory committee and providing the most useful comments and critiques.

I also thank the Portuguese Navy for the funds provided for this course, providing me with extended knowledge in Multibeam technology, which I wish will be useful in my future assignments.

There is also a number of people that contributed greatly to this thesis and to make my learning experience process very gratifying and enjoyable that I want to thank.

The Geodesy and Geomatics Department (teachers, staff and students) that helped me and supported my integration in campus life.

The Ocean mapping group personnel (Ian Church, Steve Brucker, Doug Cartwright, James Muggah, Travis Hamilton) for their continuous support and guidance when dealing with OMG software and hardware.

I'm very grateful to Auke van der Werf and Jose Lamadrid for helping me in my initial steps in Fredericton and UNB. Also to my fellow students and friends at UNB, Reenu Toodesh, Christine Legere, and Anand Hiroji for their support. And a special

Table of Contents

Curriculum Vitae

List of Tables

List of Figures

List of Equations

List of Symbols, Nomenclature or Abbreviations

DSL – Deep scattering layer

LIM – Local intensity maxima

OMG – Ocean mapping group

MBES – Multi beam echo sounder

MSR – Minimum slant range

Rc – Reception

SIS – Seafloor information system

Tx – Transmission

UNB – University of New Brunswick

WCL – Water Column

KM – Kongsberg maritime

SNR – Signal to noise ratio

AW – Apparent width

BS – Backscatter strength

NL – Noise level

1. Introduction

Hydrographic technological development has typically been focused on seafloor detection and accuracy of depth measurements. Although this is still one of the most important features in hydrography, multibeam echo sounders (MBES) can now, in addition to measuring bathymetry and sea floor reflectivity, also discriminate the acoustic scattering within the water mass by recording sampled reflectivity measurements along each beam. Water column (Wcl) imaging has been used mostly for fisheries (Mayer et al, 1997, Gerlotto et al, 1999) but it is now being used for several other applications, such as the detection of gas plumes (Jones, 2003, Gardner et al, 2009), the determination of least-depth over wrecks (Hughes Clarke et al, 2006a, Van der Werf, 2010) and noise detection (Hughes Clarke et al, 2006b).

Multibeam systems like Simrad SM600, SR240, SP270, and SA950 dedicated to fisheries were all designed to image the hemisphere below the vessel using steered beams with beam widths of about 12° (Hughes Clarke et al., 2006a) Other systems were created or also adapted for water column imaging, like the ones presented in Table 1.1 they all store the water column image of their insonified swaths.

Designation	Frequency used	Beam width used
Forward looking multibeam systems		
RESON 6012	455kHz	30°x1.5^{o}
RESON 7128	200 or 400kHz	30°x0.5^{o}
Vessel security multibeam systems		
Kongsberg SSA80	116kHz	Unknown
Fisheries research sonar systems		
Simrad SX90	20 to 30kHz	~ 10°
Simrad SH90	114kHz	~ 10°
Scientific multibeam systems		
Simrad ME70	70 to 120kHz	2°
Simrad MS70	75 to 112 kHz	500 beam (3° and 4°)
Bathymetric multibeam systems		
Kongsberg EM3002	300kHz	1.5^{o}
Kongsberg EM710	70 to 100kHz	0.5^{o} to 2°
Kongsberg EM302	30kHz	0.5^{o} to 4°
Kongsberg EM122	12kHz	1° to 2°
Kongsberg EM2040	200 to 400kHz	0.5^{o} to 1°
RESON 7101	240kHz	1.5^{o}
RESON 7125	200 to 400kHz	0.5^{o} to 1°

Table 1.1 Some multibeam systems using water column imaging
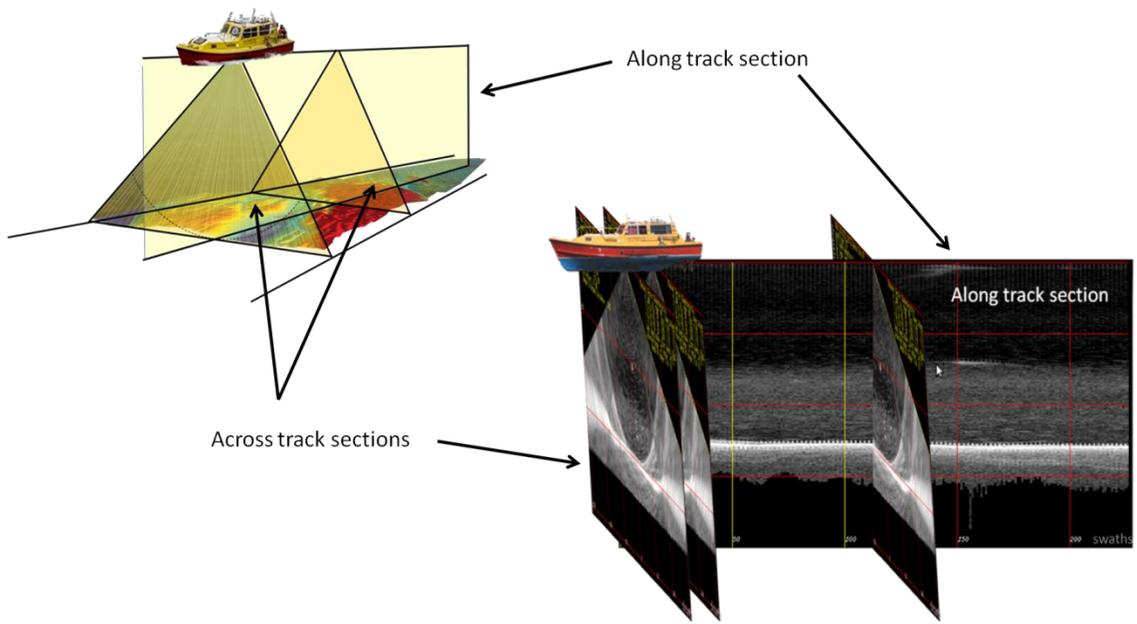
Figure 1.1 - Showing water column 3D sketch
This illustrates the two, mutually-orthogonal planes, along and across track, in which the water column data is most commonly assessed.

With MBES dedicated to seafloor tracking already storing the complete acoustic data from each beam, it is possible to present the full trace of the water column for each swath, and as the vessel progresses thus along the whole survey line (Figure 1.1). This gives the hydrographer a picture of the contents in the mid water range, discriminated in range and angle. Some more work can be done using these tools. While water column is already being widely explored for some other purposes, like fisheries (Figure 1.2), or intruder detection, its use in hydrography is still limited. Several algorithms have been created to use water column data beyond its common use for fisheries, including bubble populations (Weber et al., 2003), measuring suspended particle density (Jones, 2003), military mid water target hunting (Gallaudet and deMoustier, 2003), determination of

least-depth over wrecks (Hughes Clarke et al., 2006a, Van der Werf, 2010) (Figure 1.3) and recently mapping undersea gas seeps (Weber et al, 2012). All these applications can be further improved through analysing the water column imaging geometry characteristics Example improvements might include better positioning or better definition of objects. This thesis presents an analysis of those characteristics.

The information available with bathymetric MBES water column allows us to climb that one more step. With water column data and taking advantage of MBES narrower beam widths and lower uncertainty in positioning it should be possible to accurately position objects in the mid-water range. Typical fisheries application sonars use broader beams, poor range resolution and ignore refraction on their calculations. This is not a problem when the research focus is fisheries as there is no need to know exactly where a fish is as it is moving. On the other hand, bathymetric MBES are very concerned with positioning, that is why their water column data can be used to better locate objects.
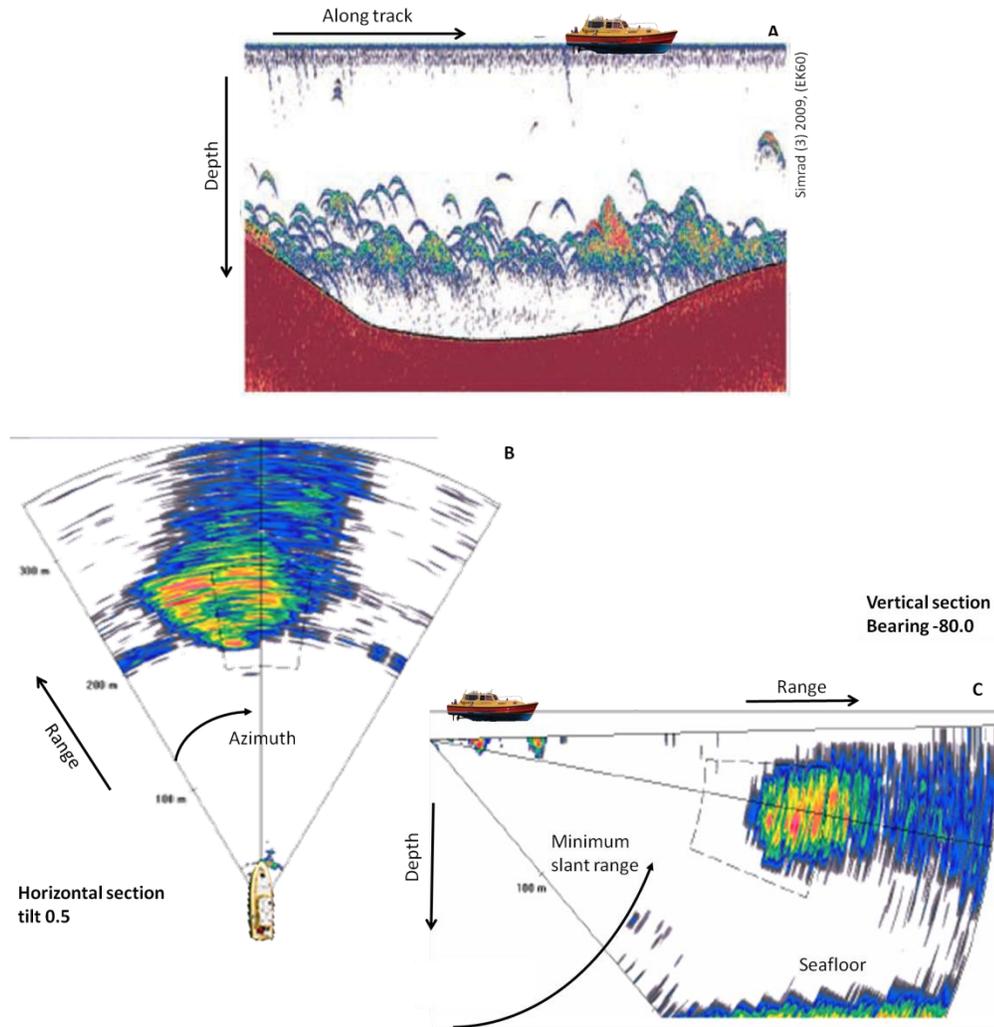
Figure 1.2 – Fisheries applications using water column.

A – Single Beam Simrad EK60 (operating at 38 kHz using 7° beams) showing a vertical profile. Note prevalence of hyperbolic echoes due to broad (~20°) beam widths. B – Kongsberg MS70 (using 3° beams) system detecting a school of herring. The system appear to have very good side lobe suppression as the fish school lies beyond the minimum slant range.

Figure A modified from Simrad 2006 (A), Figures B and C modified from Simrad 2011 (A)

5

Text visible within figure:
- 002 Ping 145
- on 0
- on 18
- 150
- db/km
- ncidence
- Rear Mast
- OMG/UNB SwathEd software
- Ribs over Hold
- Depth
- Across track
- A
- B
- Hughes Clarke et al. (1), 2006 (EM3002)
- Hughes Clarke et al. (1), 2006
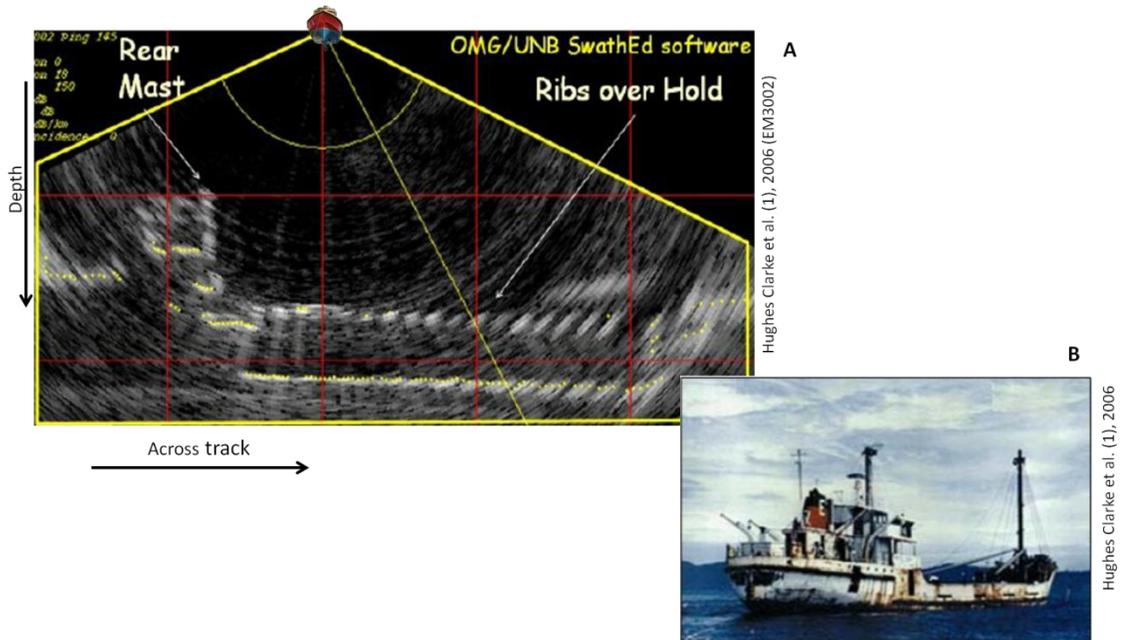
Figure 1.3 – Wreck detection using water column.

A - detecting a ship wreck, EM3002, B – the same ship shown before sinking

In this thesis the intention is to use water column imagery from bathymetric MBES data to locate and position mid water targets with the same high accuracy as the bottom detections. Taking advantage of MBES characteristics, and analysing the water column data using the multibeam imaging geometry, it should be possible to identify specific targets in the water column from amongst all the natural scatterers, and any generated noise, and position them accurately.

In order to achieve this objective several variables have to be taken into account when analysing data in the water column. MBES imaging geometry dictates how the scattering pattern around any single point in the water column appears. Transmission (Tx) beam width, reception (Rc) beam width, side lobe pattern, and pulse length are

responsible for the characteristic scattering shape of any detection in the water column, creating a 'smile' across track (common range arc) and a 'frown' along track (hyperbolic echo) (Figure 1.4). As will be explained in more detail in Chapter 2, transmission sectors, minimum slant range, yaw stabilization, and pitch stabilization limit the even sampling and usefulness of the water column data. Vessel speed, swath coverage, sound speed, refraction and, absorption coefficient, all change the way water column data needs to be analysed. This thesis will describe and explain these geometric aspects in Chapter 2. The approach of this thesis is based on identifying targets in the 3D water column volume by validating echo detections using each beam's specific imaging geometry and comparing the predicted results with the observed targets echoes. The expected imaging pattern for each detection is calculated using MBES imaging geometry, and used as a match filter to validate the detection. The algorithms developed are intentionally created not only for detecting the targets, but also for identifying all possible objects in the water column, making them useful for other possible purposes.
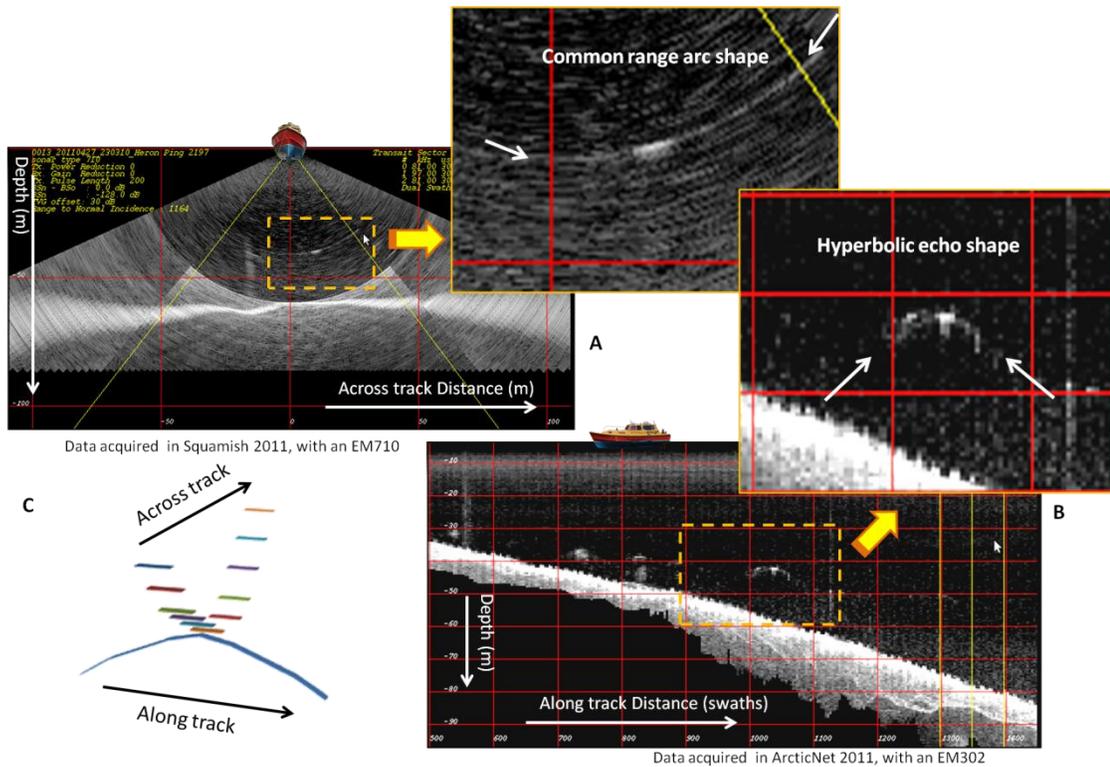
Figure 1.4 – Example MBES across track and along track imagery

A – Shows across track profile, note the common range arc pointed by the green arrows, B – Shows along track profile, Note the hyperbolic echo shape pointed by the green arrows, C – shows a 3D scheme of the side lobes effect, along and across track

A UNB project in Squamish (Hughes Clarke et al., 2011) included a specific requirement to locate mid water objects. While that could be done manually, the amount of data to be acquired requested an automatic system that could detect the desired objects uniquely and position them. The aim of the project was to track the movement of the targets. So this automation needed to be fast and reliable enough to be used throughout large volumes of recorded data with confidence that no targets would be missed.

1.1 Objectives

The main purpose of this thesis is to create a software tool to detect, mark and position special known objects in the mid water area using bathymetric multibeam water column imaging tools (Figure 1.5). The objects should be detected and geographically positioned in the 3D water mass, using the full achievable accuracy of the integrated multibeam system.

The thesis aim is to build the algorithm that finds the object and extracts its coordinates so that it can be plotted in a 3D environment imaging software along with the seafloor detection that was achieved by other software.

This thesis is divided in 5 specific objectives:

1.1.1 Assess the viability to automatically execute water column object detection

Water column data needs to be analysed and an assessment has to be made to understand if it is possible to automatically detect objects precisely in the mid water range using MBES data. Object detection is already being done manually by trained operators but the accuracy of the detection is limited by the user's precision and accuracy while using the mouse. In addition, the presence of natural objects and specious noise provide a possibility of false detection (Figure 1.5). Also this task is a very arduous exercise which is likely to create assessment errors with the operator exhaustion over time. The first objective is to simply understand how this detection can be achieved and to implement it in a test set of water column data, using only the minimum necessary data (one swath, one sector). Once automatic detection possibility is confirmed, the more general algorithm development can be started.
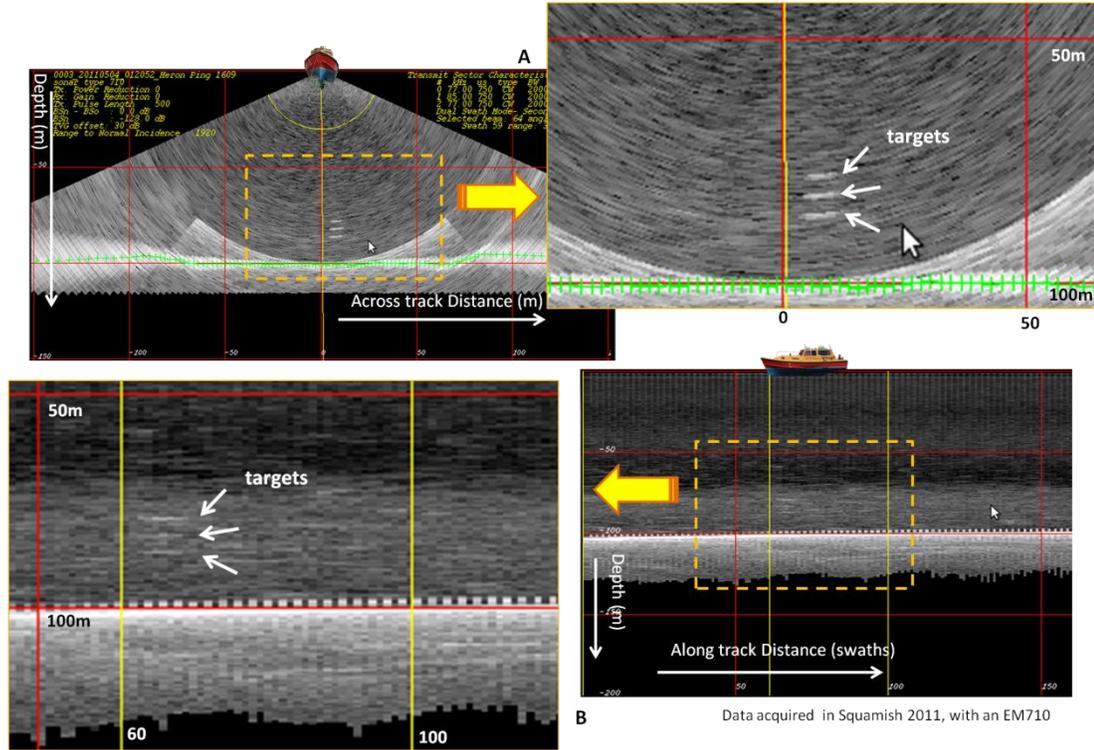
Figure 1.5 – Illustrating how target clusters appear in the water column image.
These are the 3 buoy specific geometries used in the Squamish Project. A – Shows across track profile, B – shows along track profile. Note requirement to extract target geometries from within background noise.

1.1.2 Develop the algorithm to achieve automatic object detection in the water column

The second objective is to develop the algorithm to use the water column data using single swath, one sector only and from a known depth to the minimum slant range and detect a specific known target. The complication is that it is hard to implement regular imaging analysis in water column imaging as the objects apparent shape changes across

the image as the insonification geometry changes. This analysis needs to be done in a 3D environment as the object could easily be mistaken by some other detection if using only 2D images. Using all the needed characteristics to identify the object across the swath and along the survey line the object should be detected and positioned relative to the sonar. Then, given that a singular point object is not unique, an extra step is implemented to identify specific sets of objects (target clusters, Figure 1.5).

1.1.3 Expand the algorithm to be used in a multi-swath multi-sector MBES system.

Being certain the algorithm works well in a single swath, single sector environment, the next step is to expand its capabilities to be used in nowadays most common systems, analysing the water column data stored by MBES systems that use several sectors across the swath and more than one swath along the survey line.

1.1.4 Algorithm implementation in the OMG-UNB software

Having designed the algorithm the final step is to implement it in the OMG-UNB software. This will allow its use in regular acquired data and test its scientific capabilities and contribution.

1.2 Contribution

The several significant contributions of this research are presented next:

1.2.1 Automatic detection of specific target geometries in the mid-water range

This algorithm will automate a possible but time consuming and very demanding manual task that requires trained operators that is usually subject to errors. It will also easily position the objects accurately in a geographical reference frame, while that would normally require some extra calculations from the operator (subject to mouse click precision), or the use of a special image analysis software. Using this algorithm and its capabilities it will be possible to detect most specified target geometries in the water column as long as the target scattering strength is clearly above background noise levels.

1.2.2 Automatic detection of other natural objects in the mid water range

Not only specific objects should be detected but also any other objects in the water column. If properly calibrated, excluding all the undesired noise, the algorithm should detect all discrete objects in the water column. The algorithm should have a method to train itself excluding most natural noise, like the deep scattering layer example. It should however also be possible to be manually trained by the user if objects of specific character or geometry are desired. Some examples of the objects that should be possible to detect are gas plumes and fish schools.

1.2.3 Reduce the human effort and expedite scientific research in the water column

Finally, this algorithm should work in an acceptable time frame, analyzing large sets of data in short time. It should give the user a simple way to find the desired targets

in a large set of survey lines. The user should only need to specify the target cluster geometries and survey lines (eventually some other specific needs) and the algorithm should be able to output all target locations in those lines. Any scientific research in the water column, looking for specific geometric patterns would benefit with the use of the algorithm expediting the search process. This is the main contribution, to automate the detection and location of desired target geometries in a rapid time frame. The short term goal is to have the toolkit available for the Squamish Project.

1.3 Thesis Structure

This Thesis is structured in several chapters, divided and organized according to the investigation workflow, to better understand the research development.

The current chapter provides an introduction to what the research is focused on. It explains what motivated this research and how it is positioned in the current state of algorithm development and usages. It also shows the contributions and improvements of this research to the scientific community. Finally it gives the reader an outline of the thesis structure.

Chapter 2 introduces some of the necessary theoretical background about multibeam and water column. This will allow the reader to understand the importance of several concepts in this investigation. It will show how MBES imaging geometry characteristics influence water column object detection, particularly the effect and extreme importance of main lobe width and side lobes while validating detections. Finally it should give the reader the necessary knowledge of all critical concepts to the development of this research.

Chapter 3 explains the data acquisition needs. It explains which data will be used, when and where testing data was acquired. It also gives a pre analysis of the water column data supporting the reader with enough examples of what is already achieved and what this research intends to achieve.

Chapter 4 explains the methodology used in the development of the algorithm. The main investigation and algorithm development are explained in this chapter. Algorithm training, available user interaction and possible user changes to its operation are explained here. All specifications about a target are given here. Finally, the output is explained here also.

Chapter 5 shows the results obtained by applying the algorithm. An analysis is done on the results explaining the goals achieved.

Chapter 6 is dedicated to the implementation of the resulting toolkit to the main case study in this research. The results are analyzed according to what was expected and the final conclusions are explained.

Finally the conclusions and final recommendations are presented in chapter 7. Any detected limitations are also shown. Some possible future work using this research outcome is also advanced.

Appendix A shows the software tool that was created to implement the algorithm. The specific characteristics of the tool as well as the features added to the existing OMG software are shown here.

2. Multibeam and Water Column Background

MBES now provide records of the backscattered intensity measurements along the water column, throughout the length of all acoustic beams. These records give us the possibility to create water column images that can afterwards be analyzed and interpreted (Figure 2.1).
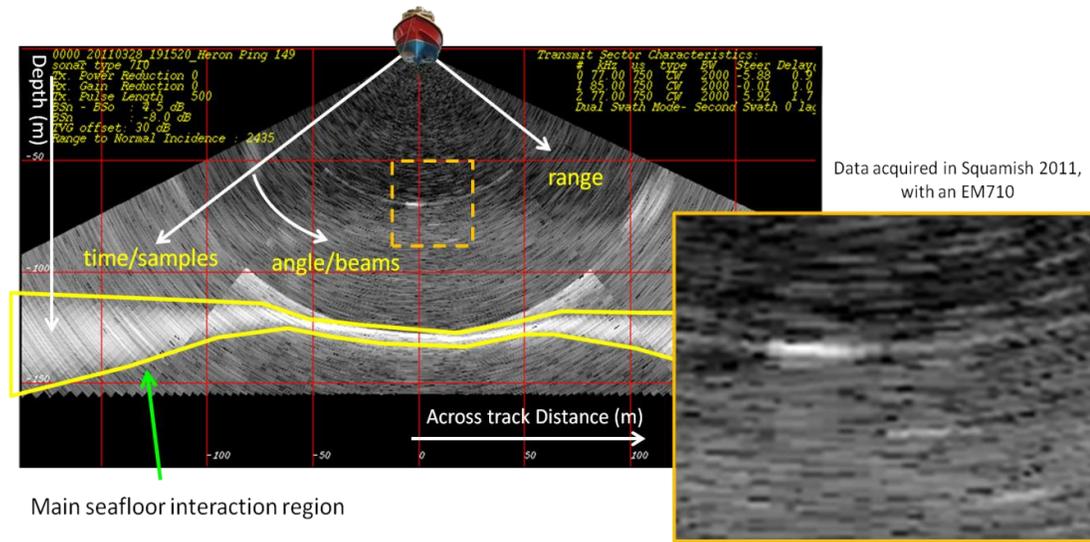
Figure 2.1 – Across track water column image for a single swath, showing each echo scattered intensity as pixelized area across the image
Note the differences in intensity from the school of fish (bright white) and the surrounding noise (grey levels). (higher intensities are brighter)

In Figure 2.1 one can see the main seafloor echo region. This is used for the primary purpose of seabed mapping. Above that region there is a 2D region that shows echoes above the seabed. Some of these reflect water column targets, but others are artifacts of the system that are not real targets. This chapter explains how to differentiate the two. This leads us to this research. To properly use the water column data we need to

understand the concepts behind MBES as well as the considerations that support the water column imagery.

2.1 Multibeam echo sounders

There are several different types and designs of multibeam echo sounders providing water column imaging. In this research the focus is only on bathymetric multibeams, specifically Mills-Cross systems using linear arrays. Slight differences may need to be taken in consideration for other system designs. Mills-Cross linear MBES are systems using at least 2 linear array transducers aligned perpendicularly to take advantage of the Mills-Cross effect (Figure 2.2 B).
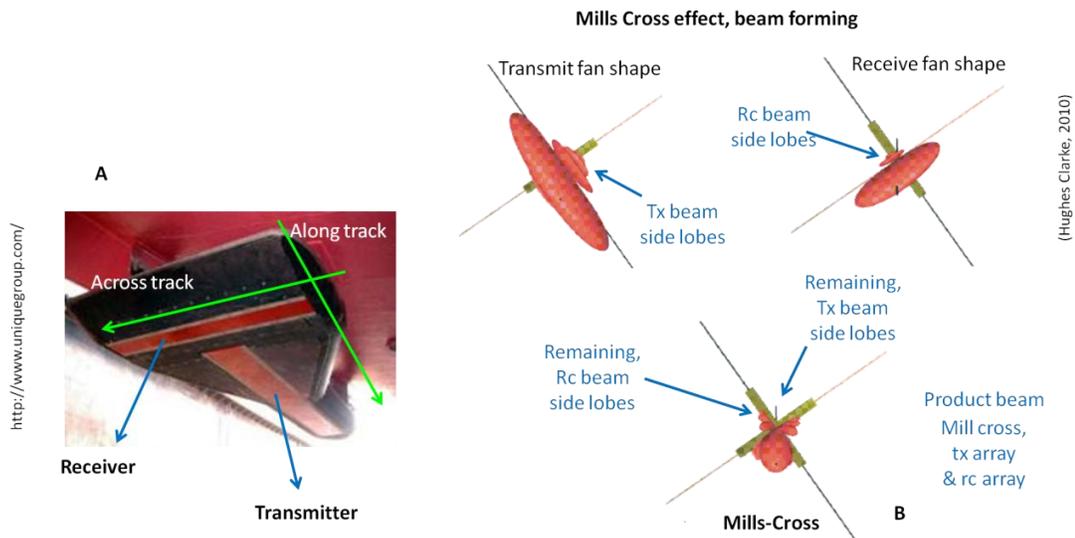
Figure 2.2 - MBES Mills-Cross beam pattern (Hughes Clarke, 2010)

A shows an EM302 photo with the usual MBES Mills-Cross configuration. In B one can see the product of the transmit beam pattern with the receiver beam pattern, creating a singular beam shape where side lobes are present along the arrays directions only.

These Mills-Cross systems are usually composed of one transmitter array and one receiver array with the transmitter mounted with the long axis of the vessel aligned with the along track direction and the receiver mounted in the across track direction (Figure 2.2 A). This way, the active system (transmitter) is only used once for each set of detections, allowing all the necessary procedures to create the directional beam to be done with the passive system (the receiver) (Figure 2.3 A). The transmitter elements are usually excited simultaneously (for unsteered transmissions) or sequentially (for steered transmissions) creating a planar fan shaped beam pattern athwart the survey platform, or in a cone shape (for steered transmissions) (Figure 2.3 B). This beam pattern is narrow in the along-track direction. The beam width depends on the linear array dimensions and wavelength (Equation 2.1).

$$\boldsymbol{\theta} \approx \frac{\boldsymbol{k} * \boldsymbol{\lambda}}{\boldsymbol{L}}$$

$$\boldsymbol{\theta} = \boldsymbol{Beam\ width}\ (\boldsymbol{rad})$$
$$\boldsymbol{\lambda} = \boldsymbol{Wave\ length}\ (\boldsymbol{m})$$
$$\boldsymbol{L} = \boldsymbol{array\ length}\ (\boldsymbol{m})$$

Equation 2.1 - Beam width equation for arrays $> \sim 10\lambda$

For unshaded arrays, k = 0.88, for typical shadowed arrays k > 1

The receiver array elements convert acoustic pressure into electrical voltage (passive operation) combining the received signals of each elements and creating a fan shaped beam pattern perpendicular to the receiver array, narrow in the across track direction again depending on the linear array dimensions and wavelength (Equation 2.1). Applying different time delays on each element of the receiver (or equivalently through

17

other procedures) it is also possible to steer this beam pattern which then also becomes conical. (Figure 2.3 C). As this is a passive system it is possible to create several successive receiver beams with a known offset receiving through a wide range of angles across the transmitted beam area (Figure 2.3 A). Combining the transmitter steering with the receiver steered beam patterns several single narrow beams are formed (Figure 2.2), using the Mills-Cross effect, with known array relative angles combining this with known array orientation, the absolute beam vector can be calculated.
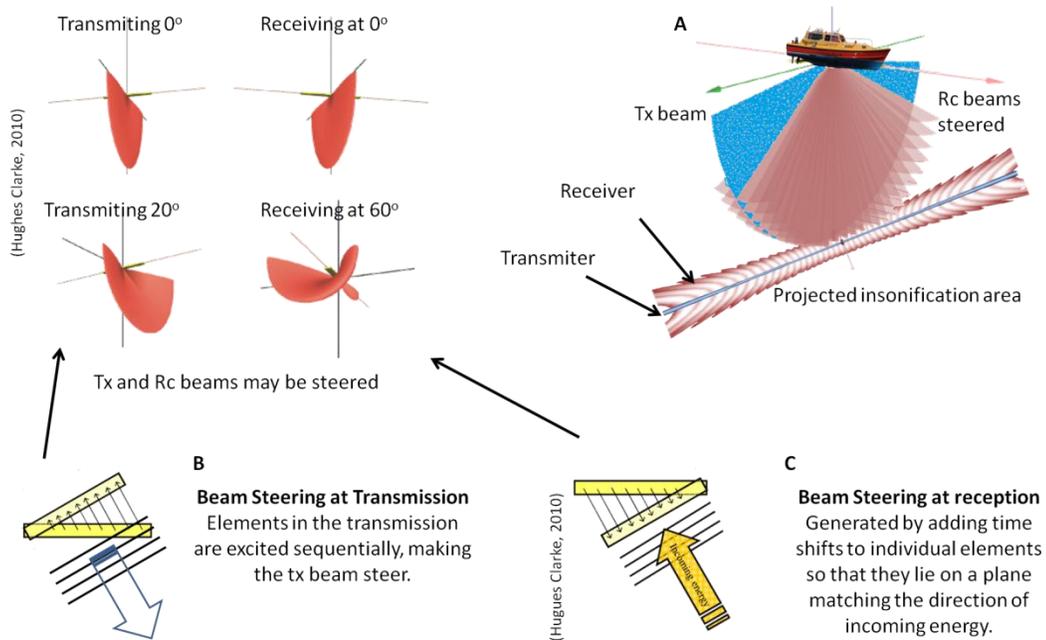
Figure 2.3 - Transmission and Receiver steering

A – Resulting projection of one transmission lobe and multiple (separately steered) receiver beams.

Note the effective array length gets smaller when steered (Equation 2.5) **increasing beam width and consequently the insonified area**

2.2 Pulse Length

The previously described interacting beam geometry controls the across swath and along track resolution of a given object. The next step is to define the along beam resolution. Along beam axis, or in the range direction, the geometry is defined by the pulse length. Pulse length, which is equivalent to 1/pulse bandwidth for simple CW systems, dictates range resolution and therefore also dictates how the object will be projected in the beam axis direction. Shorter pulse lengths achieve better range resolution (Equation 2.3). As an example, an EM710 that operates in a range of frequencies from 70kHz to 100kHz, operating with a 0.2ms pulse length, will have a pulse bandwidth of 5kHz (Equation 2.2) and a range resolution of 0.15m. Range resolution will define the projected geometry of a single point object in the water column image in the along beam axis. For a single object, its apparent water column echo dimension along the beam axis reflects the pulse length (Equation 2.3). Range resolution also reflects the capacity of the sonar to discriminate the sampling in time of echoes along the beam axis that were backscattered by two closely spaced objects. The sonar can only discriminate the objects if their echoes' time sample do not overlap. This means that the projected pulse length has to be smaller than the inter-object distance. Using the pulse length and sound speed we can calculate the effective range resolution as shown in Equation 2.3. Kongsberg Maritime (KM) systems use different pulse lengths for different acquisition modes, and even for different sectors. The pulse lengths are typically increased with increasing depth to maintain sufficient signal to noise levels. There is thus a tradeoff between range resolution and achievable range. The fact that different pulse lengths are used will have to be taken into account when analyzing the data. Another important point to be aware is

that KM systems store the water column backscattered intensities using a sampling rate decimated to be approximately the same as the bandwidth of the transmitting pulse (Kongsberg, 2011). Thus typically a target smaller than the projected pulse length should only show up in 1 or 2 samples. Knowing these two factors, it will be possible to define the expected geometry of an object in the water column image.

$$Bw\ (Hz) \approx \frac{1}{\tau}\ (CW\ pulses)\ \ Bw(Hz) = f2 - f1\ (FM\ pulses)$$

$$\tau\ (s) = pulse\ length,\ \ f(Hz) = frequency$$

Equation 2.2 - Defining Bandwidth (Bw)

$$RR\ (m) = \frac{c}{2*Bw}\ =\ \frac{c*\tau}{2}$$

Equation 2.3 - Pulse Length and Range Resolution

2.3 Beam Width

Narrow directed beams produced by MBES systems are the first step to have reliably positioned detections. The directivity of the beam is very important, and bathymetric MBES try to have this problem solved. The way the beams are formed, which was explained before, produces narrow beams (narrow main beam width) but also produces side-lobes in the beam pattern (Figure 2.4). These side lobes also play a major role in water column imaging and will be explained in section 2.4.
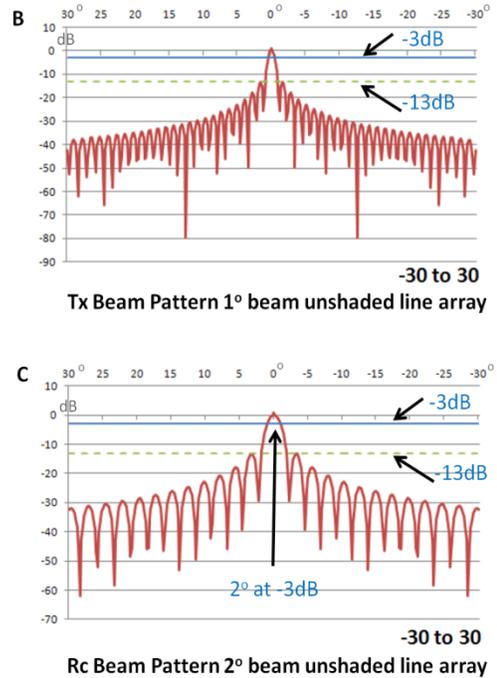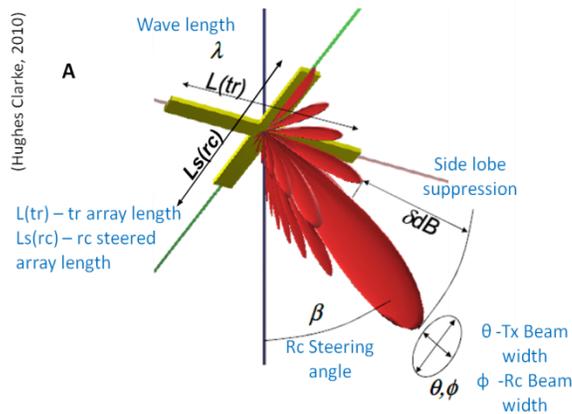
Figure 2.4 - Beam Pattern explained

A – The tx/rc beam pattern product explained (derived from Hughes Clarke, 2010). B – An example of a transmitter beam pattern, 1^O beam. C – An example of a receiver beam pattern, 2^O beam. These examples were chosen as the EM710 used in this research uses 1^Ox2^O beams.

Note the presence of side lobes along the array directions. Side lobe suppression is -13dB for both beam patterns, independently of beam width, for unshaded arrays. Typical side lobe suppression for shading used by Kongsberg MBES is -23dB.

Resultant MBES beam width depends both on the transmitter and receiver beam width. Beams are not necessarily conical as in single beam, they have a fore aft beam width, dependent on transmitter beam width, and an athwart beam width that depends on the receiver. Beam width is conventionally measured in the main beam at the -3dB limit, where the beam power reaches the half-intensity decay (Equation 2.4), and it represents the area of the main beam within which the echo is normally expected to originate. For

large objects (with respect to beam width) the whole main beam will insonify the object, but for small objects only part of the main beam will insonify the object. This fact not only reduces the sound scattered back from the object, but also creates a distortion in the object size in the water column image. Actually the distortion occurs with any object size, but is more visible in smaller objects. The object apparent size will be proportional to the main lobe width of all beams that insonify the target. The actual amount of the main lobe beam that returns a discernible echo depends on the main lobe boresite signal to noise ratio (SNR), and thus for the purposes of water column target identification, the effective beam width can be more than the -3dB limit (Figure 2.5). However, the -3dB limit is usually used for explanation purposes. The minimum possible apparent projected dimension at range, of an object (even for smaller objects) will be one beam width + object width (Figure 2.6), assuming sufficient beam spacing. However, this apparent dimension will change with range, as although the angular beam width stays constant along slant range, the beam insonified width(m) grows with slant range (Figure 2.7)

$$10 * \log(Power)$$

$$-3dB = 10 * \log(0.5)$$

Equation 2.4 - Half intensity decay equation

$$bw(tx)(rad) = \frac{k * \lambda}{L(tx)} \qquad bw(rc)(rad) = \frac{k * \lambda}{Ls(rc)}$$

$$Ls(rc)(m) = L(rc) * \cos(\beta)$$

$$\beta = steering\ angle\ (degrees), \quad \lambda = wave\ length,$$

$$k = constant\ dependent\ on\ shading$$

$$L(tx) = tx\ array\ size\ (m), \quad L(rc) = rc\ array\ size(m)$$

Equation 2.5 - Beam width equation (Tx & Rc)

For unshaded versions k=0.88, for shaded version the value of k is typically > 1.0.

$$\lambda = \frac{c}{f}$$

$$c = sound\ speed, \quad f = frequency$$

Equation 2.6 - Wave length

$$beam\ insonified\ width = 2 * SR * \tan(0.5 * bw)$$

$$SR = slant\ range, bw = beam\ width\ (radians)$$

Equation 2.7 - Beam insonified width dimension
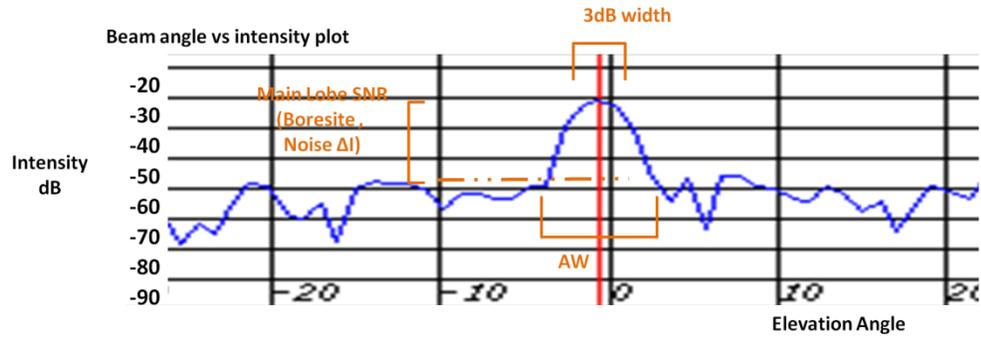
Figure 2.5 - Main lobe beam width coverage

The apparent width (AW) of the main lobe beam seen in a water column image will depend on how much stronger the boresite echo is compared to the noise (SNR)
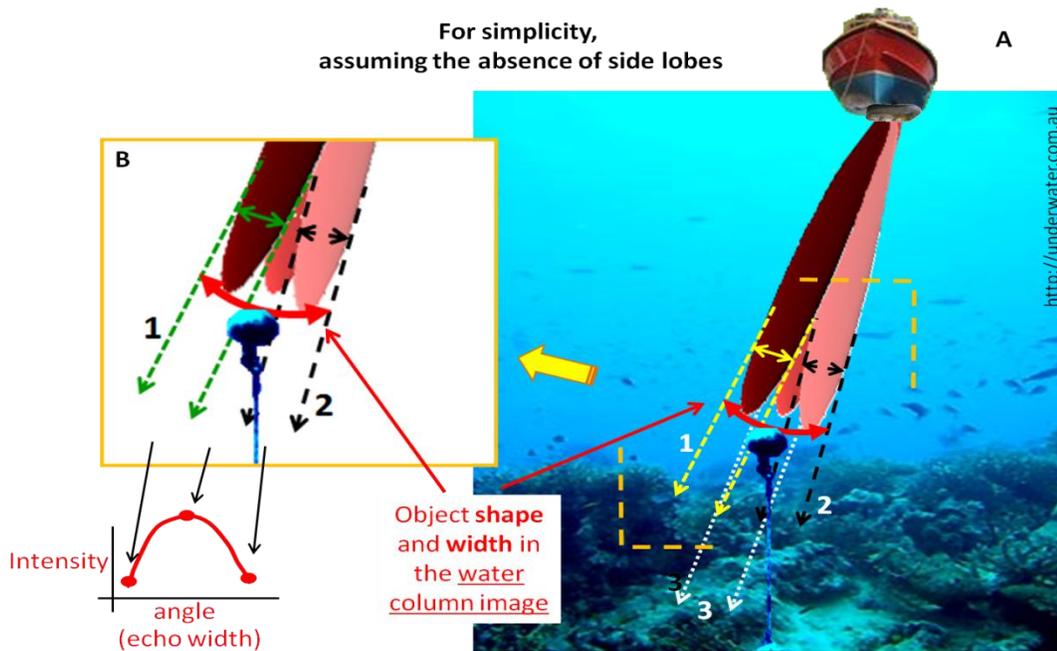
Figure 2.6 - Beam width vs object width in water column image

A – shows a sketch of the beams insonifying an object. Although beam 3 points directly to the object, depending on beam spacing, several beams (1,2,3) can all insonify the same object, defining its width in the Water column image. B – Show a zoom of A. The maximum possible perceived echo width is defined from Null to Null (main lobe width)

24

Knowing that the Tx-Rc main lobe beam width affects the apparent object imaging geometry it becomes important to know if and how beam width changes. In MBES systems, beam width is defined by Equation 2.5 and it depends on the linear array dimensions, steering angle, shading function and wavelength as shown. Wavelength (Equation 2.6) depends on frequency and sound speed, meaning it will change for different sectors, different swaths, different acquisition modes (KM systems) and different water characteristics (Equation 2.5) (Equation 2.6). Effective Array length will change with beam steering, as the array decreases size the beam width will enlarge (Figure 2.7).
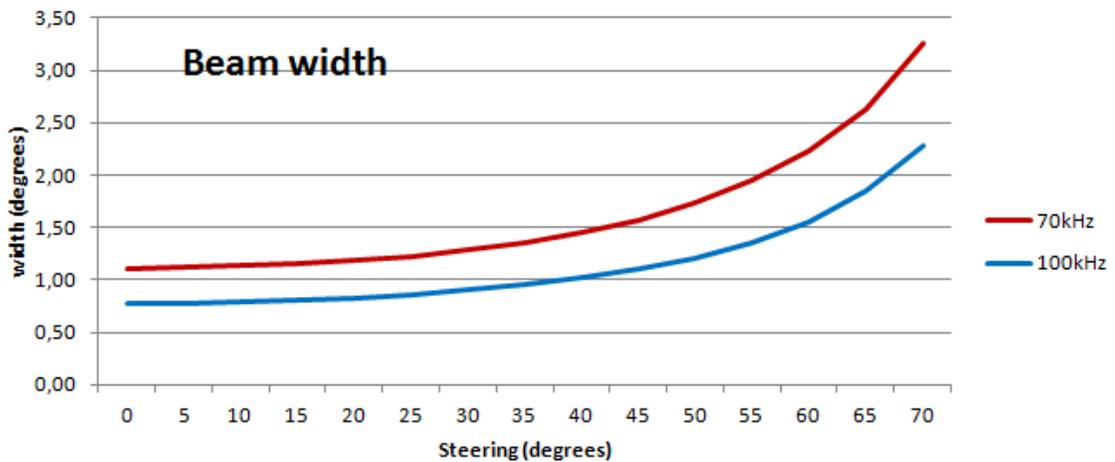
Figure 2.7 - Comparing -3dB beam width dimensions for different frequencies used by EM710 for a 1m array.

Although this change is not important for the transmission as the steering angle (used for yaw and pitch stabilization) is usually less than 5 degrees (making the effective transmission array length decrease by only 0.38%), it will be important in the receiving beam as the typical steering angles will be much larger than 5 degrees (Equation 2.5) (Figure 2.8). Figure 2.10 shows an example where the receiver beam is steered 60°. Note that at 100m range the insonified across distance (projected receiver beam dimension) is 2x wider at 60° than 0° while the insonified along distance is maintained even when the receiver is steered. Also, although depth is the same as range at nadir, at 60° 100m depth is equivalent to 200m range, and the insonified distance depends on range making it wider, as shown. In KM systems, in contrast to the sea floor detection spacing which can be multiple per physical beam, the detection in the water column is strictly done by amplitude meaning that beam spacing defines the minimum definition of angular target dimensions.
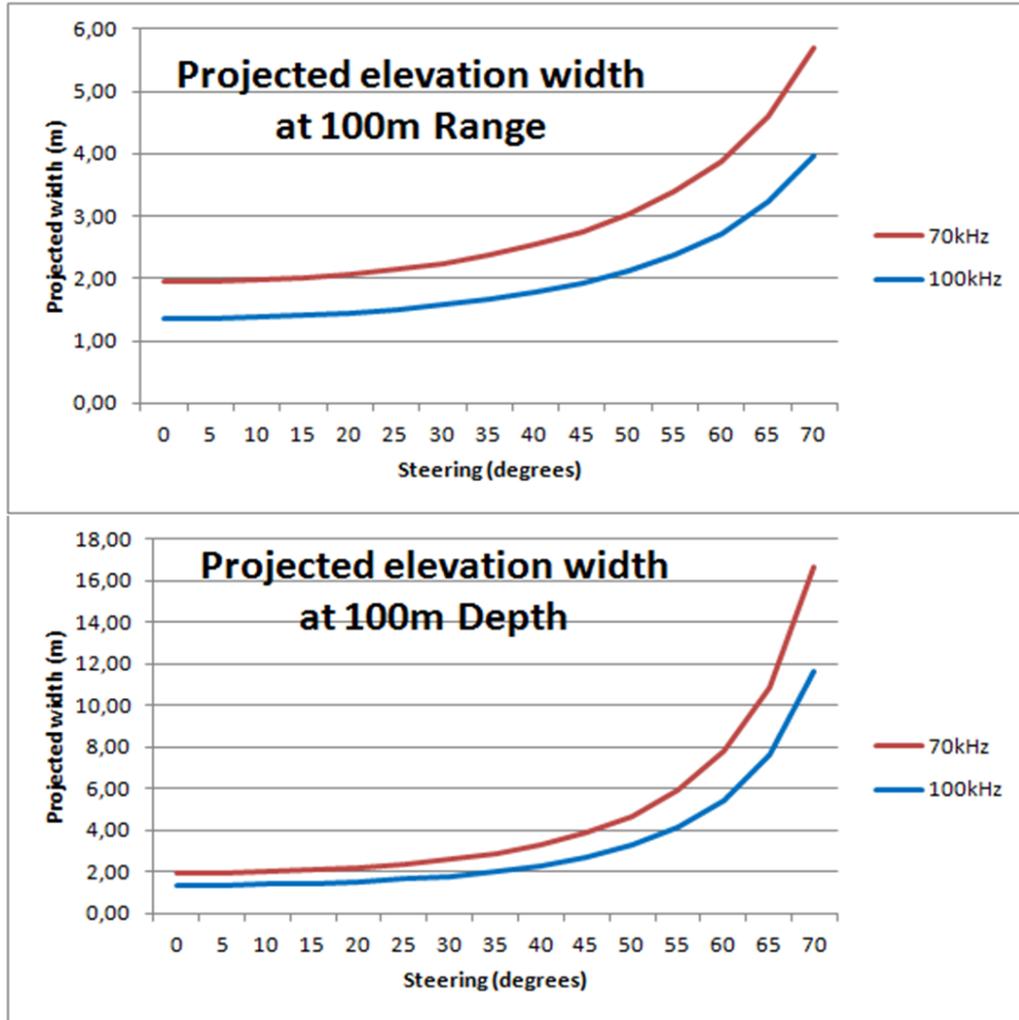
Figure 2.8 - Comparing -3dB beam width and beam projected width of the EM710 range of frequencies for different beam steering, using a 1m array.

Knowing the projected main lobe beam width and how it changes with elevation and range, one must also be aware of what controls the number of beams that will insonify the object. This depends on beam width as said before but also on beam spacing (number of available beam forming channels, equidistant, equiangular, inbetween or any other option). To guarantee all small objects (with respect to the projected beam width)

are insonified within -3dB limit the MBES system needs to ensure full coverage, meaning the spacing between beams has to be equal or smaller than the 3dB beam width. Assuming full coverage, all objects will need to be insonified at least once by one main lobe beam in the full swath of beams the MBES produces. The effective main lobe beam insonified width (the former apparent width), however, depends on the signal to noise ratio between that beam boresite echo and the surrounding noise (Figure 2.5) As the surrounding noise level increases or decreases, the effective beam width will decrease or increase respectively to a maximum that depends on side lobe suppression level. Usually in KM systems the widest beam spacing is still tighter than the 3dB limit. Figure 2.6 describes the main beam coverage and how small objects may be insonified by more than one beam (assuming spacing tighter than ½ effective main lobe width).

While -3dB is a useful dimension for specifying a discrete cut off, for the purpose of water column imaging it should be recognized that the appearance of a target will reflect the fraction of the main lobe signal that is visible above the background noise level. This is herein termed the effective beam width. For example if there is 20dB SNR then the -20dB beam width should be used. Typically this is 3x larger than the 3dB limit (Figure 2.9).
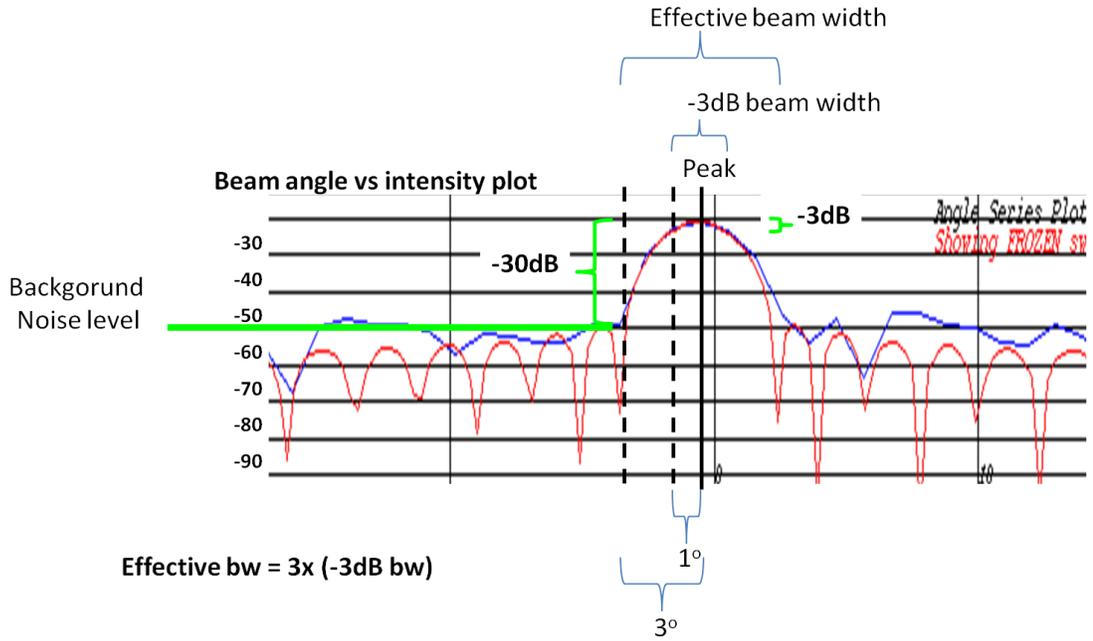
Figure 2.9 - Effective Beam width vs -3dB beam width

With the effective beam width of the main lobe beam we can calculate the along and across widths that is visibly insonified through the water column. In the transmission beam this along track dimension depends on the slant range, and effective transmission beam width, which means it will grow radially within the water column. In the receiver beam, it also depends on the steering angle, meaning it will also change across the water column. The dimensions insonified along track and across track are defined in Equation 2.7. To guarantee that a spherical object with 15 cm diameter is insonified at -3dB limit the beam spacing needs to be at least equal or smaller than the beam projected width (at -3dB) + 15 cm width, at maximum detection depth (Figure 2.6).

29

Tx Beam
Beam steered <u>**0°**</u>
insonified width (SR 100m) = **1.944m**
Beam steered <u>**5°**</u>
insonified width (SR 100m) = **1.952m**
insonified width (d 100m) = **1.959m**
(depth = 100m, SR = 100.4m)

f = 70 kHz
λ = 0.021 m
L(tx) = 0.97m
L(rc) = 0.55m
bw (tx)= 1.11°
bw (rc)= 2.20°

0°

5°   Tx
insonification

Rc Beam
Beam steered <u>**0°**</u>
insonified width (SR 100m) = **3.85 m**
Beam steered <u>**60°**</u>
insonified width (SR 100m) = **7.70 m**
insonified width (d 100m) = <u>**15.40 m**</u>
(depth = 100m, SR = 200m)

60°

Range = 100m

Depth = 100m

Rc
insonification

Figure 2.10 - Beam insonified along and across distance examples (Tx vs Rc)

Example using an EM710, at 70khz. Note that at 100m range the insonified across distance (Rc beam) is 2x wider at 60° than 0° while the insonified along distance is kept when the Rc beam is steered 60°. Note also that although depth = range at nadir, at 60° 100m depth = 200m range, and insonified area depends on range.

2.4 Side Lobes

The characteristic beam pattern of a Mills-Cross MBES system is defined by a main lobe (significantly larger than the already explained beam width at -3dB), and by side lobes that carry the remaining energy that is not in the main beam (Figure 2.4). If the side lobe energy is above the noise level it also can extend the scattering signature of those objects in the water column image. For unshaded MBES systems the side lobe suppression is -13dB (Figure 2.4) but MBES systems usually use a shading function to

30

increase the side lobe suppression, at the expense of increasing beam width (which usually is corrected by having a larger array length). These shading functions (Figure 2.11) can achieve total side lobe suppression but the cost in beam width is too large. Typically MBES systems use functions that achieve -25dB suppression, and decrease the interference of side lobes in detection. While sufficient for seafloor tracking, if the main lobe target echo intensity is 25dB or more above the background noise level, sidelobe responses will be shown in water column data, and so they are also important in water column detection.
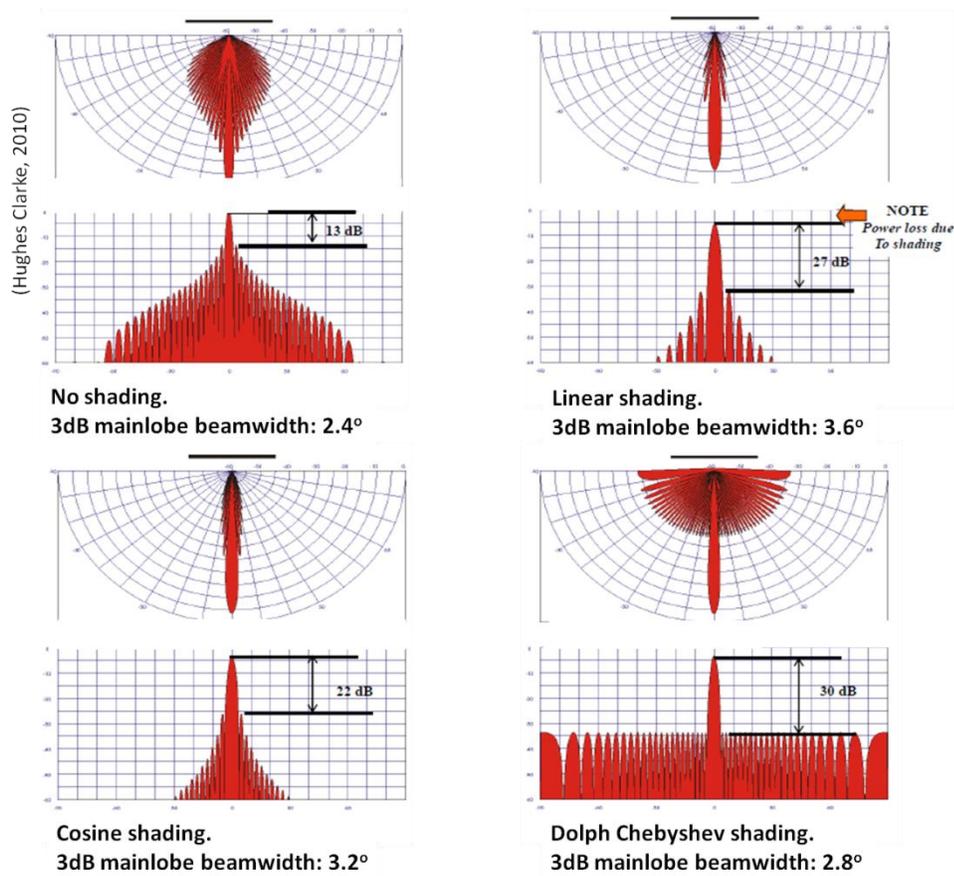
Figure 2.11 - Shading functions example (Hughes Clarke, 2010)

Note the beam width increases with amount of shading and there is a loss of power in the main lobe.

KM systems shading function is unknown at the moment.

Side lobe signatures can be particularly noticeable in water column imaging because MBES systems record the total intensity received from each beam, which includes all parts of the transmission and receiver beam pattern product. Figure 2.12 illustrates what a typical MBES beam pattern looks like and how objects outside the boresite contribute. MBES systems record samples of intensity captured in short time frame as the hemispherically expanding pulse travels away from the source. All targets within two hemispheric shells spaced a pulse length apart contribute. How much each point in that volume contributes is the product of its target strength and the beam pattern at that angle off boresite. At each time frame the MBES records the total intensity captured by the beam (the whole beam pattern), assuming it came from the main beam boresite (the maximum response axis). But as it was shown in Figure 2.4 the beam has significant sensitivity below -3dB. This sensitivity may be enough when detecting high scatter objects located off the actual beam axis to give a discernible echo. So all the energy captured by side lobes are added to the energy captured by the main beam. The misleading effect here is that if a high intensity echo is detected by a side lobe, the MBES system stores it in the main beam boresite direction, at a slant range corresponding to the time frame when it was detected. This can create false echoes that are confused with real ones. So it is possible to point the beam to 0° and detect an object at 30°, and MBES water column projection will incorrectly map this object where the main beam was pointing (0°) (Figure 2.12 (A)).

Beam Pattern (unshaded line array)

Showing the beam pattern of 1 beam only

Side lobes beam width

3rd side lobe (51°)
2nd side lobe (33°)
1st side lobe (18°)

main beam width
5° at -3dB

Object A is detected with the 2nd side lobe and projected to the main lobe **a** at the same slant range it was detected

Object C is detected with the main beam, even though only part of it is inside the side lobe insonified area, and projected to the beam angle in c

Object B is not detected as it lays between the 1st and the 2nd side lobe, facing a Null location

Object D is detected with the main beam

Figure 2.12 - Showing an object detection example across the beam pattern

For simplicity main lobe width at -3dB is used, although the real value needs to be calculated.

Side lobes will cause one particularly important limitation in water column detection. The limitation is created by the side lobes detecting the closest high scattering object (large in the beam axis). Having the MBES transducer as the reference, this closest high scattering object that constitutes a problem is usually the seafloor. Sea floor usually has very high scattering characteristics (when compared to everything else in the water) and it is a large (virtually infinite) object in the beam axis. When side lobes detect the seafloor, the intensity scattered back is so high relative to typical water column echoes (see Table 2.1) that, even with side lobes at -25dB the echo will obscure mid water targets. This effect creates a high intensity mask after the Minimum Slant Range (MSR) in all the beams whose side lobes had hit the sea floor, masking all the water column true detections. The Figure 2.13 depicts MSR effect. Although the sea floor directly below is

usually the problem, vertical rock formations or off nadir rock walls will create the same effect at a range equal to their closest approach to the sonar. And similarly, a particularly bright mid water target will show up in multiple beams away from its actual location due to side lobe detection at the same slant range (Figure 2.14), thus can mask weaker real targets at other elevation angles at the same slant range.

Type of detection	Backscatter
Targets (Buoys)	-20 dB
Fish	-30 to -20 dB
Fish School	-10 to 0 dB
DSL (krill)	-60 to -40 dB
Krill layer	-20 to -10 dB
Gas plumes	-40 to -35 dB
Seafloor (Squamish)	0 to 10 dB
Water	-70 to -80 dB

Table 2.1 Typical backscatter strength for different detections

Data acquired in Squamish 2011, with an EM710
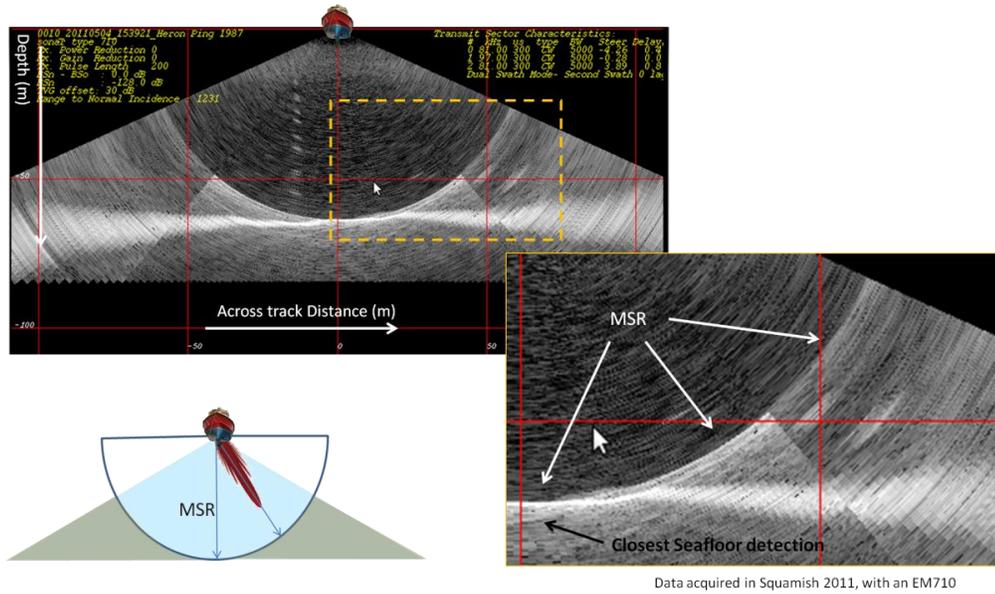
Figure 2.13 – Side lobes creating the Minimum Slant Range effect

Intensity measurements are affected by side lobes detecting sea floor after the closest seafloor detection - minimum slant range (MSR).

Data acquired in Squamish 2011, with an EM710
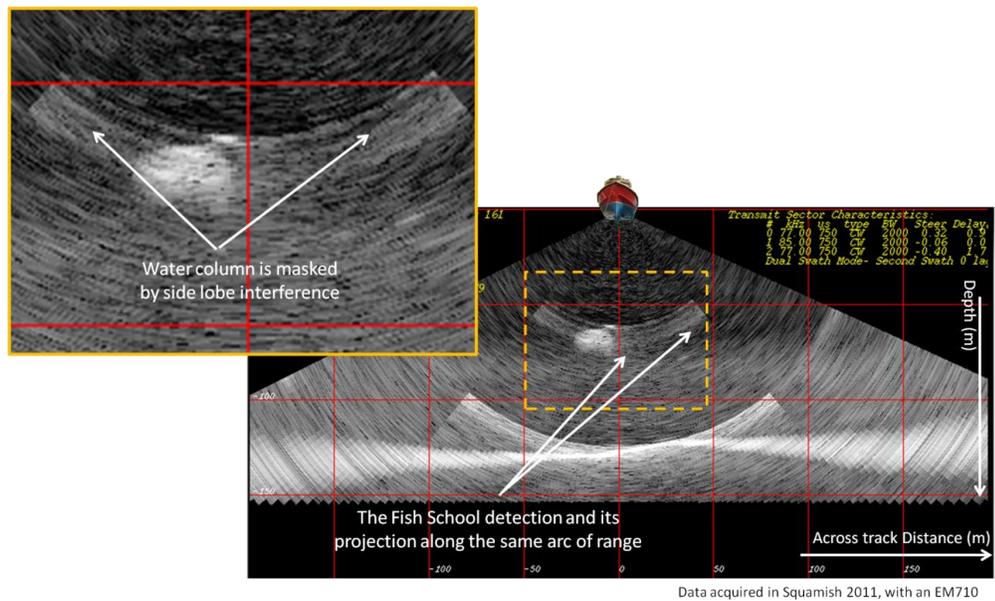
Figure 2.14 - Fish school side lobe mask effect, similar to MSR

Note the high intensity common range shadow around this fish school, also note it does not interfere with the other sectors

35

Being aware of the MSR limitation in water column detection, we must focus on side lobes interference in water column imaging. Because of the side lobe detection effect shown in Figure 2.12, side lobes distort any object that backscatters enough energy in two characteristic ways, depending on which side lobes detect the object. In Section 2.3 it was shown that each MBES beam was created by joining the transmission and receiver beams, each one with its own side lobes (Figure 2.2). The result was an MBES beam with side lobes typically on the axis of the transmitter and receiver array. Each direction of these side lobes corresponds to the respective transmitter and receiver beam. The distortions are created separately by the 2 different source types of side lobes, the receiver beam side lobes and the transmitter side lobes Figure 2.15.
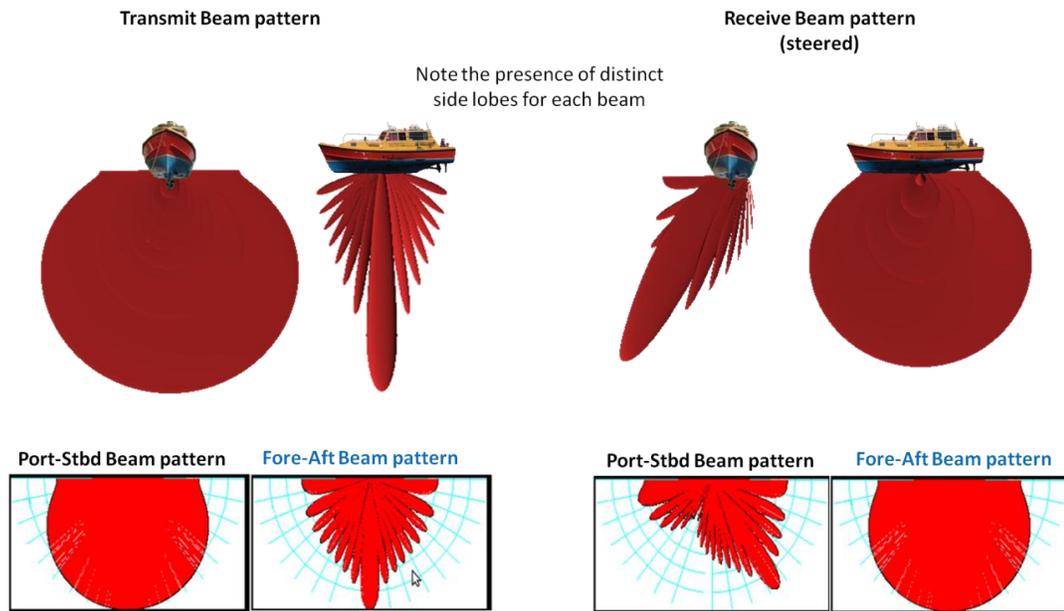
Figure 2.15 - Tx and Rc beams and side lobes

As the vessel moves forward between successive pings, the transmitter beam side lobes create a hyperbolic shaped echo in the water column image, in a plane defined by the object detection angle and swath (Figure 2.16), similar to the one seen in single beam detections. As the survey platform moves towards the object the consecutive transmitter beams start to insonify the object in the water column with their side lobes even before the main beam points to the object (Hughes Clarke, 2006). The slant range will then be larger than the one that will be detected by the main beam, as the object is still far from its closest point. The higher intensity detected by the side lobe is erroneously positioned as if it were located in the main beam boresite vertically below the vessel, at that same slant range it was detected (Figure 2.16A). As the survey platform moves closer to the object, the slant range at which the side lobes will detect the object will decrease. Once within the field of view of the main lobe the echo will increase to a maximum at the closest point. After passing at the closest point, where the main lobe insonifies the object directly, as the distance to the object increases the recorded detections will appear at increasing slant ranges. This effect creates the hyperbolic echo, centered in the real object detection. Figure 2.16 A shows how the hyperbolic echo appears and reinforces the idea that this effect is seen in a plane defined along track by the vessel track and the vector to the target when it lies in the main lobe boresite (Figure 2.16 C,D). The radial thickness of this along track hyperbolae will be controlled by the pulse length. Figure 2.16 B shows this hyperbolic echo shape seen in the water column image. The size of the shape depends on side lobe suppression and the objects scattering capacity.
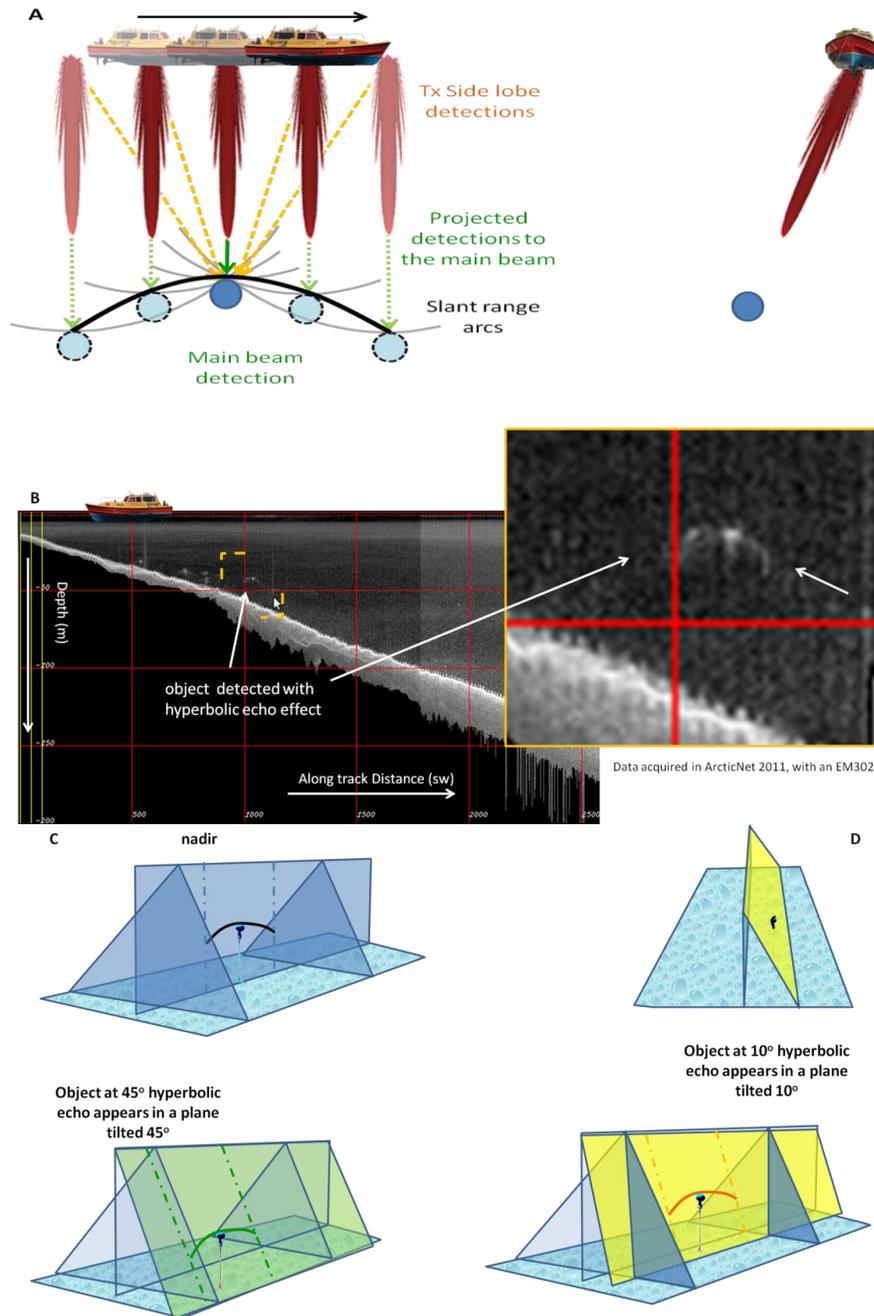
Figure 2.16 - Hyperbolic echo explained

A –illustrates the vessel movement while pinging creating the hyperbolic echo shape, B – shows an example of the hyperbolic echo seen in a water column image, C – illustrates an example of the hyperbolic echo seen at nadir and 45 degrees in a perspective view, D – illustrates another example of the hyperbolic echo seen in a perspective view and front view.

Across track, not only the receiver main lobe but also its side lobes will detect the backscattered energy from the transmitter main lobe and the detected intensity will be erroneously positioned as if it were located in the main lobe, at the same slant range. This creates a common range arc seen across swath as several adjacent beams detect the same target with their side lobes (Figure 2.17 A). This effect is visible along the same range through the whole sector where the object is detected (Figure 2.17 B). The width of the common range arc depends on side lobe suppression and the objects scattering capacity. The effect is seen across the swath, together with the beam width projection (Figure 2.17 B, C). The common range arc is a discontinuous higher intensity arc as it reflects not only the side lobes but also the nulls between the side lobes (where no scattering intensity is registered). This effect actually reflects a composite beam pattern that is created from the successive discrete sampling of all the adjacent receiver beams patterns (as will be explained later in Section 4.2.5). Each intensity value in the common range arc, mapped in the water column image, comes from the edge of the main lobe or the side lobe detections of each separate beam at that same range (Figure 2.20). The sampling of the receiver common range arc depends on the physical spacing of the beams. Better than - 3dB limit is a common standard. Finer spacing is achievable at the expense of angular sector.

A – illustrates the mechanism that creates the common range arc echo shape

Text within figure A (right panel):
Rc Side lobe detections create Projected detections in the main beam

Common range arc

Main beam detection

Text within figure B:
0013_20110427_230310_Heron Ping 2197
sonar type 710
Tx. Power Reduction 0
Rx. Gain Reduction 0
Tx. Pulse Length 200
BSn - BSo : 0.0 dB
BSn : -128.0 dB
TVG offset: 30 dB
Range to Normal Incidence 1164

Depth (m)

object detected showing side lobes common range arc

Data acquired in Squamish 2011, with an EM710

Across track Distance (m)

Text within figure C:
nadir

Object at 20°, common range arc appears tilted 20°

Figure 2.17 - Common range arc explained

A –illustrates the mechanism that creates the common range arc echo shape, B – shows an example of the common range arc echo seen in a water column image, C – illustrates examples of the hyperbolic echo seen at nadir in a perspective view and at 20° in a front view.

40

Both across track side lobe effect and the MSR limitation are minimized with the use of sectors, limiting its effect to the respective sector. The transmitted power is focused on each sector with minimal power transmitted to adjacent sectors, and different frequencies isolating the sectors. This effectively blocks the detection of objects in adjacent sectors. As an example, for an outer sector, the sound radiated in the nadir direction is minimal reducing the MSR effect (Hughes Clarke, 2006). Figure 2.18 shows that the MSR effect is minimized but not removed, while the common range arc effect effectively disappears.
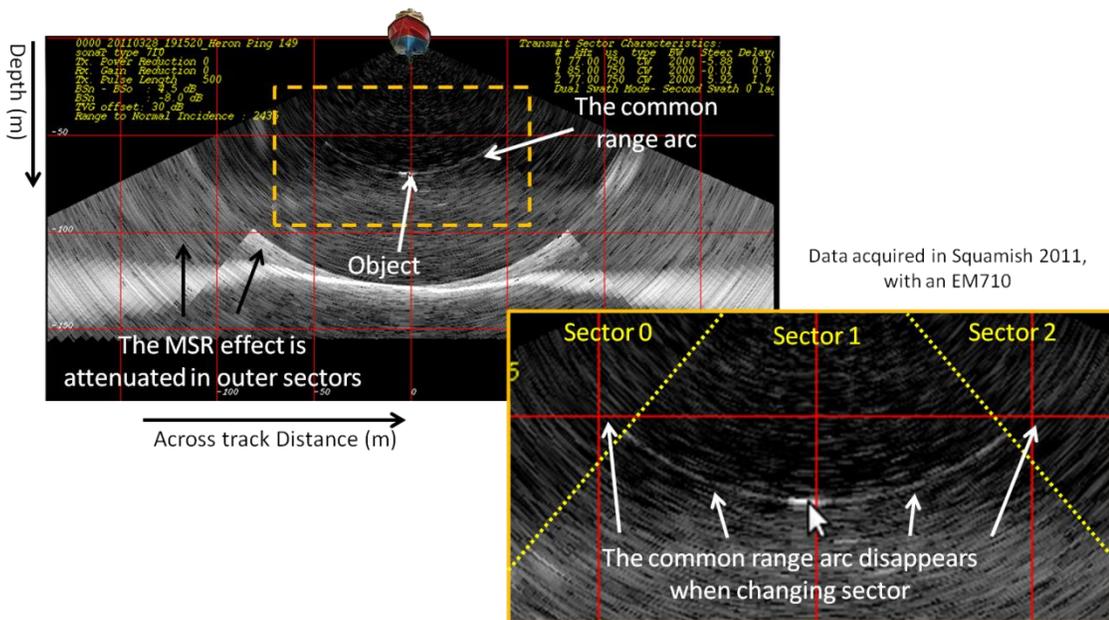
Figure 2.18 - The common range arc limited by sectors

Looking at Figure 2.19 (A) we can see that side lobes are not continuous. They are presented as lobes with a maximum response axis and a null between each side lobe. In order to fully predict how an object's geometry will be defined in the water column imaging one needs to know the location of these nulls and the side lobes spacing. The way these lobes are created depends on the effective array length, frequency and shading function as shown in Figure 2.19 (B). As it depends on the effective array length, it will also depend on the beam steering (Equation 2.5). Both receiver common range arc shape and transmitter hyperbolic echo shape distortions will be registered in a specific beam depending on the presence or not of a side lobe pointing at a discrete target, and this marks the importance of knowing the location of the nulls between side lobes as well as the side lobe centre and their level of suppression, and consequently the side lobe spacing. Figure 2.20 illustrates that because of discrete side lobe spacing the common range arc shape will not be a continuous line.

The Rc beam pattern shown in a water column image is a product of all beam's beam pattern. The pattern observed is not just the receiver pattern for a single beam. Rather it is discrete (at beam spacing) sampling of the beam pattern of many beams. The pattern is almost equivalent but not quite the same. Ideally one can model the beam pattern. Actual patterns however, rarely match these. For the purpose of this thesis, sections through particularly strong targets (example Figure 2.20) will be used to design match filter shapes for use in target detection.
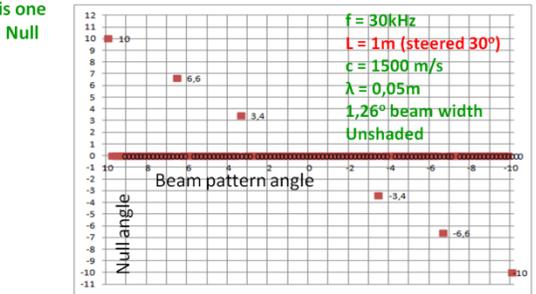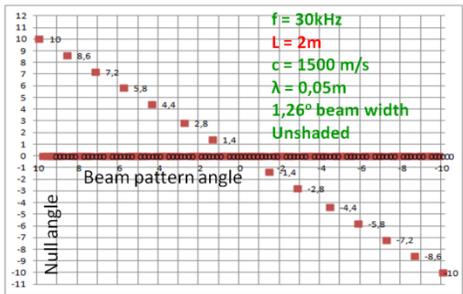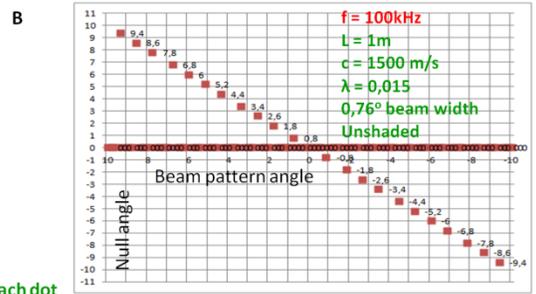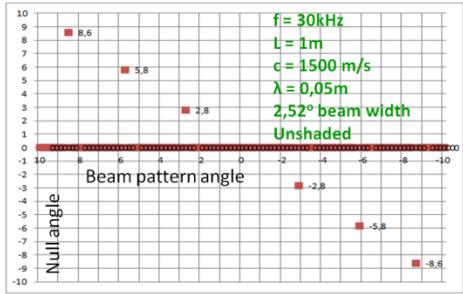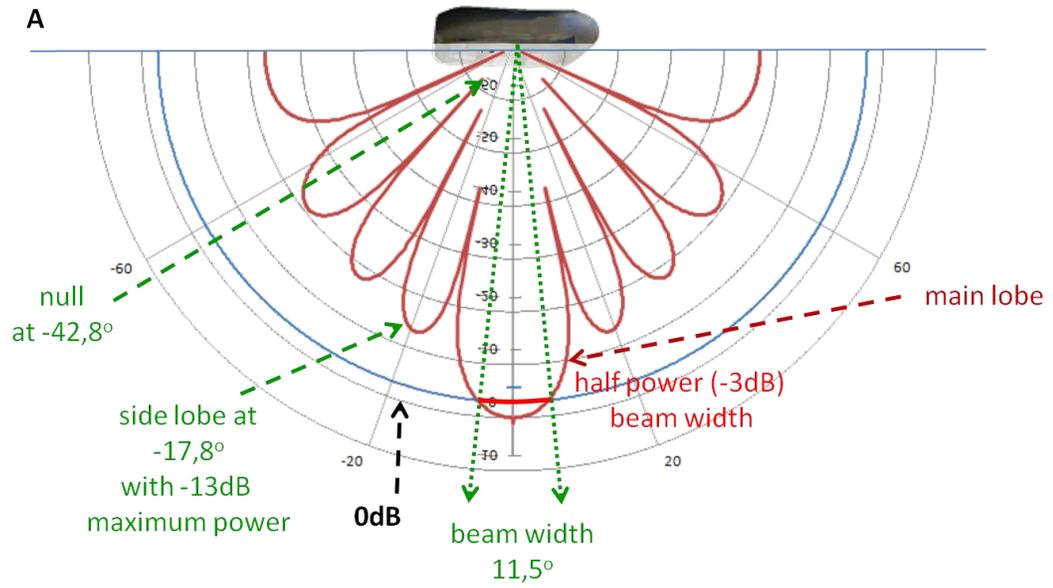
Figure 2.19 - Showing side lobes and Nulls location in a specific beam pattern

Note the location of the nulls changes when changing frequency, the array length and when steering.
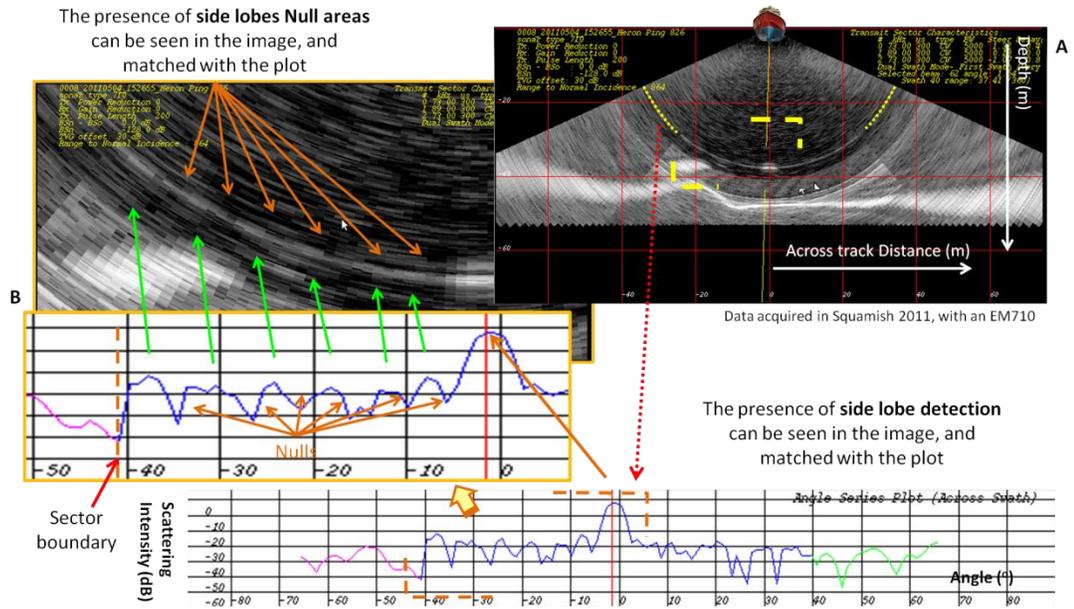
Figure 2.20 – Strongly scattering fish school showing the existence of nulls between side lobes

A – shows the fish school being detected in the water column image with side lobes intensity stored in contiguous beams, B – shows a zoom of the side lobe area, and a match with the intensity plot along the same range arc.

2.5 Sectors

In order to maintain yaw stabilization, MBES systems split their transmitting fan into several sectors. These sectors are then transmitted at different transmit steering angles conserving along track coverage homogeneity. Although along track coverage is maintained, across track there is discontinuity in the water column data when considering a single swath, increasing its gap as the transmitting tilt angle increases. Figure 2.21 illustrates the transmitting sectors and the swath discontinuity across track.

This significantly complicates target pattern recognition as a single swath is composed of multiple sectors and this does not define a common plane.

44
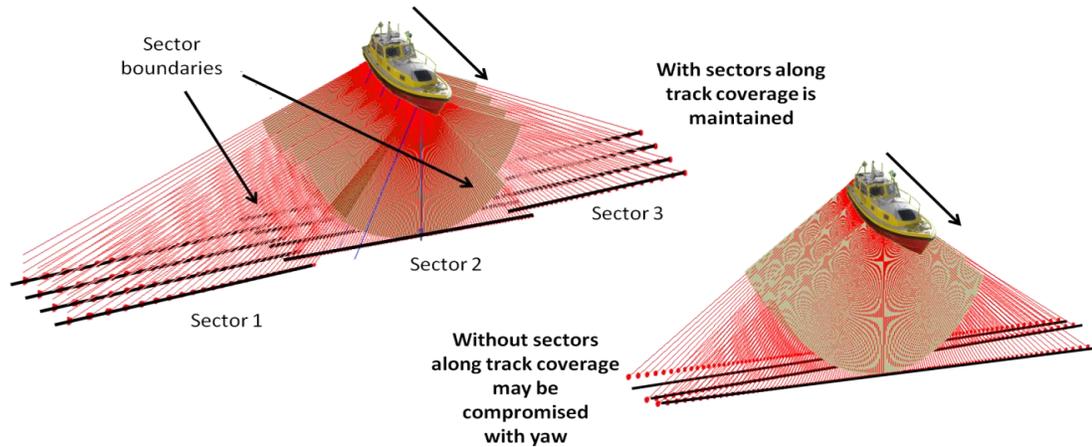
Figure 2.21 - MBES Sectors and yaw stabilization

2.6 Detections, LIMs, targets and objects

Before moving to the next chapter, a small elucidation is required. Along the next chapters the words 'LIMs', 'detections', 'objects' and 'targets' will be used several times. 'LIMs' (local intensity maxima) is a specific phrase used for potential detections done at step 4 of the algorithm (Search for LIM), as they are simply the highest intensity in a defined volume and not truly a final detection. 'Detections' is used when the algorithm chooses to consider a LIM as a valid detection point. The decision will take place for the LIM when the scattering pattern about the LIM matches the expected geometry. 'Object' is effectively whatever there is in the water column to be detected (can be a fish, a buoy, gas, etc). This is distinct from LIM's that may represent artifacts that are not related to a real object. Finally, a 'target' is only used for specific geometrically defined clusters of objects the user might be looking for (clusters of detections).

45

3. Data Acquisition and pre-Analysis

Most data used in this research came from the case study in Squamish (Hughes Clarke et al, 2012) (Figure 3.1 A) using an EM710. But in order to demonstrate the general utility of the algorithm it was tested also on two other sets of data. The requirements were that data needed to have been acquired by any Kongsberg Maritime bathymetric multibeam that could also record water column data. As to the survey settings for the case of Squamish data, the experimental design specifically was set up to optimize imaging the suspended targets that were deliberately laid along seafloor channel axes. The survey lines were run so that the targets would be detected close to the nadir in the water column image, using the central sector. For the other examples the data were derived from an opportunistic passing over mooring hardware and a submerged structure only as part of a regional survey.
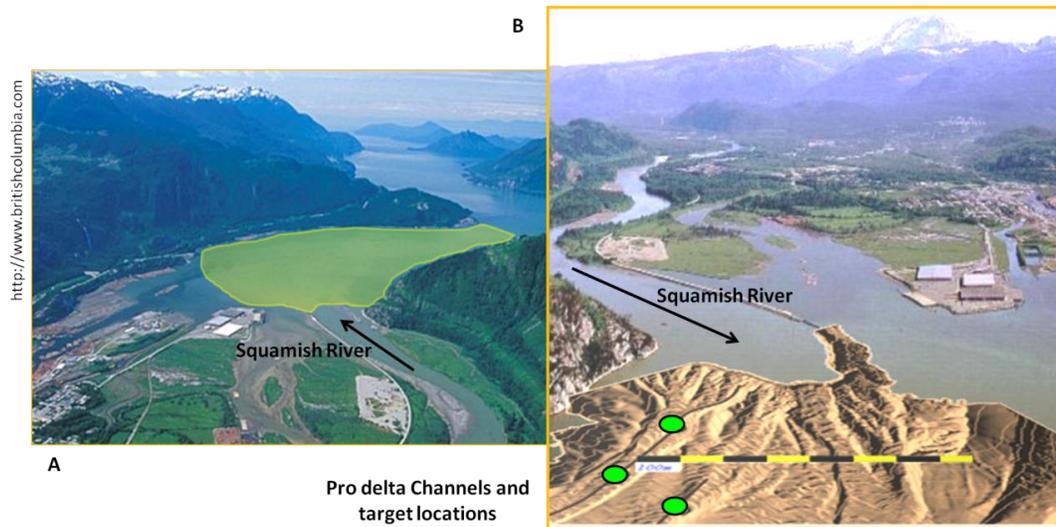
Figure 3.1 - Squamish project survey area, river pro-delta

A – Survey area, at the pro-delta of Squamish river, B – 3D view of the pro-delta revealed from multibeam surveys showing some buoys location example as green circles.

For the algorithm purposes several KM system characteristics need to be considered. EM710 systems operate in different acquisition modes, named Very shallow mode, Shallow mode, Medium mode, Deep mode, Very deep mode and Extra deep mode. In these modes the MBES changes some important parameters including pulse length, centre frequencies and sampling rate (Table 3.1, Table 3.2). If nothing is specified the system automatically switches modes according to depth (Table 3.1,Table 3.2).

MBES systems are designed to improve bathymetric resolution by decreasing the beam width and pulse length whenever possible, thereby improving angular and range resolution (going from deep to shallow mode). Beam width will change with frequency, so assuming the array size is kept constant, it will be considerably better in shallower modes where higher frequencies are used (depending on the sector and single/dual swath mode). For target detection, however, there are other considerations to take into account. As higher frequencies are used in shallower waters (as attenuation is less of an issue), decreasing pulse length and consecutively increasing range resolution, the signal to noise ratio will however decrease as two terms of the sonar equation change related to ensonified area and band width.

$$SNR = SL - 2 * TL - NL + BS + DI$$

$$BS = S_b(\theta) + 10 * Log(A)$$

$$NL = N_c + 10 * Log(W)$$

$$W = receiver\ bandwidth, \qquad Nc = Noise\ center\ frequency$$

Equation 3.1 - Sonar Equation, signal to noise ratio

47

Analyzing the terms that make up the signal to noise ratio (SNR) (Equation 3.1), when all other parameters are fixed the backscatter strength (BS) and noise level(NL) are the terms that can alter with pulse length and bandwidth. In the shallower modes the pulse length is usually set to provide sufficient SNR for the seabed echo (seabed echo is typically -20dB). But the water column echoes are typically 10^3 times weaker ($\approx$ - 50dB). Backscattered signal level will therefore decrease, with the shortened pulse length thus decreasing signal to noise level. Superimposed on this is the greater noise due to higher receiver bandwidth. The system will therefore have better range resolution for loud targets like the seafloor. However, while still having better potential resolution for strong water column targets, it will show poorer discrimination of those weak targets whose echoes are only slightly above background noise level.

The overall result is better for bathymetric detection, however the decrease in signal to noise ratio can create increasing difficulties in water column detection. The sea floor is a strong scattering object, while small objects in the water column are unlikely to be. Therefore the decrease in signal to noise is not significant for bathymetric purposes, but it can be a very significant issue in water column detection while trying to detect weak scattering objects in waters crowded with marine life or suspended sediments. To improve weak target SNR longer pulses are favored, but do compromise range definition of the targets. However, as illustrated earlier, typical range resolution ~< 1m whereas projected beam dimensions are several meters. As by increasing pulse length discrimination in range also becomes a problem, it was operationally found that the best mode to detect objects in the water column using an EM710 for depths shallower than 200m seems to be the shallow mode considering pulse length.

48

Mode	Pulse	WCL Sample Rate	Auto crossover depth	Used in Squamish
Very Shallow	CW	6.94 kHz		X
Shallow	CW	2.31 kHz	100 m	X
Medium	CW	0.51 kHz	200 m	X
Deep	CW + FM	0.51 kHz	300 m	
Very Deep	FM	0.51 kHz	500 m	
Extra Deep	FM	0.51 kHz	1000 m	

Table 3.1 - EM710 modes, sampling rate

Mode	Pulse Length	Bandwidth	Frequencies used Single and Dual swath	Range resolution
Very Shallow	0.2 ms	5Khz	73, 97, 85 kHz 73, 89, 73; 81, 97, 81 kHz	approx: 0.15m
Shallow	0.5 ms	2Khz	73, 85, 79 kHz 73, 81, 73; 77, 85, 77 kHz	approx: 0.375m
Medium	2 ms	0.5Khz	73, 79, 76 kHz 73, 77, 73; 75, 79, 75 kHz	approx: 1.5m
Deep	~= 2ms	0.5Khz	73, 79, 76 kHz 73, 77, 73; 75, 79, 75 kHz	approx: 1.5m
Very Deep	~= 2ms	0.5Khz	73, 79, 76 kHz	approx: 1.5m
Extra Deep	~= 2ms	0.5Khz	73, 79, 76 kHz	approx: 1.5m

Table 3.2 - EM710 modes, range resolution

The main case study was on the Squamish pro-delta (Figure 3.1 B) in depths of 50-150m, where specially configured targets were placed in the mid water range so that they could be tracked. This survey, in 2011, used an EM710 mounted in a gondola on the hull of the CSL Heron. In Squamish targets were designed with different geometries using 15cm and 20cm targets spaced 2 to 5m apart so that they could be uniquely identified in the water column (targets will be carefully explained later in Section 3.2).

In the depths investigated (10-210m) EM710 uses pulse lengths of 0.2ms, 0.5ms and 2ms, with effective range resolution of 0.15m, 0.35m and 1.5m respectively. Comparing these values with the size of the buoys we can see the range resolution is usually larger than the size of the buoy. This means that buoys are not easily discriminated if close to each other. The targets separation used distances several times greater than the range resolution between the buoys to guarantee this problem does not exist. But still, there is an issue with target size to be aware. As the sampling rate is bandwidth dependent, reflecting the range resolution, the water column will be sampled in sizes equal to the range resolution. As the convolution of the pulse with the buoy may be an echo with 1 or more pulse lengths, the apparent echo length of the buoy along the beam axis in the water column will be equal to at most 2 samples (2xrange resolution). This will affect the construction of the pattern match filter (Section 4.2.5), as it will need to check that objects with a specific size have their specific geometry in the along beam axis. For the case of smaller objects than the pulse length it is always 1 or 2 x the range resolution at most.

As to the beam dimensions, in Section 2.3 it was demonstrated that beam width defines the object geometry along track (Tx beam), and across track (Rc beam) in the water column image. The EM710 used has 1° and 2° beams in transmission and reception respectively. The 20cm buoys are small enough to be smaller than the 1° beam (at -3dB) insonified area after a slant range of 12m. How many beams hit the buoy along track and across track actually depends on speed and ping period (along track), and beam spacing method used (across track). As shown in Figure 2.10, at 100m which is a close depth to the ones used for the targets, assuming 1° transmitter beam and 2° receiver beams (at -3dB), the transmitter beam will insonify a fore aft dimension of 1.94m and the receiver beam will detect a port starboard dimension of 3,85m at nadir. If the target echo intensity is well above the noise level even greater dimensions will be visible (as the effective beam width will be wider). This is the minimum size the buoy will appear as in the projected dimensions, along and across track on the water column image. Assuming the same depth, but steering the receiver beam 60°, the geometry of the buoy in the water column image will have a dimension along the same range arc of at least 15,40m.

Another important set of data that was tested was the ArcticNet Program data, acquired using an EM302 to survey in the Arctic. All tests were run on data acquired in the Beaufort Sea in 2011.

To test the algorithm in detecting man made structures, data from a survey in the Gulf of Mexico was used. The survey was done with an EM2040 mounted on a ROV using single swath, traveling at a speed lower than 1 knot and using a ping rate of 4Hz.

All the acquisition in Squamish and the ArcticNet Program was done using Kongsberg Maritime acquisition software SIS (Seafloor Information System) which controls the transceiver configuration and collects and stores the water column data together with soundings. It also enables the user to modify specific sonar settings which allows some tests to determine the optimal suspended target imaging configuration.

3.1 Survey Platforms

In Squamish, data was collected using the survey launch from OMG-UNB the CSL Heron (Figure 3.2). As mentioned, the 'Heron', a 10m launch, is equipped with a Kongsberg EM710. The version installed is a 1°x2^{o} mounted on a hull gondola. The 'Heron' also has an AML SVP to get sound speed and temperature near the transducer, and a Brooke Ocean MVP-30 installed, used to get the necessary sound speed profiles. Sound speed was acquired regularly, usually every 70m to 700m along track depending on depth, and typically only to 30m depth and a maximum of 80m depth. Then the remaining sound speed profile was extrapolated using the SIS software or using a static sound velocity profile. For positioning the 'Heron' is equipped with a CNAV system from C&C Technologies using Real-Time Gypsy solution (C&C Technologies, 2011) and feeding an RTCM correction to the POS/MV v.4 GPS aided inertial system also mounted on board. POS/MV then generates inertially smoothed differential solutions used to get the transducer position. Alternatively position can also be obtained in post processing by either using PPP, Precise Point Positioning, or PPK Post Processed Kinematics, using CNAV logged raw pseudo range. A Cansel Can-Net base station is

used for the PPK solutions. About vertical positioning, several options are available with the data that was acquired. Observed tides from DFO/MEDS online service was stored for posterior use, while initially predicted tides for Point Atkinson (35 km away) were used. Attitude from the survey platform was recorded by the POS/MV and applied directly with the SIS software.

CSL Heron

MVP 30 at the back of Heron

EM710 1°x2°

Surface Sound Speed Probe

EM710 and SSS probe
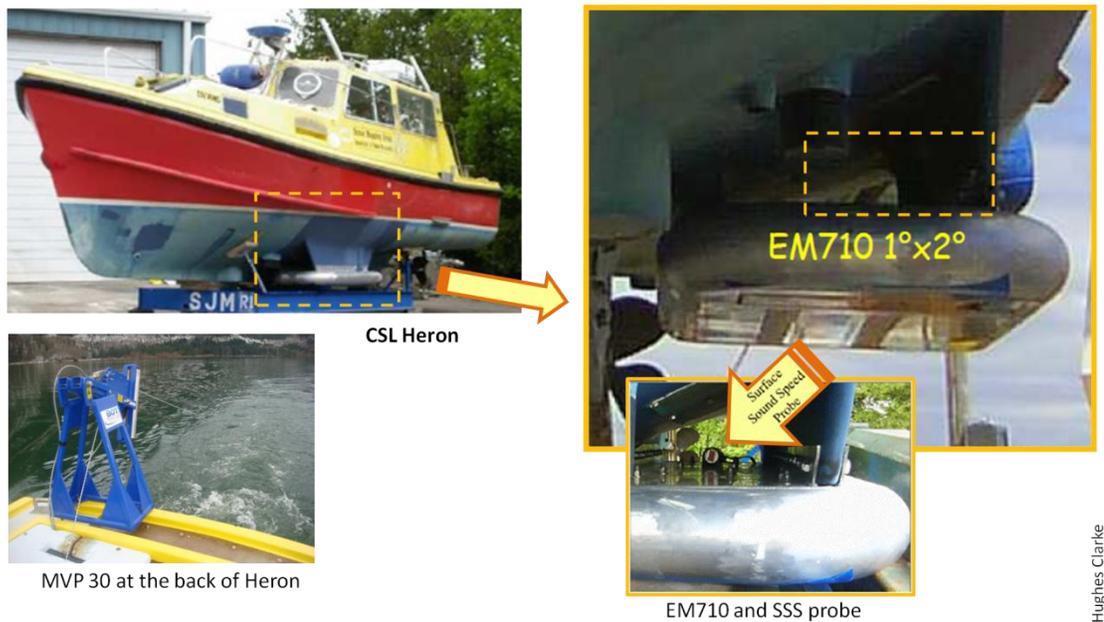
Hughes Clarke

Figure 3.2 - CSL Heron (Hughes Clarke, 2010)

As for the ArcticNet data, the collection platform was the CCGS Amundsen (Figure 3.3) a 98m 1200 class icebreaker fully equipped for long surveys in the Arctic. In the CCGS Amundsen was mounted an EM302, a $1^{o}x2^{o}$ system working at 30kHz. This system is installed directly in the hull of the vessel using a titanium-polymer window, keeping it a flush system. This multibeam system has the transmission array design

constrained to 65 degrees only, and the receiver array is tilted to port side by 6 degrees and has a 10dB attenuation because of the way it had to be mounted behind ice windows. To acquire sound velocity profiles, the vessel is equipped with a BOT (Brooke Ocean Technology) MVP-300 (Moving Vessel Profiler) capable of acquiring water column information while being towed and dipping constantly behind the vessel. For positioning a CNAV (C&C Technologies) system was used, with differential corrections. Attitude motion was recorded using the Applanix POS/MV 320 system.

MVP 300

EM302 Tx array (1ox2o system), and titanium polymer ice window

CCGS Amundsen

EM302 location

Hughes Clarke

Figure 3.3 – CCGS Amundsen

Despite positioning being probably the ultimate purpose of target detection, this thesis focus is mainly on the target detection itself. Leaving position accuracy analysis apart and focusing on object detection, both these survey platforms are well equipped for water column target detection as both EM710 and EM302 systems store water column

data. EM710 pulse lengths go from 0.2ms to 2ms, as already discussed. Beam spacing may be selected by the user to equidistant, equiangular or hi-density equidistant. The Squamish survey was always done using hi-density equidistant as it is the best option for bathymetry. For target detection equiangular is the best solution, as the projected geometry of the object in the water column image would not change across swath, for the same slant range. Using equiangular, the angle between beams does not change with across track distance making it easier to compare with the expected beam pattern. With equidistant the distance spacing at the seafloor is maintained across track by changing the angular spacing between beams across the swath. With angle between beams changing from beam to beam, the sampling across the swath may not be enough to validate real echoes. This clearly complicates any comparison with a calculated expected beam pattern. As hi-density equidistant beam spacing is created using multiple phase detections within a single beam, the actual physical beams are spaced equiangular anyway and water column samples are only collected in physical beams.

EM302 uses frequencies around 30 kHz (26.5 to 33.5 kHz) with pulse lengths of 0.75ms, 2ms, 5ms, and 15ms, having range resolutions of 0.56m, 1.5m, 3.75m and 11.25m in single swath mode. In dual swath mode the shorter pulse length is switched to 1.1ms with 0.83m of range resolution. Everything else stays the same. The configuration depends on the mode being used. For the examples used in this thesis the targets were suspended between 500m and 1000m depths that by default would employ very deep mode, using 2ms pulses with corresponding range resolution of 1.5m. Assuming depths of 500m and 1000m, using 1° transmitter beam and 2° receiver beams and considering 1m diameter buoys, an example of how a single buoys would be projected in the water

column image can be calculated. 1° transmitter beam at 500m insonifies an along track distance of 9m, and 18m at 1000m depth. The 2° receiver beam will detect a distance of 35m at 1000m depth across track for nadir beams and 140m at 60°. These values correspond to the minimum projected dimensions (at -3dB limit) of the buoy in the water column.

Beam spacing used is also hi-density equidistant, once again having the best beam spacing for bathymetric detections, and also for water column detection (with physical beam spacing being equiangular as explained before).

The EM302 installed in the Amundsen is installed directly in the hull which leaves the MBES system very susceptible to have signal to noise issues with the air bubbles that flow naturally along the ship's hulls (the bubble washdown). This effect actually creates serious problems to the MBES system in rougher seas. Another problem that is easily seen in the EM302 is noise created by interference of other systems. The Amundsen is equipped with several other acoustic systems, and without proper synchronization (the example deliberately illustrated herein) its interference is recorded in the water column images. An example will be discussed later when presenting the results obtained with the algorithm (Section 5.1). The solution to have water column data free of interferences is to use synchronization. Although it solves the problem of noise, synchronization introduces another problem. As systems have to be synchronized to fit the longest transmission period, the along track sampling interval in the water column may not be enough to guarantee full coverage as expected (which can always be solved by reducing survey speed).

As to the 2040 system, the data was not acquired by OMG personal and there is no clear information about the equipments or survey parameters used. It does not fulfill the purpose of target location, but it will however, show how the target detection algorithm works when detecting structures.

3.2 Targets

In Squamish several targets (Figure 3.4) were created for the specific purpose of this research as explained before. Each target was composed of three air filled buoys with known size, attached by a rope to 2 or 3 cement block (approx. 12kg each) acting as a mooring set. The vertical spacing of the buoys was planned so that each target would be unique and this way easily identified in the acquired water column images. Also the distance from the last buoy to the cement weight was pre defined so that the depth of the target set was known. Figure 3.6 describes the targets configuration

B

3 x Concrete Block Markers
(approx: 36 kg total)
Identified by 3 yellow 20cm
submerged targets

Hughes Clarke

Green = 15cm
Yellow = 20 cm
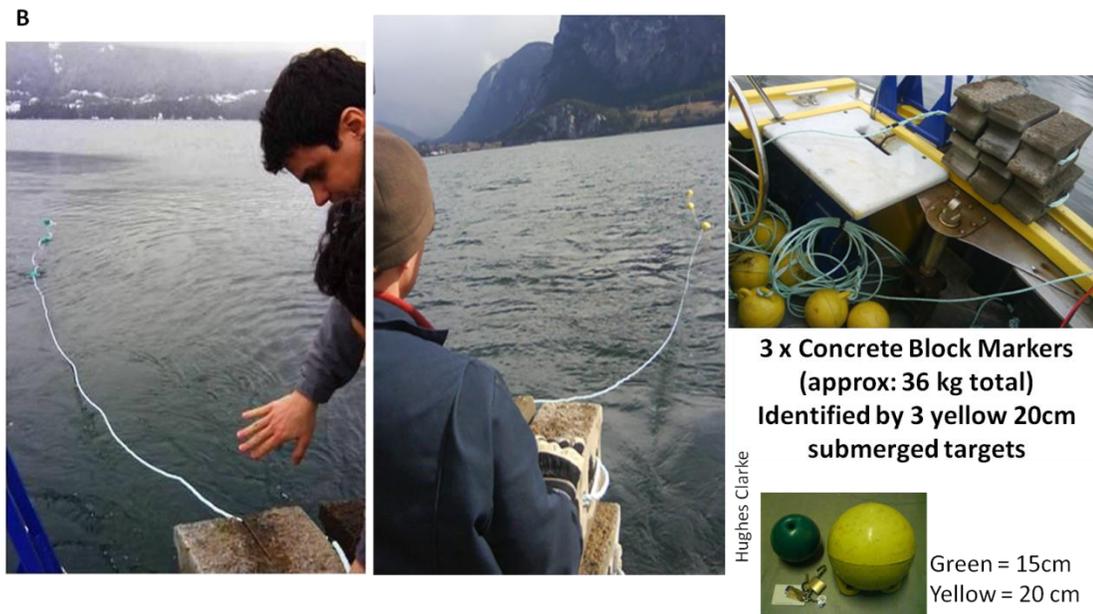
Figure 3.4 – Showing the block markers and targets (A) and their deployment (B)

Each target was then deployed in different places within channels of the pro delta slope so that landslide events could be detected (Hughes Clarke et al, 2012). The deployment site was then immediately surveyed with several check lines to assure the target location and stability with regular currents. Figure 3.5 shows a map of the surveyed area with the target's initial locations. Table 3.3 describes the planned configuration of the targets.

Target	Configuration (size) spacing (m)	Channel	Depth (m)
0	(0,15) 2.5, 2.5, 7.5	North	50
1	(0,15) 5, 5, 7.5	North	80
2	(0,15) 5, 2.5, 10	South	50
3	(0,15) 2.5, 5, 10	Center	80
4	(0,2) 4, 4, 15	South	80
5	(0,2) 4, 8, 15	South	110

Table 3.3 – Targets planned configuration
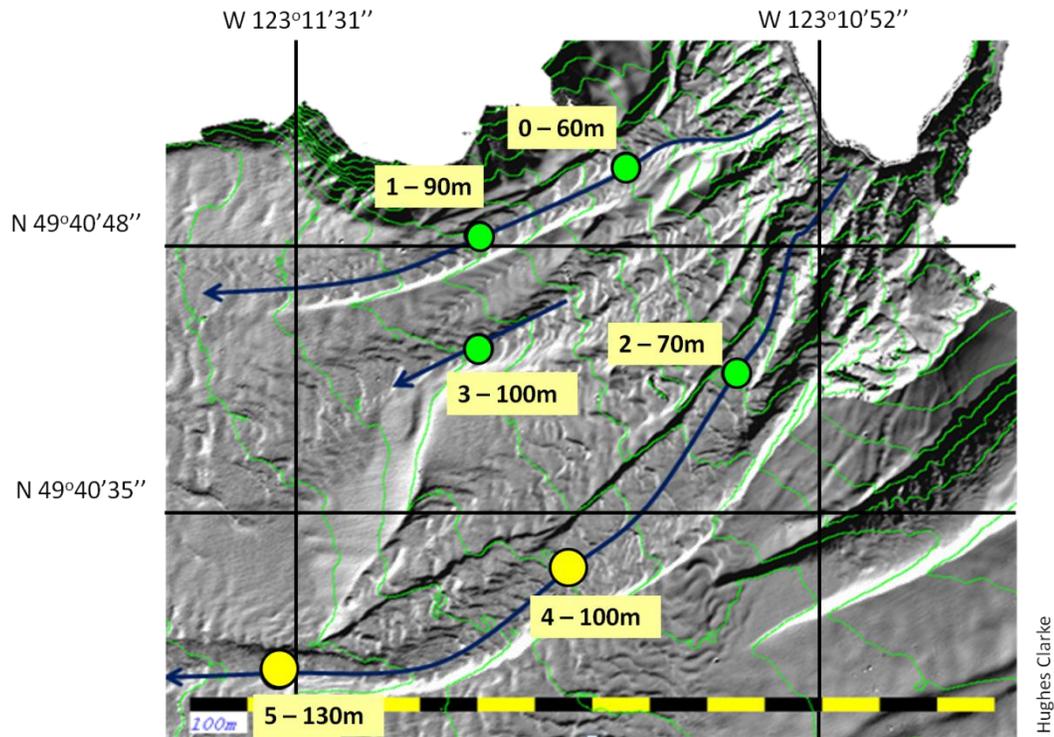
Figure 3.5 - Targets initial location

Targets are labeled with their number and initial depth, and shown using their respective colors.

During the year of 2011, from April to July, the area was surveyed several times a week in order to keep track of any eventual target movement. Early in the year of 2012, data began to be analyzed. The next list (Table 3.4) shows the initial targets check survey lines, surveyed immediately after the targets were deployed, well before any seabed displacement were likely to occur.

Survey Line	Date	Target
0002_20110301_200932_Heron.merged	01 Mar 2011	0
0003_20110301_201103_Heron.merged	01 Mar 2011	0
0004_20110301_201226_Heron.merged	01 Mar 2011	0
0005_20110301_201420_Heron.merged	01 Mar 2011	0
0006_20110301_204442_Heron.merged	01 Mar 2011	1
0007_20110301_204621_Heron.merged	01 Mar 2011	1
0007_20110301_204621_Heron.merged	01 Mar 2011	1
0008_20110301_204808_Heron.merged	01 Mar 2011	1
0009_20110301_204941_Heron.merged	01 Mar 2011	1
0010_20110301_205123_Heron.merged	01 Mar 2011	1
0005_20110304_184735_Heron.merged	04 Mar 2011	2
0006_20110304_184921_Heron.merged	04 Mar 2011	2
0007_20110304_185051_Heron.merged	04 Mar 2011	2
0008_20110304_185240_Heron.merged	04 Mar 2011	2

0009_20110304_185414_Heron.merged	04 Mar 2011	2
0000_20110304_183645_Heron.merged	04 Mar 2011	3
0001_20110304_183849_Heron.merged	04 Mar 2011	3
0002_20110304_184019_Heron.merged	04 Mar 2011	3
0003_20110304_184150_Heron.merged	04 Mar 2011	3
0004_20110304_184310_Heron.merged	04 Mar 2011	3
0000_20110328_191520_Heron.merged	28 Mar 2011	4
0001_20110328_191728_Heron.merged	28 Mar 2011	4
0002_20110328_191941_Heron.merged	28 Mar 2011	4
0003_20110328_192212_Heron.merged	28 Mar 2011	4
0004_20110328_192722_Heron.merged	28 Mar 2011	5
0005_20110328_192926_Heron.merged	28 Mar 2011	5
0006_20110328_193152_Heron.merged	28 Mar 2011	5
0007_20110328_193419_Heron.merged	28 Mar 2011	5

Table 3.4 – Targets initial confirmation survey lines

Having defined distances serves the purpose of uniquely identifying the targets in the water column. The next figure (Figure 3.6) shows the target's actual configuration. Also, Table 3.5 shows each target's final configuration and location.
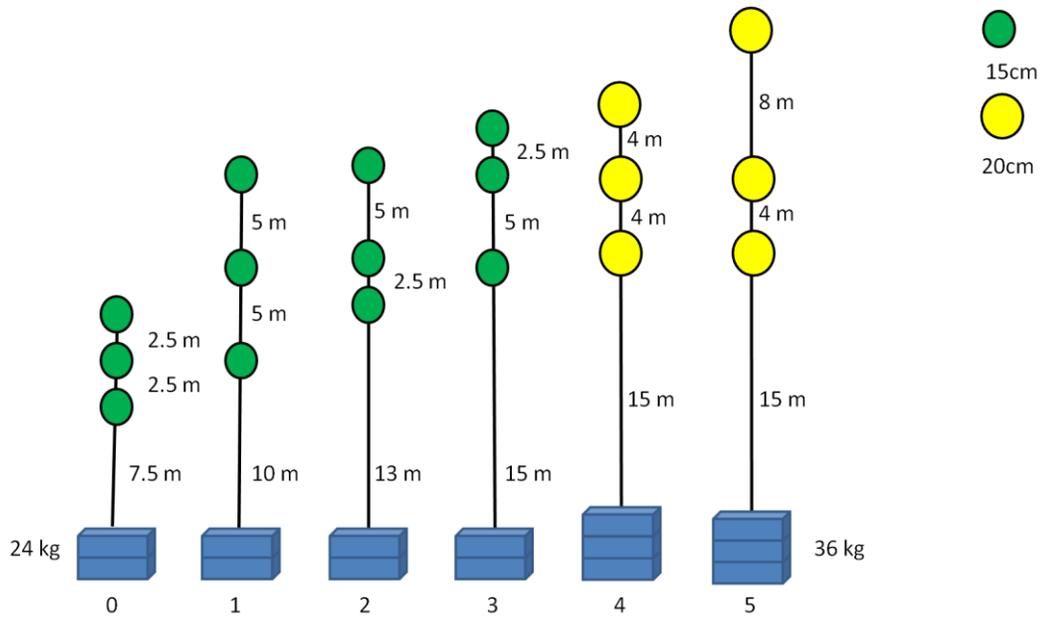
Figure 3.6 – Targets final configuration

Target	Configuration (size) spacing (m)	Latitude (^{o})	Longitude (^{o})	Depth (m)
0	(0,15) 2.5, 2.5, 7.5	49.680885	-123.184384	54.27
1	(0,15) 5, 5, 10	49.679950	-123.187866	79.92
2	(0,15) 5, 2.5, 13	49.677792	-123.181733	54.68
3	(0,15) 2.5, 5, 15	49.678205	-123.187741	79.73
4	(0,2) 4, 4, 15	49.674323	-123.185607	85.88
5	(0,2) 8, 4, 15	49.672531	-123.192576	110.46

Table 3.5 - Target configuration and initial deployed location

3.3 SIS Settings (Installation parameters, Runtime parameters)

Running SIS on the survey platforms, for the depth encountered in these experiment it would be better to have the systems setup using shallow mode (in Squamish) and Very deep (in the Arctic) increasing signal/noise, using the central sector, or beams close to nadir. Another custom configuration that these systems need is an adjustment to the dynamic range used for data logging. By default KM systems record water column intensities in samples using 8 bits only. This allows only to record 256 levels of intensity. As logarithmic intensities are given in 0.5dB resolution, there is only room for ±128 signed values, meaning the default minimum intensity that will be captured is -64dB. Typically the seafloor will scatter energy much higher that -64dB. But for example zooplankton scattered intensity lies between -50dB and -80dB (depending on the species) thus being clipped by this default system setting. Also, smaller objects such as the small buoys may scatter energy close to the lower boundary of the default dynamic range. The buoys used in Squamish seem to be detected around -20dB to -40dB. As KM systems internally record values at higher dynamic range (24bit), these systems also actually detect intensity values lower than -64dB, even though they are not stored by default, so there is an option to set an offset to the values recorded in the water column sampling 'xLog_offset ##' that offsets the scale by ## dB values. This way the KM system will record lower intensity values if needed (Figure 3.7). The offset used in Squamish was 'xLog_offset 30' allowing the system to record values as low as -94dB. While this change also shows more noise, it also shows clearly the mid-water detections.
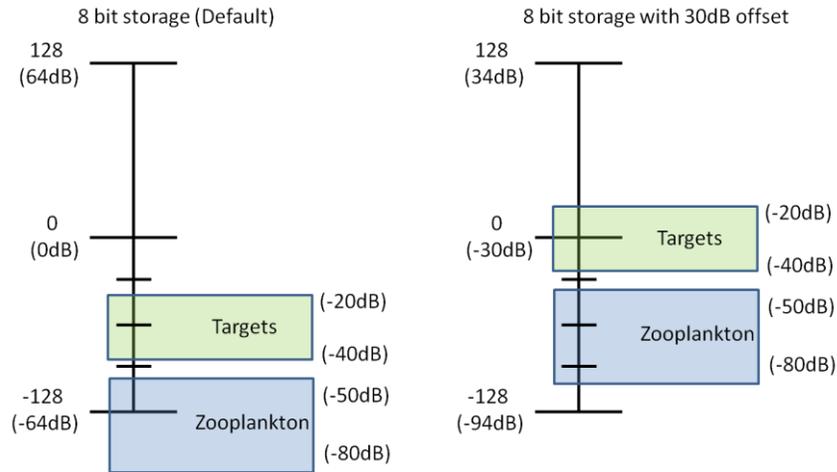
Figure 3.7- 8bit storage and xLog_offset

3.4 Survey Lines planning

The first time targets were deployed in Squamish, short survey lines (Table 3.4) in a star shape pattern were run in order to capture the targets from different azimuths and using different elevation angles. In a pre-analysis to these survey lines it was decided that targets were easier to detect if they were in the central sectors, closer to nadir, where angle deformation would be smaller as the receiver beam pattern's main lobe was narrower.

Survey lines were then planned keeping in mind the main aim of the Squamish research. In order to unambiguously identify integration artifact effects, the regular survey lines were run alternately parallel and perpendicular to the fjord direction. As to the targets location, 5 days each week an extra set of survey lines was acquired covering the targets probable path. The lines were run along the axis of each active channel in the river pro-delta assuming the targets would move that way. All the lines were run so that

64

the axis of the channel was near nadir in order to survey the targets with the central sector, and also minimizing any bathymetric errors. Next figure (Figure 3.8) shows the example of the planning.
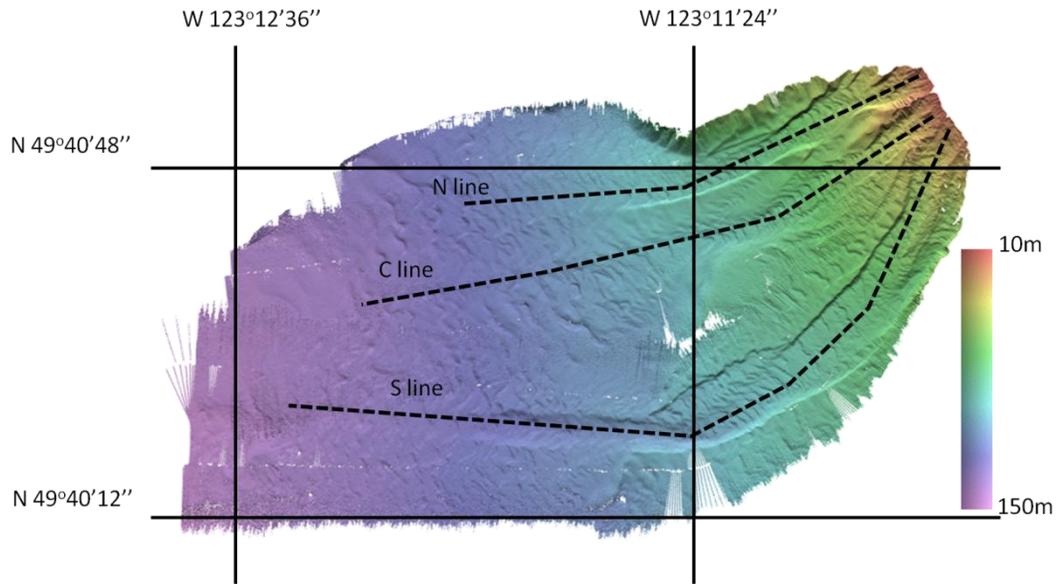
Figure 3.8 - Survey lines planned along the active channels (pro-delta of the river).

3.5 Water Column Images

From the Squamish Project survey, with 90 days of surveys all collected with 3 channel lines per day, we need to examine approximately 2800 minutes of data, surveyed with the EM710, with depths that range from 10m to 200m. This makes a total of about 270 survey lines, 90Gb of data, totaling near 714,000 swaths or 2D water column images to be analyzed.

In the pre-analyses to gather information on how to create a detection method, the initial post-deployment lines were processed and checked for any target appearance.

Lines were short and the amount of time spent analyzing the lines was acceptable. All targets could be located by trained operators although sometimes it could require a second analysis. The following figure (Figure 3.9 A) shows target 1 (5m.5m.10m) being detected in a 2D across track and along track water column images (line 0038 4thMar2011). Although the buoys are spherical they do not appear in the 2D water column image as a circular shape, as they would in a regular photographic image. The buoys appear as an arc with a specific size, with this shape depending on multibeam imaging geometry as explained in Chapter 2.

Looking at the time series of intensity plot of the beam that hits the target (Figure 3.9 B), we can notice that the intensity peak is abrupt, increasing and decreasing in a few samples. As explained before, as the target is smaller than the beam pulse length the resultant image geometry in the water column will be at least 1 pulse length echo, but cannot be more than 2 (Figure 3.10).

Looking at the intensity plot by angle of the same slant range in several beams across swath (Figure 3.9 C), we can verify that the target is also detected with contiguous beams. This depends on two factors, the beam spacing and beam width (beam coverage effect). This effect is created by the receiver beam pattern. This beam pattern, is characterized by the main lobe beam, with a specific known beam width at -3dB. Note that as the target echo is ~20dB above the noise level, the visible main lobe is much wider than the nominal 3dB limits reflecting the shape of the intensity fall off outside the 3dB limits. It also carries the side lobes as shown previously in Section 2.4. This side lobes interference is always present, although in this case its intensity is below noise level.

66
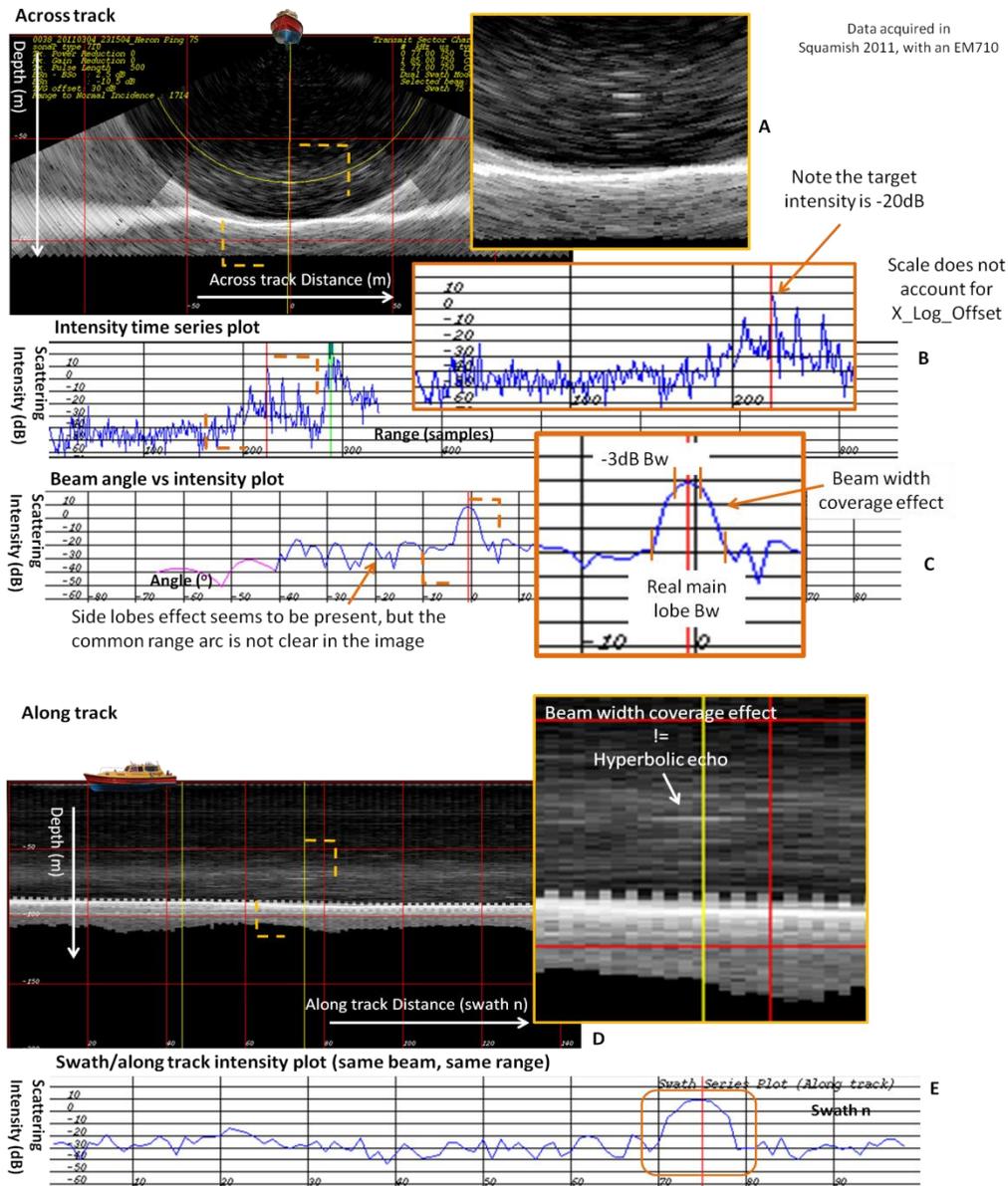
Figure 3.9 - Targets being detected in a 2D water column swath image

A – Targets detected and labeled in the WCL across track image, B – Time series, showing target intensity (note that values need -30dB offset applied), C – A plot across the swath, intensity at same slant range. Note the visible main lobe Rc beam width is more than -3dB, as it depends on SNR, D – Along track image, Tx beam width coverage effect is present, E – Along track intensity plot (dual swath), note that main lobe beam width coverage effect is seen at same range as the curvature of the hyperbolae is lost with the large internal sampling of MBES.

67
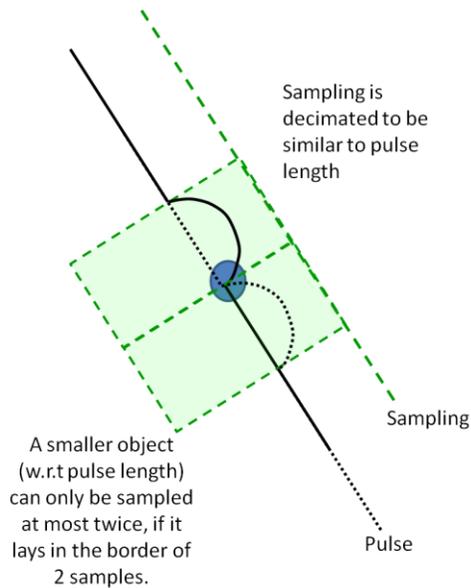
Figure 3.10 - Pulse length vs target

The pattern seen in the intensity plot in Figure 3.9 (C) reflects the visible receiver main lobe beam width being larger than the -3dB limit, with several contiguous beams also capturing the target. Considering this is a 2° receiver system, using 128 physical beams, using a swath coverage of 65° to each side, and knowing it is a equiangular system, we have roughly 1° beam spacing. With this beam spacing we would have at least 3 hits on the target if just considering -3dB limit, and we are actually seeing 5 to 6 hits, meaning the main lobe is observed insonifying the target well beyond the -3dB limit. This effect (beam width coverage) controls the length of the continuous arc, with the angular width defined by the effective receiver insonified width (beyond -3dB). This distortion is similar to the common range arc created by the side lobes. But although the common range arc is presented showing the nulls between side lobes (Figure 2.20) the

beam width coverage effect presents itself as a continuous arc. This effect is created by adjacent beams detecting the object within their main lobe.

Having an effective beam width (over -3dB) the transmitter main lobe will insonify the object before the vertical perpendicular plane that contains the object (6° beam width achieves around 10m width coverage at 100m depth) and the backscattered intensity will be stored by the receiver. This creates a hyperbolic echo with the angular width defined by the effective transmitter beam width seen along track.

As to the side lobes effect, in this image their presence is not clearly seen. The backscattered intensity captured by the side lobes has an intensity that is too close or below the natural water column noise intensity. This way the side lobes are masked by the noise and seem not to be present as is explained in Figure 3.11. It seems hard to characterize side lobe pattern unless main lobe echo is more than 30dB above background noise.
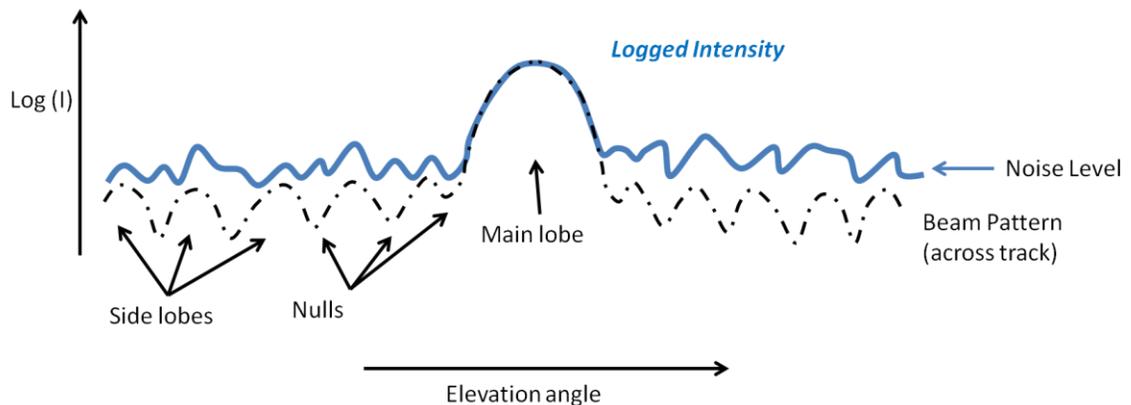

Figure 3.11 – Sidelobes intensity compared with background noise

In this figure's case, occasional side lobe peaks may even be seen although they are not significantly above noise level.

A similar effect to the one seen in the receiver beam seems to be present due to the transmission beam pattern in the along track image (Figure 3.9D). A continuous line is seen along track created by the main lobe beam width (< -3dB) coverage effect with the transmitter beam pattern. This is shown by analyzing the plot shown in Figure 3.9 E). We can see that the target was detected along track for several swaths (with the vessel speed of 3m/s, pulse rate of 2.1 Hz, the along track spacing for each ping is about 1.41m, and the beam width coverage seen corresponds to 6.38m distance), always by the same beam, almost at the same range.

Together with this transmit main lobe beam width coverage effect there is usually the hyperbolic echo pattern. This hyperbolic echo distortion is harder to see in this image. That is because there are few pings along track spreading the side lobes more than usual. Analyzing other water column data acquired in Squamish, one could see that for the typical survey speed (6 knots) and depths of 80m the hyperbolic continuous echo could be seen along track for about 7m and the side lobes would spread for about 30m before and after the continuous hyperbolic line. The example in Figure 3.9 shows only 196 m along track water column data, so assuming the side lobes are still there, the complete hyperbolic echo with side lobes should be seen spread almost one third of the survey line distance. Re-inspecting this same survey line carefully, and analyzing several slant ranges after the target detection we can pick the side lobes. Figure 3.12 (A) shows a zoom of the target area, pointing out the side lobes. Zooming out again, compressing the image, and increasing contrast in Figure 3.12 (B) it is possible to see the hyperbolic pattern created with the side lobes detection before and after the main lobe detection as pointed out in Figure 3.9. Note the scales of each image are changed intentionally when the image is

compressed. Using the image from Figure 3.12 (B) another image is created Figure 3.12 (C) to show the hyperbolic shape drawn over the water column image as it appears in the detections. The intensity plots shown in Figure 3.13 (A) (B) and (C), show intensities along track, showing the same beam angle (0°) at 3 different swaths and ranges. Forward side lobe detection was captured in swath 65 (91m along track) at a range of 73m, the main lobe detection (where the target actually is) was captured in swath 71 (105m along track), at a range of 71m, and the aft side lobe detection was captured in swath 87 (121m along track) at a range of 73m. This points out the target (swath 71) and two of the Tx side lobe detections fore-aft that help create the hyperbolic echo pattern.

This pre-analysis allows the conclusion that the hyperbolic effect seen along track is also composed by the Tx main lobe beam width coverage effect together with the transmitting side lobes. It is discontinuous as the nulls between the side lobes are below the background noise level. Similarly the constant range arc shape seen across the swath is composed by the receiver main beam width coverage effect and side lobe effect also.
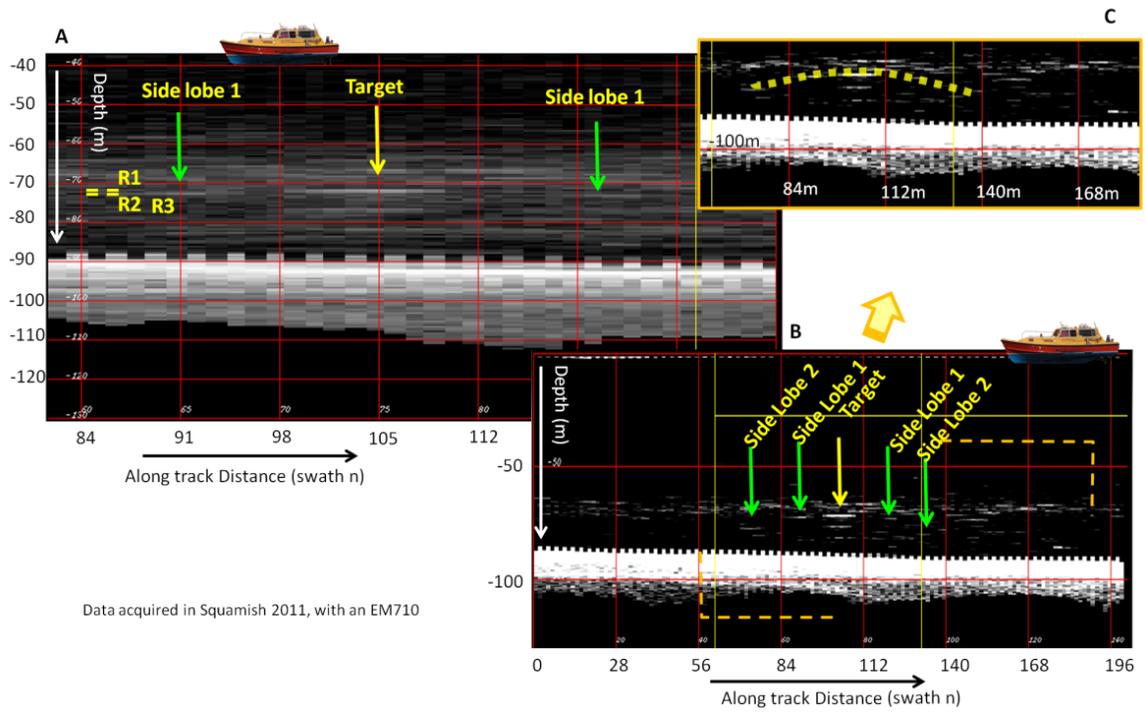
Figure 3.12 - Hyperbolic pattern seen along track

A – Zoom in on Figure 3.12 showing the hyperbolic echo shape and beam width coverage effect. B – The full survey line image compressed and with contrast increased so that the hyperbolic echo shape is more perceptible. C – shows a sketch of the hyperbolic shape drawn over the echoes
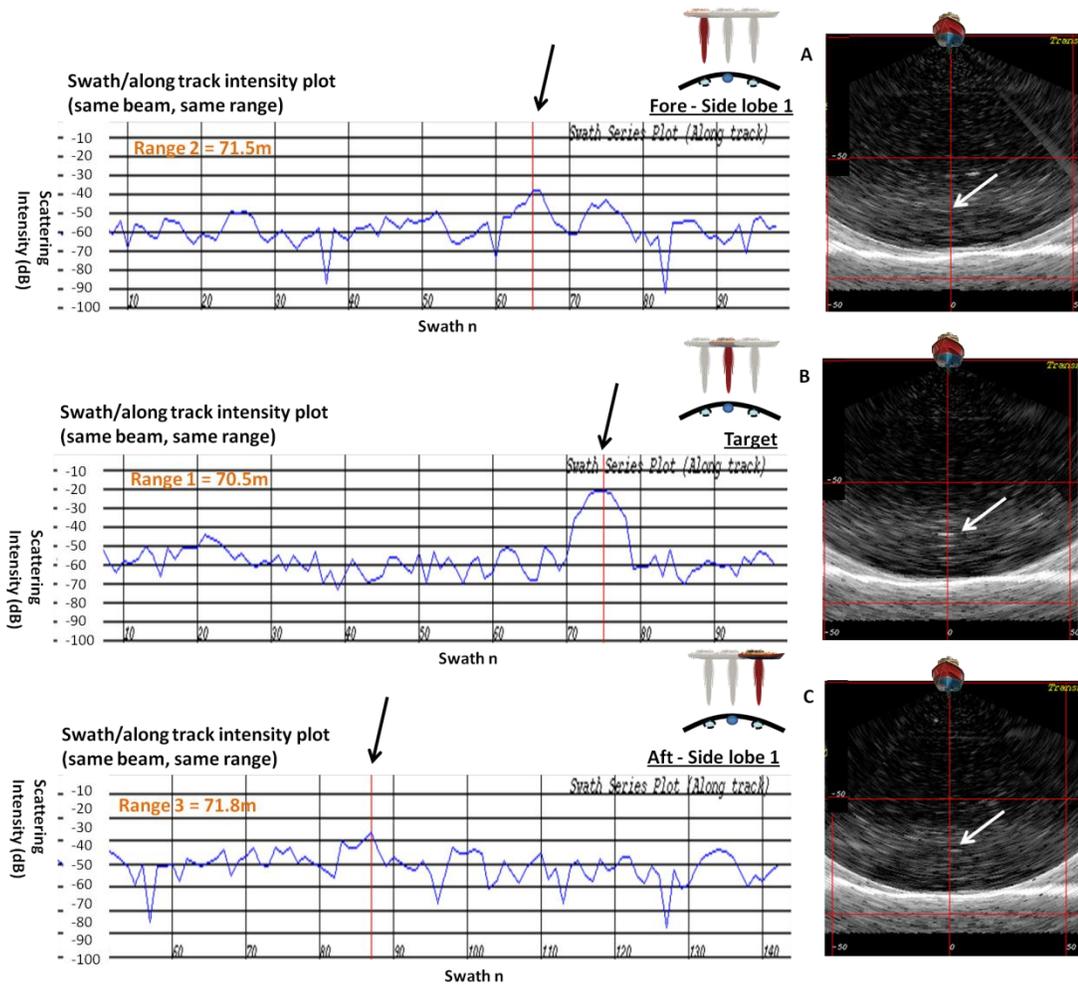
Figure 3.13 – Plotting the hyperbolic pattern seen along track

A – shows the intensity plot at 0o beam angle, swath 65, range 71.5m. B – shows the intensity plot at 0o beam angle, swath 75, range70.5 m. B – shows the intensity plot at 0o beam angle, swath 87, range 71.8m. Note the distinct side lobes appearing in the intensity plots A and C.

4. Methodology

4.1 Algorithm design and constraints

For the purpose of positioning something in the water column, the first objective will be to detect it. To do that one needs to know its actual dimension and scattering properties and how that compares to the sonar range and angle resolution and background noise level. It should be an easy task to look for large objects that are big with respect to the beam and pulse dimensions. But trying to find objects small with respect to beam dimensions and pulse, whose target strength differs little from natural scatterers is a complex and difficult task. In order to distinguish valuable detections from regular water column noise one needs to be aware of the water column characteristics, the sonar characteristics, its specific water column imaging geometry, and what a valuable detection is, separating it from the noise.

While the target shape and the contrast between target and water physical properties control the target strength, as explained in Chapter 2, MBES aspects determine how that strength will be described in range and angle space. Transmitter beam width, receiver beam width, side lobe characteristics, pulse length (or equivalent bandwidth), transmitter and receiver steering angles, sectors and sector boundaries, minimum slant range, slant range itself and vessel speed are all attributes that define a unique water column imaging geometry (Figure 4.1) and to correctly interpret the water column image they have to be known.
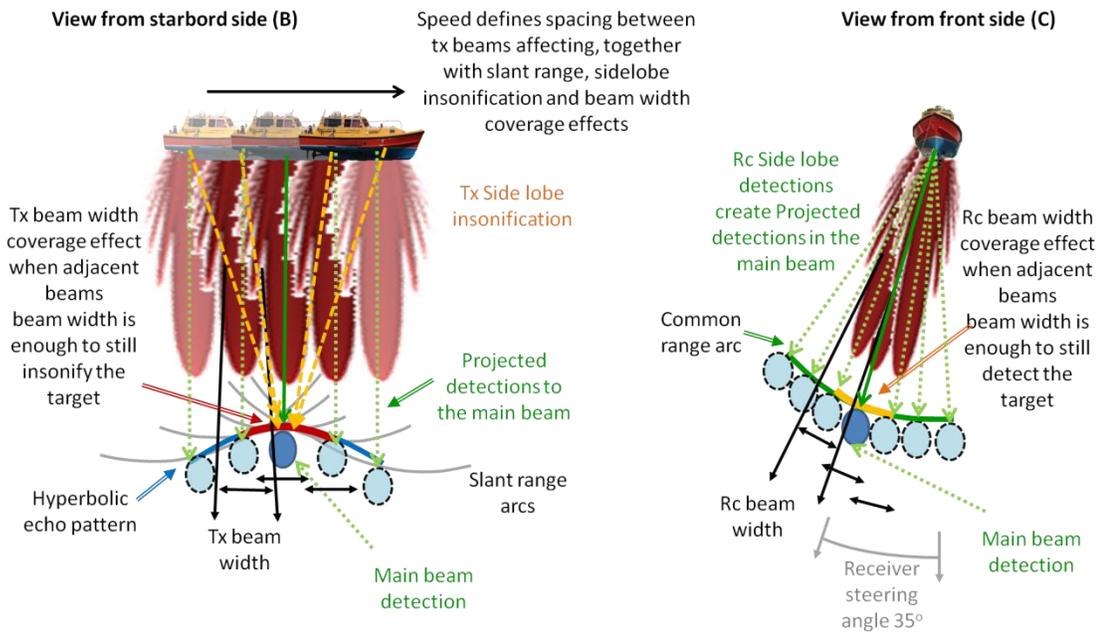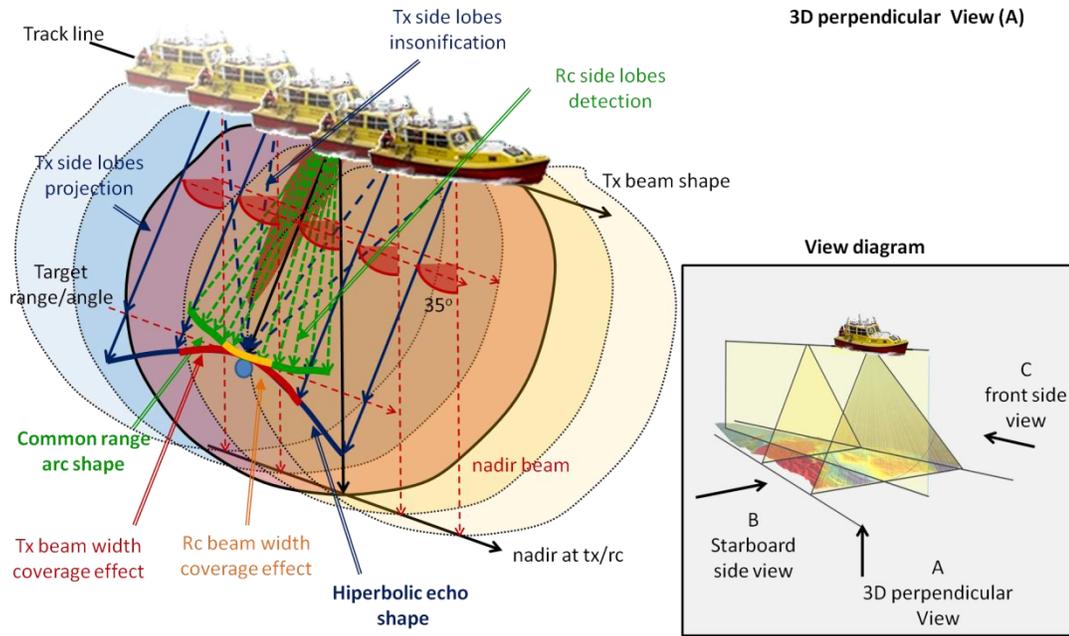
3D perpendicular View (A)

Track line

Tx side lobes insonification

Rc side lobes detection

Tx side lobes projection

Tx beam shape

View diagram

Target range/angle

35°

C front side view

Common range arc shape

nadir beam

B Starboard side view

A 3D perpendicular View

Tx beam width coverage effect

Rc beam width coverage effect

nadir at tx/rc

Hiperbolic echo shape

View from starbord side (B)

Speed defines spacing between tx beams affecting, together with slant range, sidelobe insonification and beam width coverage effects

View from front side (C)

Tx Side lobe insonification

Rc Side lobe detections create Projected detections in the main beam

Tx beam width coverage effect when adjacent beams beam width is enough to still insonify the target

Rc beam width coverage effect when adjacent beams beam width is enough to still detect the target

Projected detections to the main beam

Common range arc

Hyperbolic echo pattern

Slant range arcs

Tx beam width

Rc beam width

Main beam detection

Receiver steering angle 35°

Main beam detection

Figure 4.1 - Water column detection sketch

Illustrating all the components of the sonar imaging geometry that contribute to the scattering pattern observed.

75

There are 2 main points to notice before even trying to do any detection. First of all is that with the use of yaw stabilization, correlating detections across sector boundaries seems impracticable as the sectors simply may not match at the boundaries (Figure 4.2). Another insuperable task seems to be to detect something after the minimum slant range, as the side lobes contamination from the sea floor seems to mask everything in the water column after it (Figure 2.13).
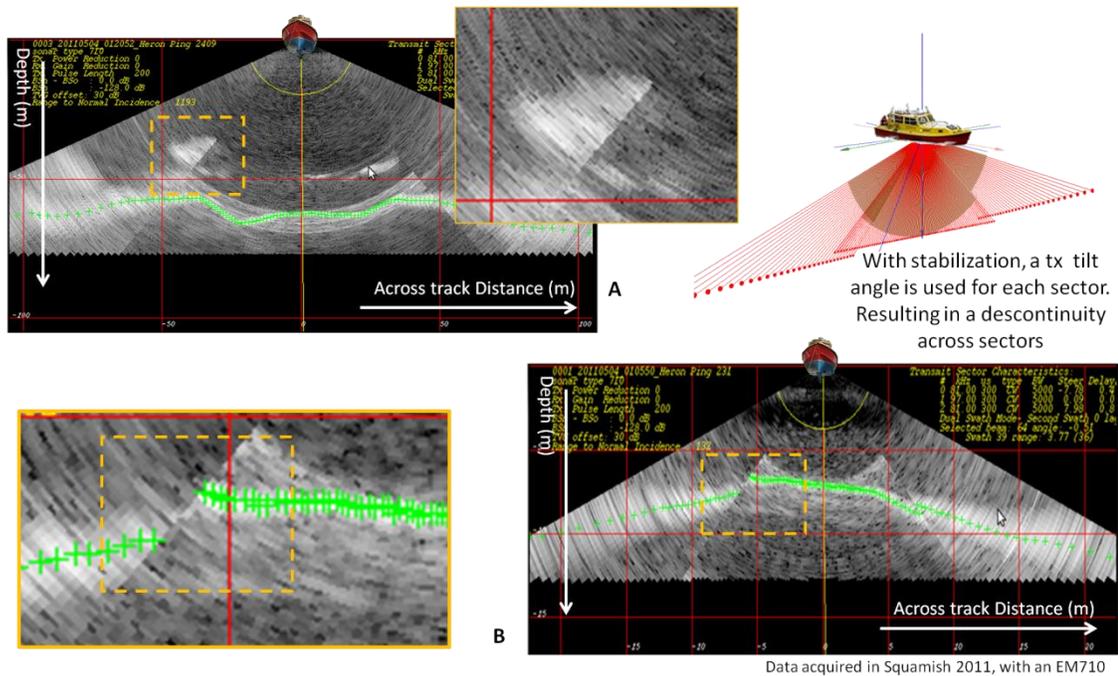

Figure 4.2 – Discontinuities at sector boundaries in the water column image

A – In the zoomed window, note the school of fish on sector 0 (left) does not appear on sector (1) right. B – Note that across sectors the sea floor (in green) seems to have a step, it is not continuous, consequently there is also no continuity in the water column data across sectors.

76

The first approach to the detection problem was to calculate the potential 3D water column scattering pattern shape of a target at each sampled point in 3D space and then, by running this pattern as a match filter through the all water column, search for potential targets at those products. Taking advantage of the fact that the highest echo should be at the target location, rather than run the match filter over every location, the filter was only applied to all intensity peaks. This saves significant processing time.

4.2 Development overview

The method that is herein defined (Figure 4.3) tries to use as much information as possible and automatically do the detection. Using the knowledge from the previous chapters an algorithm was designed and implemented. The algorithm target detection is done in 3 separate parts:

1. An initial local intensity maximum detection process (looking for the highest intensity peaks),
2. checking whether the fall-off intensity about the peak point matches the expected water column point target scattering field
3. a target geometric match filter process (checking if the detections spacing correspond to the desired targets).

This method allows the user to define most of the needed parameters for each step, even allowing improbable values as long as they are within acceptable values. This will be explained later. Even though the user can override default parameters the algorithm still calculates everything automatically by default if no parameters are defined.

The detection process (1 and 2) was deliberately separated from the target shape match filter (3), so that, if desired the algorithm can act simply as an object detection algorithm. In the detection process it will mark all the intensity peaks found above a specific threshold, using the MBES system characteristics (using a beam pattern match filter). If desired, the target match filter process is then used on all the detections, and those that match the requested target geometry are marked as targets. Also if desired, all the detections except those that match the targets are eliminated and a list of the targets is created with the position, depth and ID for each target. This algorithm searches through as many sectors as asked, with the search being always independent, using each sector separately. Dual swath is also considered, and detections are done separately for each swath. Finally the size of the water column data slots (water column loaded into memory at one time) is also customizable, so that the algorithm can be adjusted according to the computer being used and its speed maximized.
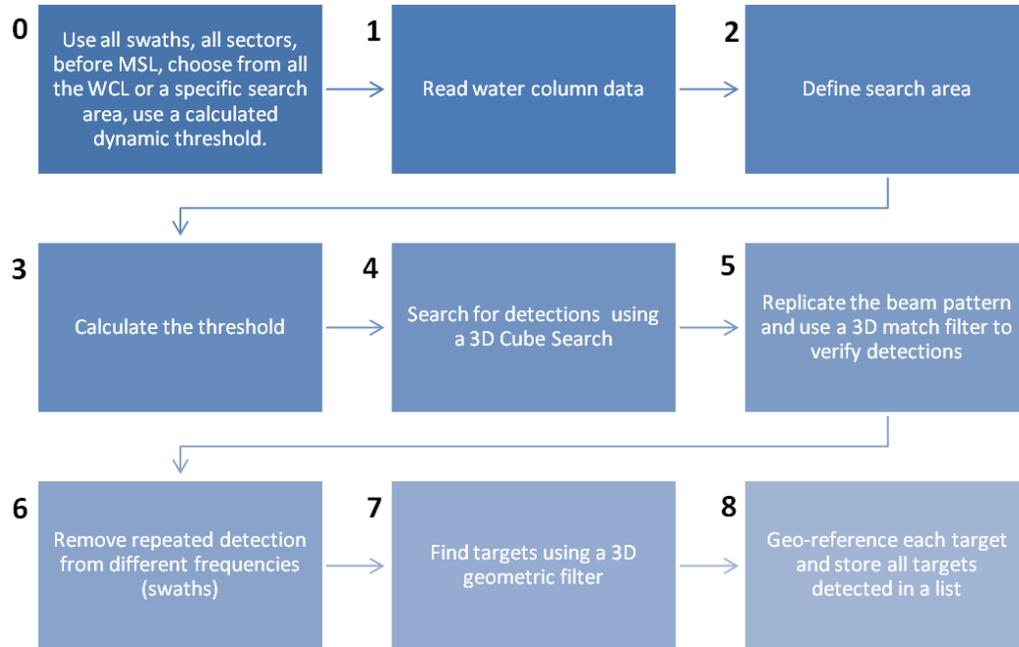
| 0 | Use all swaths, all sectors, before MSL, choose from all the WCL or a specific search area, use a calculated dynamic threshold. | 1 | Read water column data | 2 | Define search area |

| 3 | Calculate the threshold | 4 | Search for detections using a 3D Cube Search | 5 | Replicate the beam pattern and use a 3D match filter to verify detections |

| 6 | Remove repeated detection from different frequencies (swaths) | 7 | Find targets using a 3D geometric filter | 8 | Geo-reference each target and store all targets detected in a list |

Figure 4.3 - Final algorithm workflow

The algorithm can be separated in 9 parts, (Table 4.1) 5 of which take an important part in the object detection and target identification process (steps 3 to 7). The algorithm starts by reading the water column data (step 1), then defines the search area according to the needs and available data (step 2). It then uses an automatic threshold calculation (step 3) after which it starts searching for detections. This search is done using a 3D cubic search (step 4) to isolate credible detections. At this point only a peak detection (Local intensity Maxima – LIM) is done, irrespective of any intensity variations around the peak detection. Then a 3D match filter is used (step 5), using a specific detection pattern. This is where the intensity along, across and through the detection (around the peak) is examined. And finally any repeated detections (from dual swath) are removed (step 6). Once all valuable detections were found a last filter (step 7) is run through all detections

using another 3D filter to uniquely detect user-specified target geometries. Finally the targets are geo-referenced (step 8) and a list of targets is created and stored (step 9).

The algorithm that is explained next was implemented in the OMG software as it is shown in appendix A.

	Algorithm step designation	New Code ?	Needs User Parameters	Optional	User Configurable Parameters
1	Read water column data	Code + OMG code			
2	Define search area	Code			X
3	Calculate intensity threshold	Code			X
4	Search for detections (3D cube search box)	Code			X
5	Check beam pattern (3D pattern match filter)	Code		X	
6	Check different frequencies (dual swath)	Code		X	
7	Lock on desired targets	Code	X	X	X
8	Geo-reference targets/detections	OMG code			
9	Store results	Code + OMG code			

Table 4.1 - Algorithm summary

The design of the filter is based on a 3 dimensional coordinate system defined in 3 axes. Those include:

- swaths, from the beginning of the survey line to the end, representing each ping of data (1 or 2 swaths).

- beams representing each physical sound beam (at a different angle) created by the multibeam transducer.

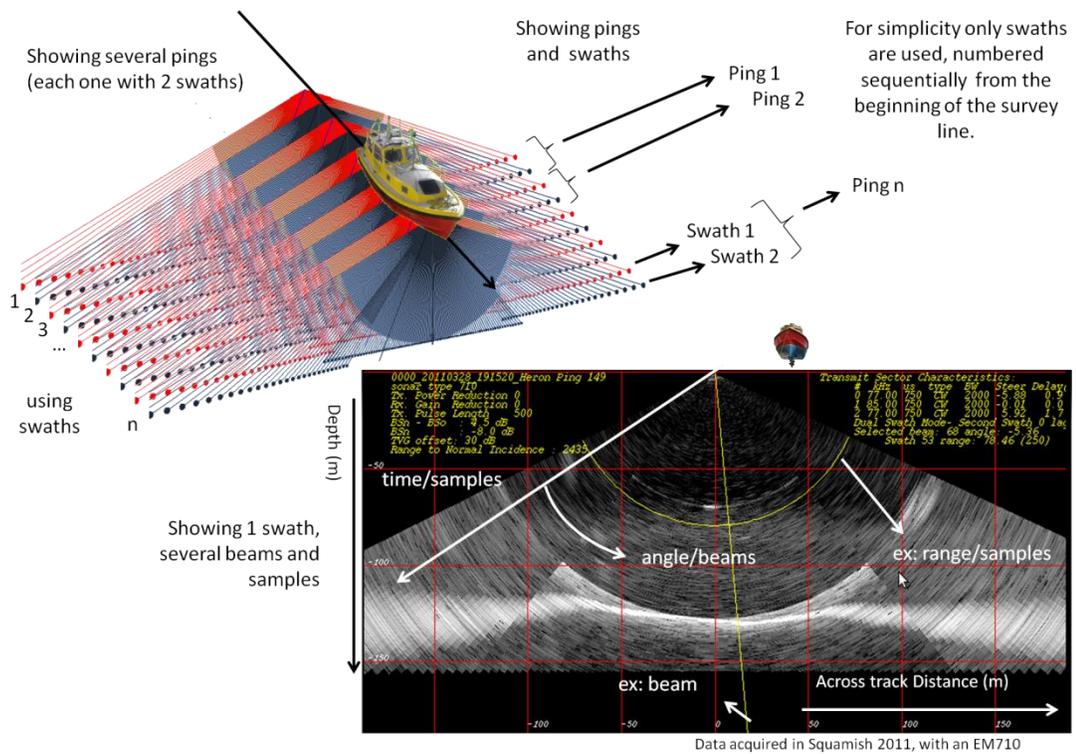- samples (time), representing a sampled range of backscattered intensity measurement along the beam (Figure 4.4).

Figure 4.4 - Water column image explaining beams, samples and swaths

4.2.1 Reading data

Initially the algorithm starts by reading all the user defined variables. In the process call phase, the user can define several boundaries to the way the algorithm works (as can be seen in Appendix A). This method tries to be as automatic as possible, so that the only values that need to be defined by the user are which survey lines or survey area is to be checked, and the expected target's geometry.

The initiation process would obviously need to be to read the data. The algorithm was initially designed to work on Kongsberg Systems so the designed process reads the data from Kongsberg datagrams converted into OMG format and stores it in a specific structure that allows posterior access to survey line water column data and all other survey line data in a quicker access method. Using sonar system water column imaging characteristics, all water column data is stored in a format similar to an image format, so that the following processes can work on it as an image (Figure 4.5).
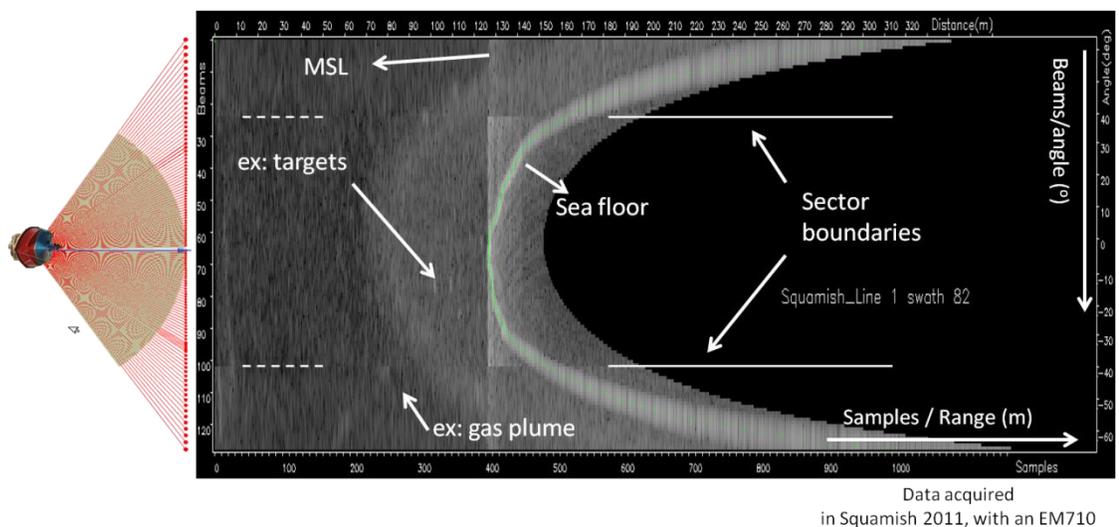
Figure 4.5 - Water column time-angle image, swath 82 line 0001 Mar 28th 2011

As an example, Figure 4.5 shows a time-angle plot of a swath, showing exactly the water column 2D image of a swath that is used to work on the following steps. This image shows the internally utilized perspective of the multibeam system, showing the data as it is acquired in time and receiver elevation angle. All artifacts, and multibeam distortions are present in this type of image, but it uses time and angle axes. While doing calculations it is easier to work on time angle plots (2 of the 3 coordinates of the search), and all the algorithm works on this type of image. Although the time/angle image (Figure 4.5) gives a more comprehensive view of the water column, the reference is time and angle, making it harder to be understood by a human being. Having this in consideration, all water column swath images presented are shown on polar plot images, ex: Figure 4.6, which shows exactly the same data, but the reference is now depth and across track distance, meters on both axis.
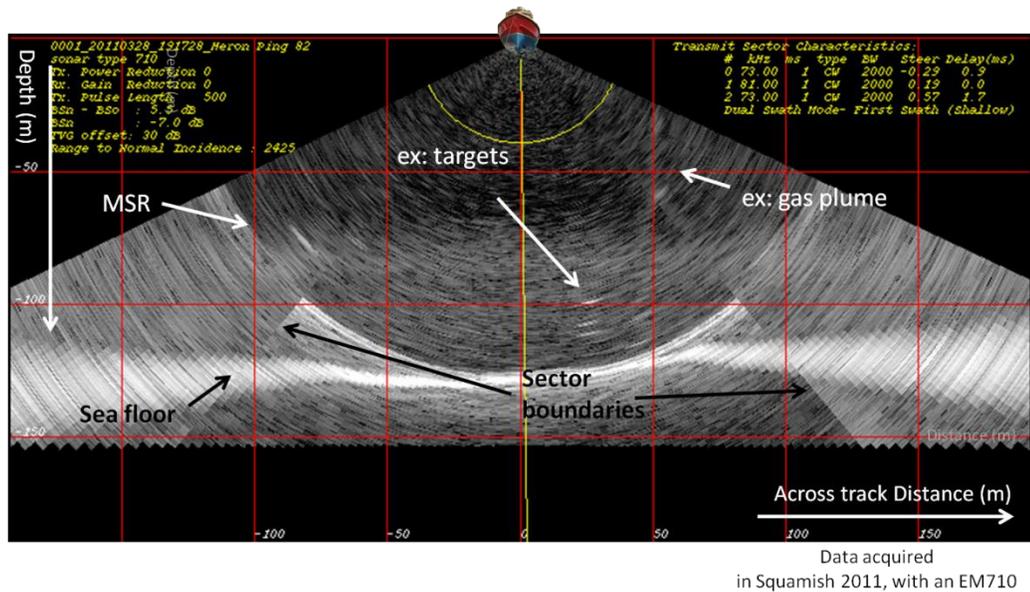
Figure 4.6 - Water column polar plot image, swath 82 line 0001 Mar 28th 2011

Same data as Figure 4.5

The algorithm identifies the survey lines to be analyzed, either by user input specifically or by calculation using a square area of input geographic coordinates. Then it uses a water column slot size, default or user defined, to speed up the analysis process and to deal with available memory on the user's computer. The algorithm analyzes each line separately. And instead of reading the whole line of water column data, it reads the line in slots as depicted in Figure 4.7. In order not to lose any data, each slot starts a specific amount of swaths before the last slot ended. The amount of swaths to go backwards on the survey line, depends on the size, in swaths, of the cube box (explained in Section 4.2.4) used to search for detections. If this size is calculated automatically, which should always be the case (unless for specific testing purposes), this size is dependent on the transmitter beam width, vessel speed and ping rate.

Also, the target's list file needs to be created. This list is shared with other OMG tools, and is actually created by other OMG subroutines (Beaudoin, J., unpublished 2011). If this list file exists it just needs to be read as some targets may have been identified already. This process reads the file, identifying all previous targets, making sure they are not repeated in the detection identification process. In the end all identified targets will be added to this targets file.
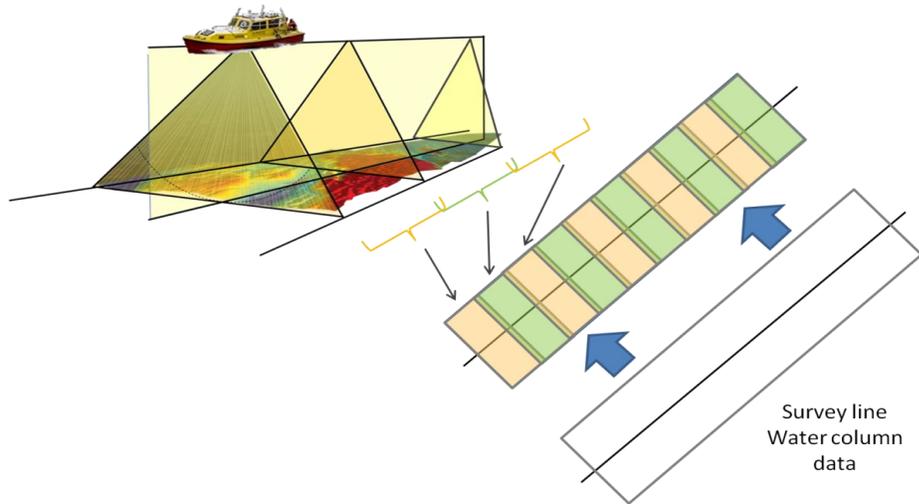
Figure 4.7 – Water column survey line split in slots

Water column data is split up in equal parts, overlap by the 3D cube size in swaths and each one analyzed at a turn. What actually happens is that the program uses a buffer, loads m swaths of data into it, analyses this data and stores the results. Then cleans the buffer, shifts back n swaths in the data, loads another m swaths of data into the buffer …
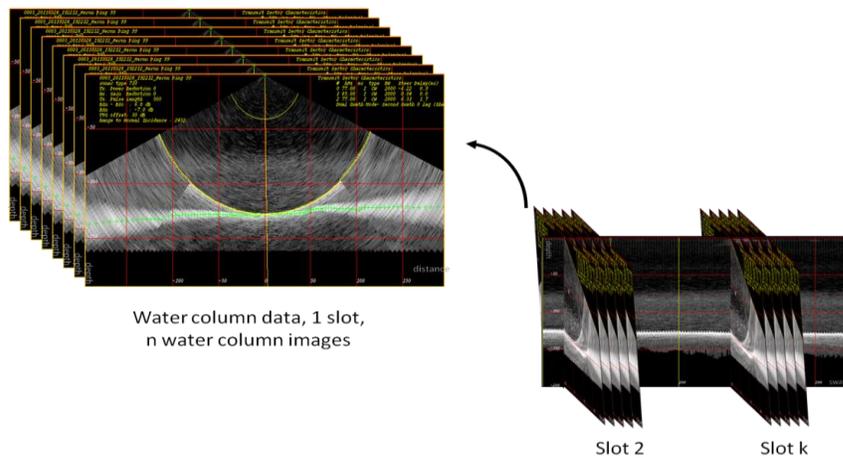
And keeps working until the end of the line.

Figure 4.8 – One slot of water column images.

The algorithm selects one slot of water column data, and uses each swath as an image, executing the target search on it. Once it is finished, another slot is analyzed, until the end.

4.2.2   Defining the Search Area

After having read all user defined variables and transforming the water column data into water column time/angle images, the algorithm defines the search area. This search area is defined in beams, samples and swaths. If there is no special input from the user, the algorithm tries to read all the water column data. It reads all swaths available in the slot of water column data. Then it starts by trying to find how many sectors are being used in the available slot of data and selects each one to be used. Within each sector from each swath, and still within the available slot of data, it checks for the minimum and maximum beams. Finally it checks what the minimum slant range (MSR) is and selects the corresponding sample number, limiting the search area to before that sample.

The later was the automatic default process, but the user can decide which area needs to be checked. Actually the area can be limited using sector numbers (Figure 4.9), minimum and/or maximum samples (Figure 4.10), minimum and/or maximum beams (Figure 4.11), minimum and/or maximum swaths (Figure 4.12), all together or a combination of any of these options (Figure 4.13, Figure 4.14,) . As samples and beams are somehow an unusual unit for humans to work with, the algorithm also allows the user to define a minimum and/or maximum range and angle. Having some or all of this optional variables defined, the algorithm limits the search area accordingly taking into account all the multibeam system boundaries. The user is never allowed to search outside usable data. Although several sectors can be used, because of sector boundary problems the search is always done on each sector separately. Both these problems can probably be solved with more research on these subjects.
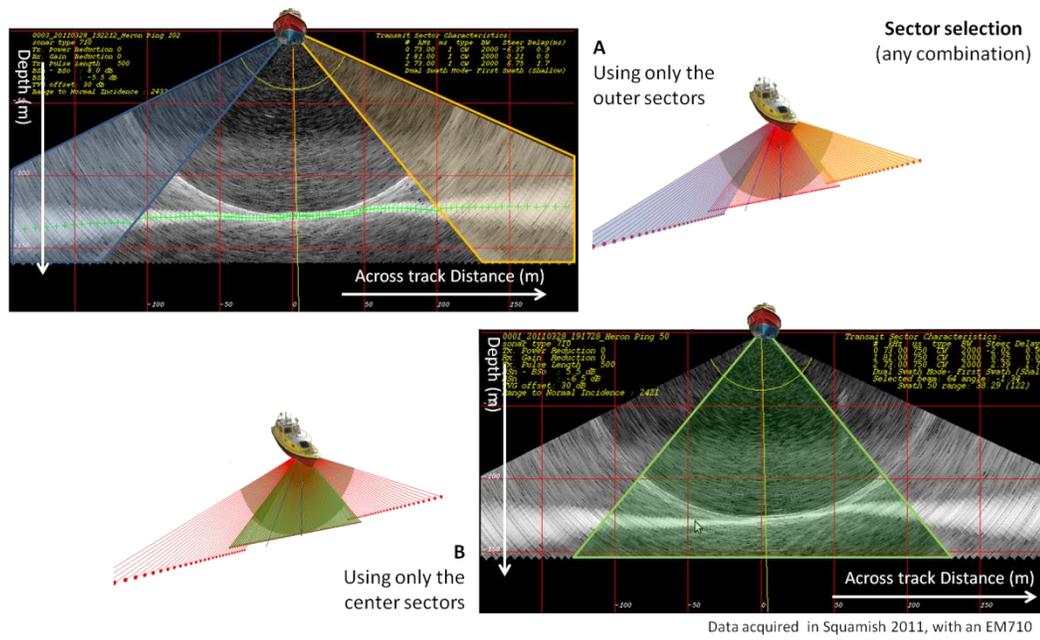
86

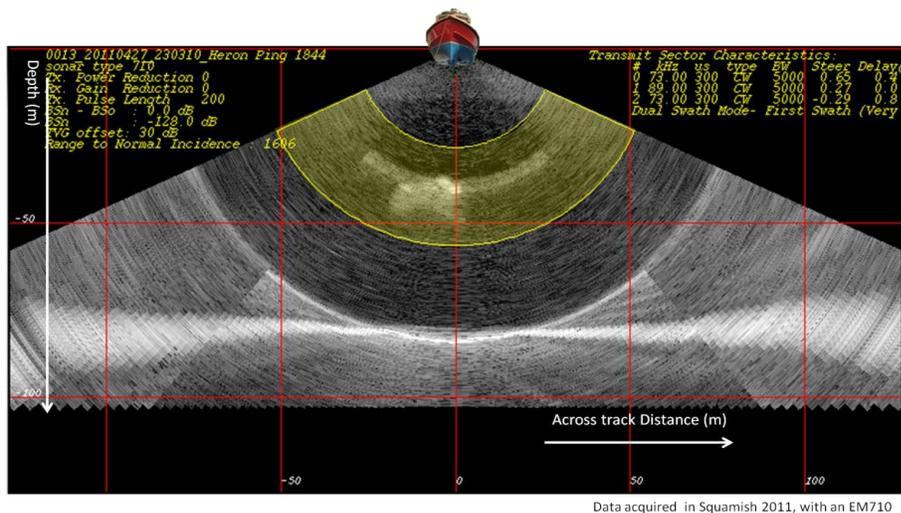**Figure 4.9 – Searching area using sectors. The user can decide in which sectors to search.**

Figure 4.10 - Searching area defining minimum and/or maximum samples/range.

Data is presented in samples and all the calculations are done using samples. The algorithm allows the specification of range (in m), automatically converting to samples according to the sample rate.
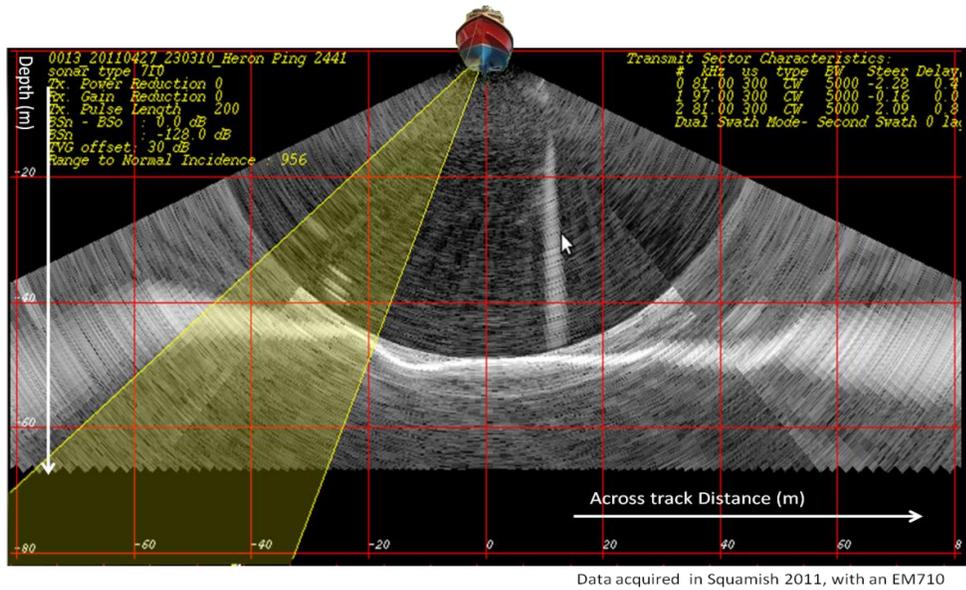
Data acquired in Squamish 2011, with an EM710

Figure 4.11 - Search area using minimum and maximum beams or equivalently elevation angle.

Data acquired in Squamish 2011, with an EM710
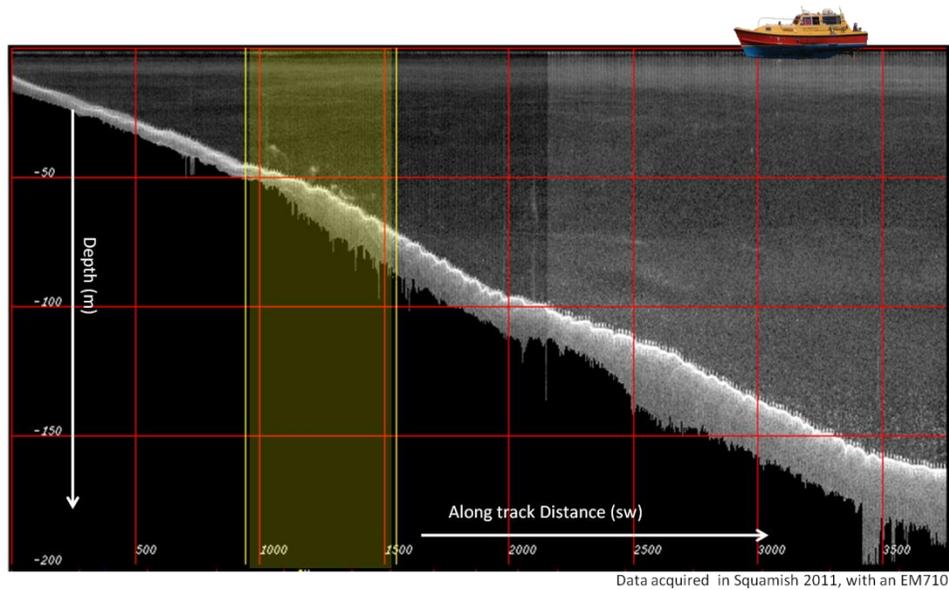
Figure 4.12 - Search area using a minimum and maximum swath.

This allows the user to search only in a part of the survey line.
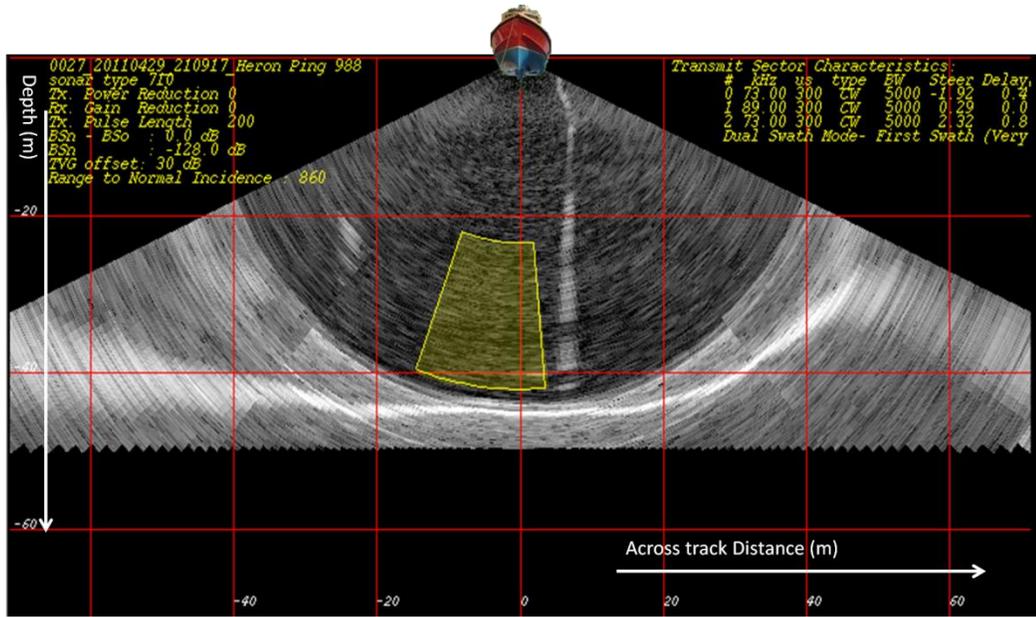
Data acquired in Squamish 2011, with an EM710

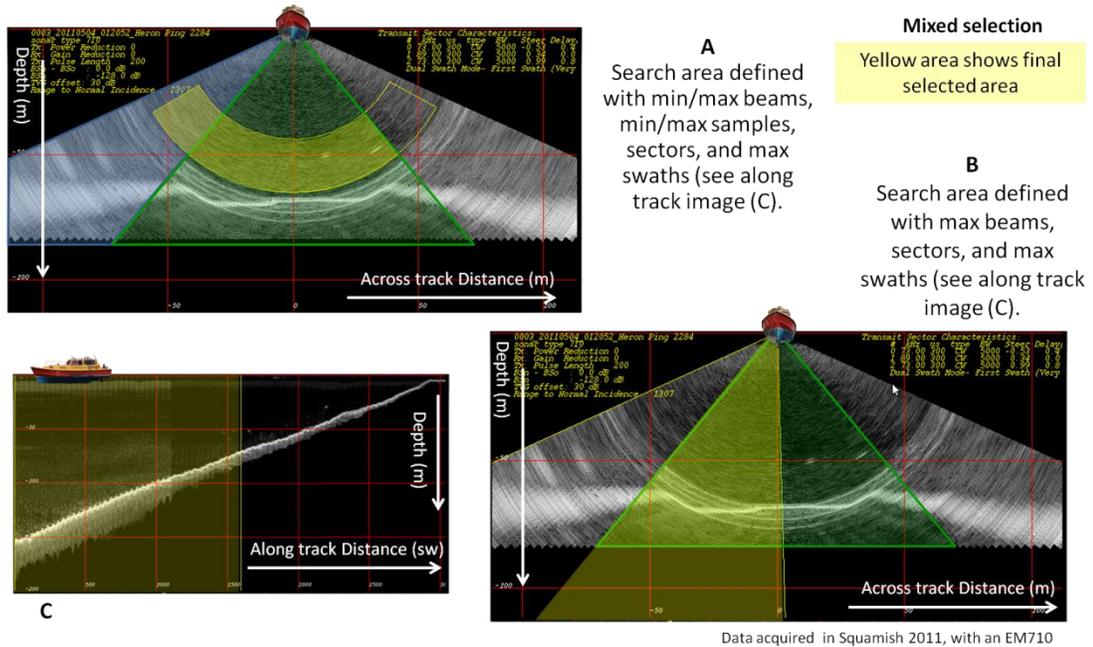**Figure 4.13 - Search area (combination of samples/beams)**

A
Search area defined
with min/max beams,
min/max samples,
sectors, and max
swaths (see along
track image (C).

Mixed selection
Yellow area shows final
selected area

B
Search area defined
with max beams,
sectors, and max
swaths (see along track
image (C).

Data acquired in Squamish 2011, with an EM710

Figure 4.14 - Search area (combination of sectors/samples)

Note that all search areas intercept and define a new custom area. Sectors can intercept with range

(A) and beams (A) (B) and swaths (C).

89

A successful algorithm implementation requires data before and after the point of investigation on all 3 axes. This causes the algorithm to avoid the search in intensity samples that lie ½ the cube size in samples, swaths or beams (step 3) from the sector and survey line boundaries, or whenever data is not available (ex: reduced swath width along consecutive swaths).

A final note needs to be pointed out in this section. This search area is defined only to search inside the selected files (survey lines). The geographical square box that allows the user to define an area to look for survey lines was used in the previous step (Section 4.2.1) and deals exclusively with survey lines. If any data of a survey line is inside the defined geographical box, the line will be selected (step 1) and unless any limitations are imposed in this step (step 2) the whole line will be read. To search only in a specific geographical area of the survey line, the algorithm only provides the swath selection method. Figure 4.15 distinguishes these two concepts.
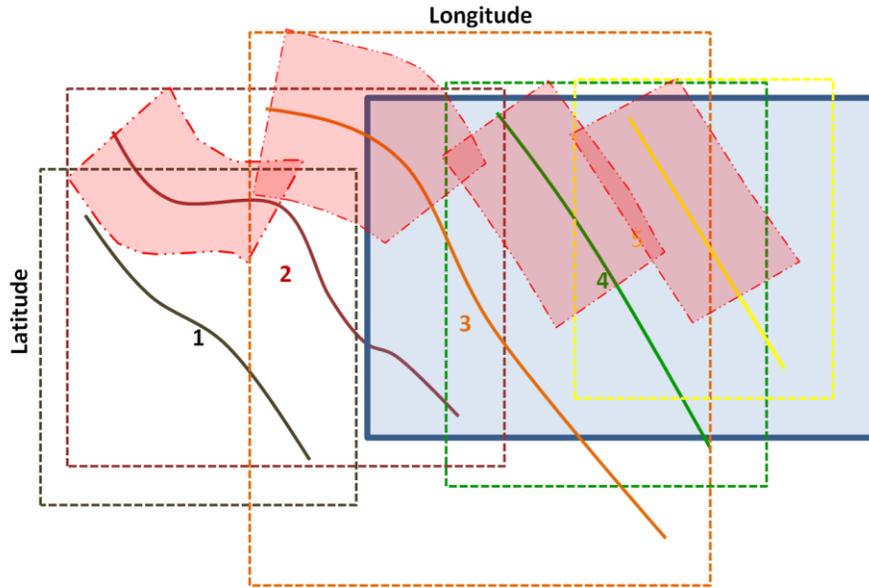
Figure 4.15 - Geographical area vs search area

Dotted boxes define each survey line geographical area. Having selected all available lines and defined the blue box as a geographical area to execute the search, the algorithm will select all lines except line 1, that is the only one which geographical area does not intercept the geographical box defined by the user. As an example, also defining swaths 0 to 100 would execute the search in the highlighted red areas only. These areas are already defined in the OMG code, using min/max Latitude/Longitude used in the line.

4.2.3   Calculating the intensity threshold (step 3)

After importing the data available to be used, and having the search area limits defined in 3 dimensions (swaths, beams and samples), there is still one dimension where some boundaries can be imposed, the intensity dimension. The water column image carries a large amount of data with logarithmic scattering intensity values stored for each sample distance at each beam in each swath typically ranging from -94dB(minimum possible) to -10dB (typical backscatter seafloor echo). These scattering values can imply

several different detections in the water column. Also, as the water column is populated with biological life, and other components that may reflect sound, the water column image is usually abundant in low but still significant intensity values (Figure 4.16). In Squamish large clouds of zooplankton, assumed to be euphausia (Everson, I. 2000, Robertis,A. 2002) were found. Zooplankton, like krill, will be represented in the water column image with higher intensity values than regular salt water, being detected usually as layers or clouds (Figure 4.18). Typical target strength for krill like animals are within -105 to -65dB range for 70kHz, the frequency at which krill has higher backscatter strength (Conti, S. et al. 2005, Calise, L. and Knutsen, T., 2011, Figure 4.18). This effect of detecting zooplankton creates in Squamish a deep scattering layer (DSL) (Figure 4.16). Small algae will also have a similar effect on intensity values, probably with different values, and several other examples can be found for this effect. All these typical but undesired water column reflections are considered noise for the purpose of this research. Another example are gas plumes. A significant natural scattering target in the water column at Squamish was found to be columns of rising gas (Figure 4.16). This gas plumes have a typical backscatter strength within -40 to -35dB range (Table 2.1) and can sometimes be detected with configurations similar to the targets.
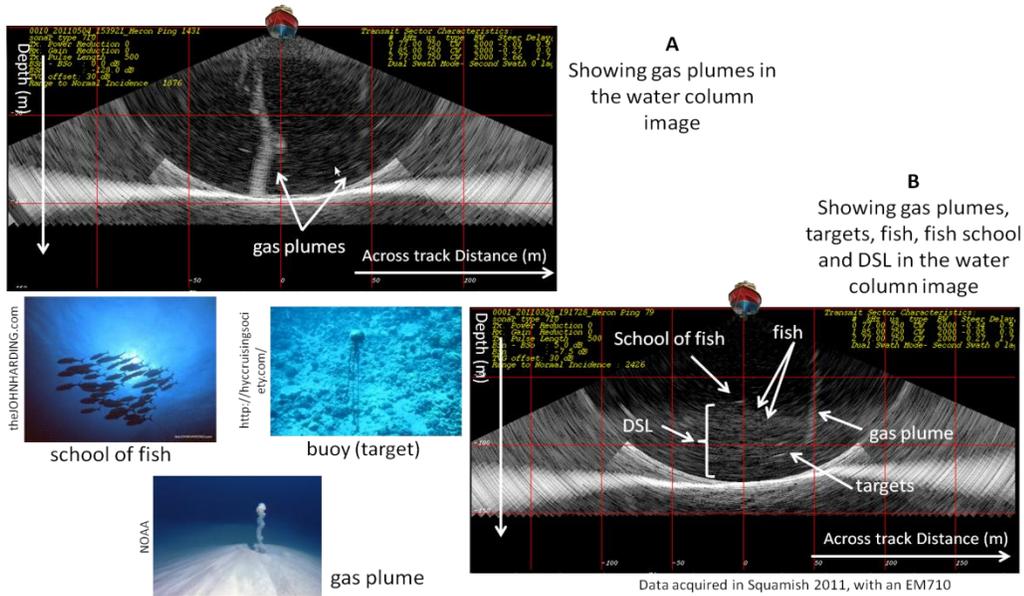
Figure 4.16 - A water column image showing typical noise intensity values

In Squamish, using a 70 to 100 kHz system. A shows gas plumes. B shows other possible objects seen in the WCL including a DSL. For reference some photos show examples of how those objects may look.
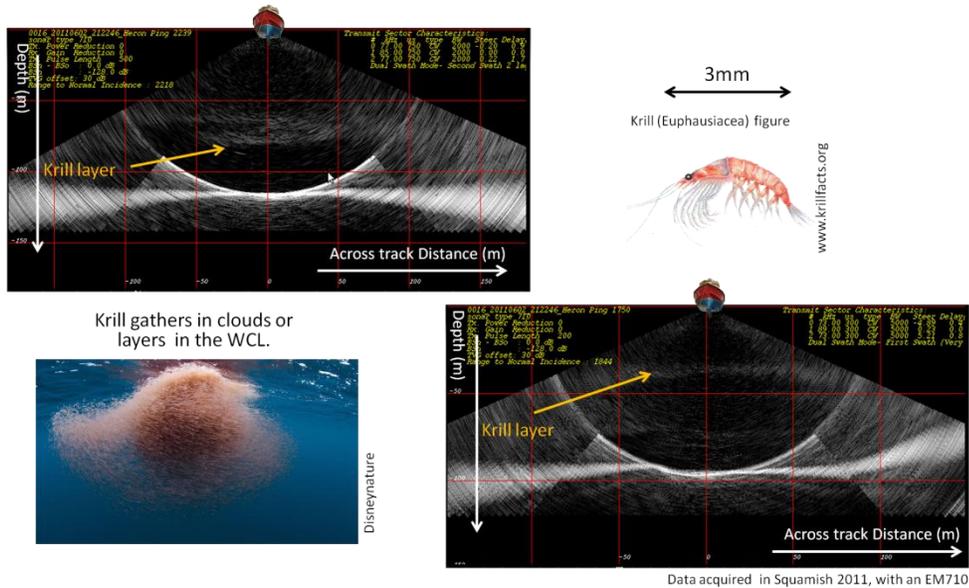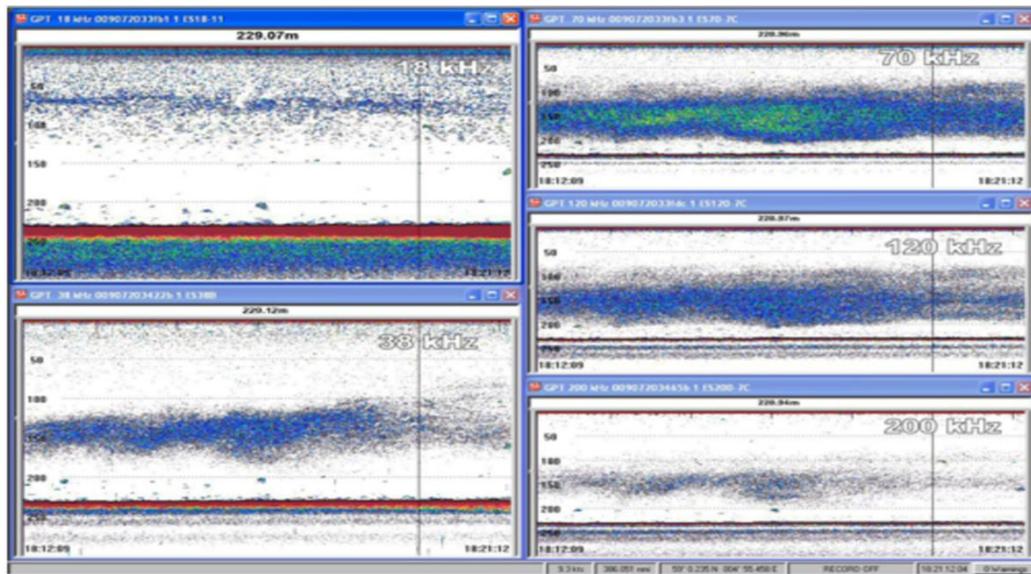

Figure 4.17 - Image showing assumed krill detection near the river delta

93

Figure 4.18 - A layer of krill being detected using a Kongsberg EK60 system (SIMRAD, 2006 a). The images at the left show the same krill cloud/layer being detected at different frequencies using an EK60 scientific echo sounder system, from Simrad. It is notable that it reflects differently at each of the tested frequencies, having its best reflection at 70 kHz a frequency used by EM710.

Obviously, larger animals, like fish (Figure 4.19) plants or other objects are also detected and the intensity values in the water column image will indicate that. Those detections however may have a comparable or higher scattering intensity value than the objects we are looking for, making them a possible false target. The example of a fish school can be used to show this, comparing an image where both a fish school (Figure 4.19) and the targets were detected (Figure 4.20). Note that the side lobes along, and across track (hyperbolic echo and common range arc) are easily seen in the fish school (Figure 4.19), even though they are not clear in the intensity plot. The targets (Figure 4.20) are detected with lower intensity values and the side lobe effect seems to be mixed with noise. Apart from that both cases are very similar and may need to be distinguished.

94

A table with backscatter strength and typical dimensions of these more common detections found in the water column is presented in Table 2.1. In Squamish all operation occurred during day time, and a deep layer of krill (deep scattering layer - DSL) is usually seen in the water column (Figure 4.16). The presence of the DSL produces a need to define a lower intensity boundary, threshold, in order to improve the algorithm speed and effectiveness. Note that the result could still be the same, but without the use of a threshold, the algorithm would have to work with more data, and probably would find more spurious detections (intensity peaks), increasing the chances of classifying them as targets.
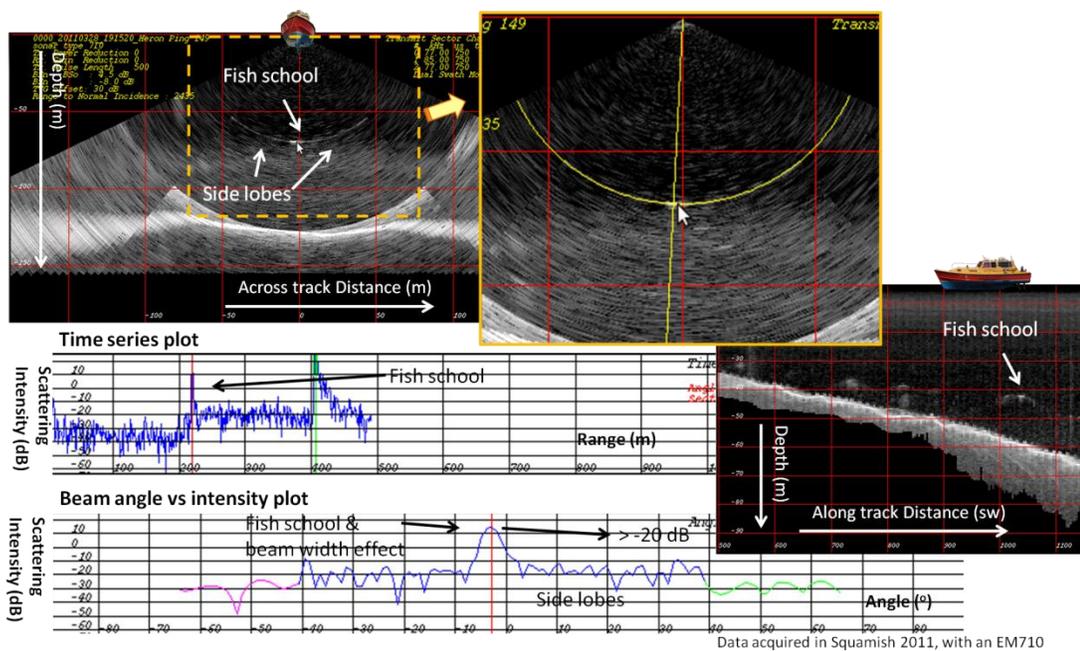
Figure 4.19 - Water column image showing a fish school being detected

(Note that values need -30dB offset applied)
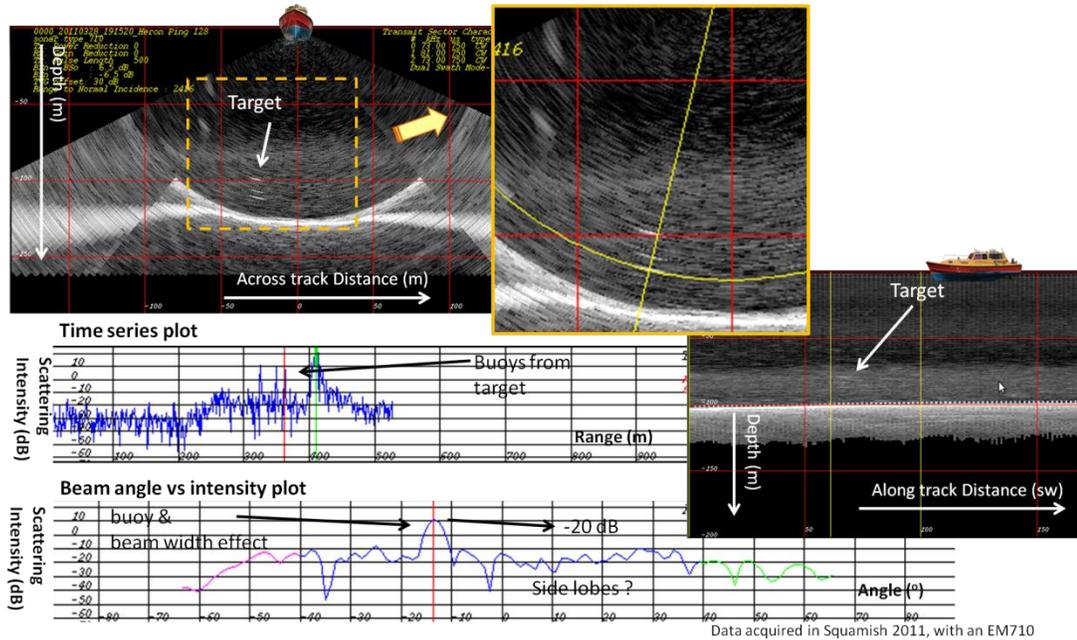
Figure 4.20 - Water column images showing a target, with intensity plots

(Note that values need -30dB offset applied)

As a first iteration a single, minimum intensity threshold based on the whole average scattering strength of swath water column from surface to MSR was calculated, rejecting all water column data that had an intensity value below that threshold. This initial method was later discontinued as it revealed to be inadequate to deal with clearly horizontal layers of water column data with a large range of noise values, like the DSL example (Figure 4.21). Nevertheless, this is still a good method if the specific scattering intensity values of the targets are known to be well above average background levels. And it could even work better when used together with a top intensity boundary, excluding echoes known to have higher intensity than the desired targets, like several fish schools (Table 2.1).

96
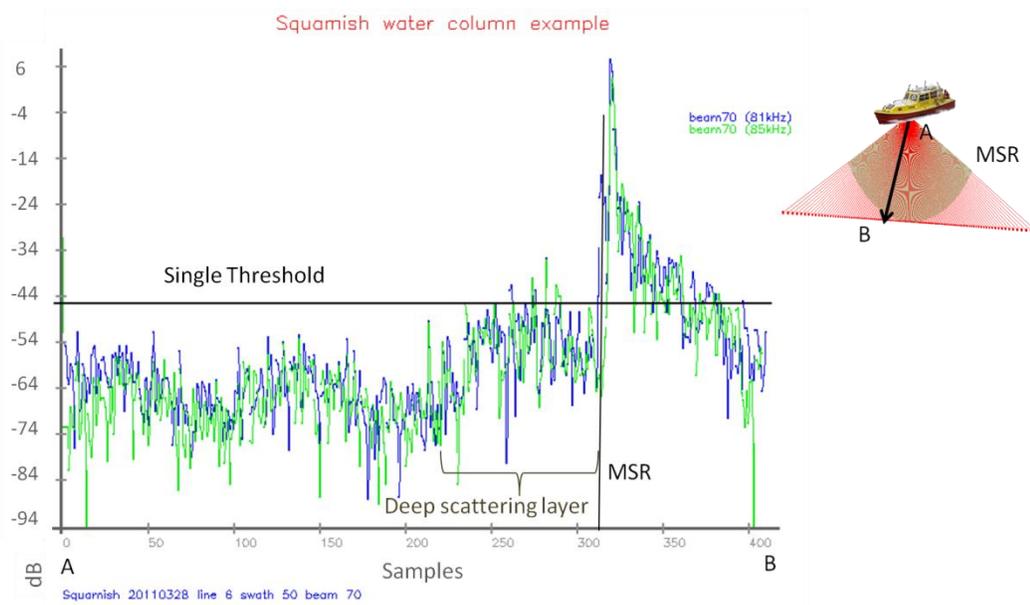
Figure 4.21 – Time series of a single (near nadir) receiver channel showing the single threshold. Note the DSL intensity level increasing and going over the threshold, even though there are no objects being detected.

Building on the previous method to calculate the threshold, a new method was developed to make the threshold follow depth variations in the noise data trend. Assuming most natural changes in the water column occur vertically, this new method divides the water column into horizontal depth layers (the size of this layers can be user defined), then analyzing the whole water column of data in the swaths that lay inside the volume under investigation, reads all the intensities along each beam, in each swath, and calculates the average peak, and average trough values for each depth layer (Figure 4.22). Then calculates the difference between them, and adding a percentage of that difference to the average peak value it creates a water column depth layered threshold. Depth layers are calculated reflecting the range resolution being used, so that each layer at the nadir would carry approximately 10 intensity samples. This value '10', used to obtain the size

97

of the depth layers was tested for the 3 systems used (EM710, EM302, EM2040) and revealed to be the most reliable, and it guarantees a significant amount of samples in each layer (>2000). Smaller values increase the sensitivity of the threshold to any strong noise spikes, and larger values make the threshold lose its sensitivity to large echoes as their intensity is averaged with the remaining data. The threshold now follows data intensity noise bias, creating a more accurate 'cut' on the water column noise (Figure 4.23). This method was found to be considerably better than the single threshold when working with unknown data characteristics. If the reflectivity value of the targets is unknown, or if the user just wants to use the default values, the performance increases substantially using a layered threshold. The fact that the threshold is calculated through several swaths (3D cube size in swaths - step 3 – Section 4.2.4) should help to average out strong local echoes like gas plumes and fish schools. Averaging through a larger number of echoes could average out changes in larger environment echoes like the example of the survey line crossing an area where the krill layer changes its vertical position.

The depth varying method is now the default process to calculate the threshold. But, as both methods have advantages and disadvantages, the user can still define the threshold using either, a single value or a layered one. Defining a single value is useful if the user wants to search above a specific intensity value. Defining a layered threshold, allows the user to adjust the threshold as desired so that weaker targets can be detected or stronger noise can be excluded.

The algorithm accepts a multiplier value to use on the value added (the peaks-troughs difference) to the average peaks when creating the layered threshold. By default this value is 1, lower values will approach the threshold to the noise data, and higher

values will distance the threshold from noise. Note that this optional multiplier only shifts the threshold up and down (Figure 4.24 A) so that the user can adjust the threshold calculation, and bias approximation, for 'cleaner' or 'noisier' data.
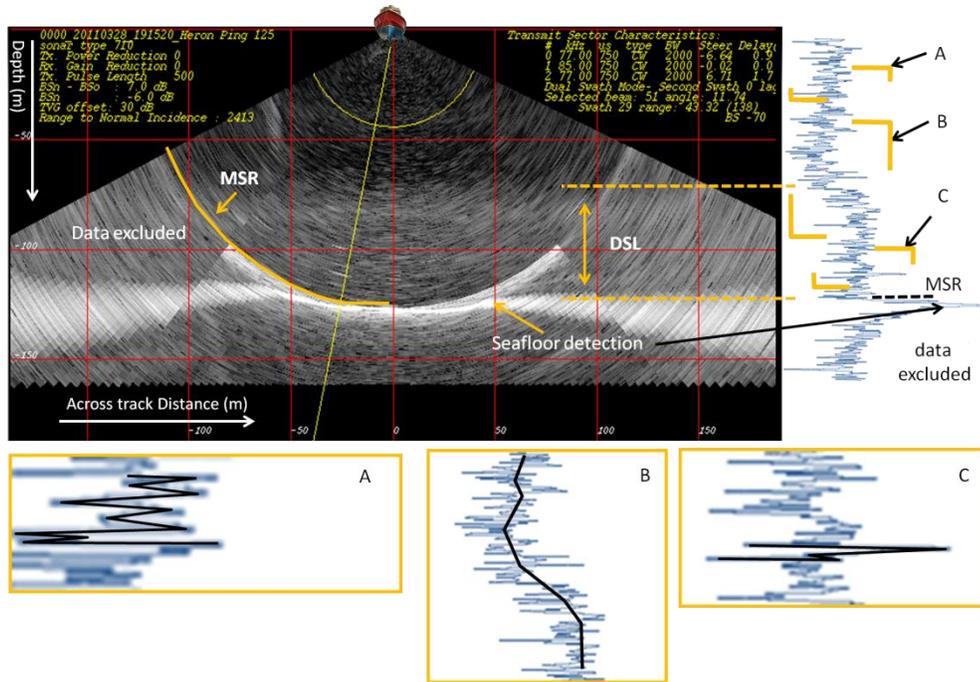

Figure 4.22 – Dynamic threshold layer size definition shown in one beam intensity plot

As the intensities along depth reflect variations in the water column, the algorithm needs to calculate a threshold that follows those variations (macro scale - B), ignoring small variations (micro scale - A), without excluding intensity peaks produced by objects in the water column (C)
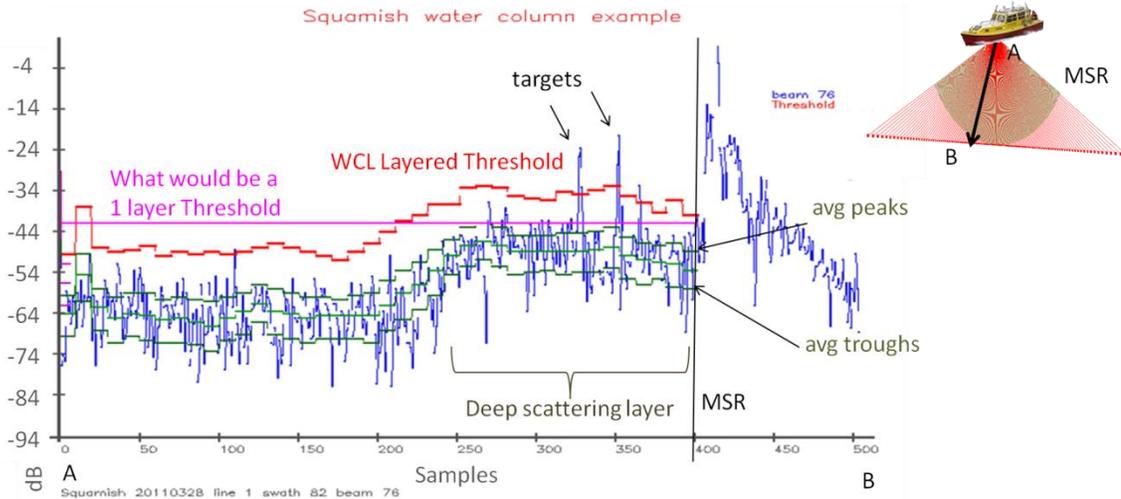
Figure 4.23 – Along beam intensity time series plot showing layered threshold.

Note that the layered threshold follows the DSL intensity level rise and does not disturb object detection. The layered threshold offset to the data may be changed by the user. This threshold is calculated once per swath, using the swaths that fall inside the cube area.

Finally, the user can also define the pulse length multiplier that defines the depth layers. This will modify the threshold shape with depth. Larger layers approach the single threshold effect, not following the data trend. Smaller layers have less intensity values contributing to the calculations, capturing smaller oscillations in intensity values (shorter noise wavelengths) (Figure 4.24 B). Knowing this fact, the default layer size was defined using a multiple (default 10x) of the range resolution, trying to keep the number of intensity values contributing to the calculations reasonable.

Figure 4.24 – Time series intensity plots showing 4 different size for depth layer threshold

All plots show the intensity of beam 64, a layered threshold (red) and a single threshold (green). Beam 64 was chosen because it shows 2 objects in the water column (fish schools)

4.2.4 Search for Local Intensity Maxima (3D cubic search box) (step 4)

At this point where all boundaries are defined, the algorithm starts its search for LIMs. It has to be pointed out here that it is not searching for clusters of targets at this stage, it is solely searching for local intensity maxima (LIM), which means a broader search, that actually can be used for other purposes beyond target cluster search.

This search process, searches for LIMs on every swath, beam and sample inside the search area. LIMs are defined at this stage simply as a peak in intensity in all 3D dimensions (Figure 4.25). This means the algorithm will classify as a LIM each sample that is a peak in the samples axis, the beams axis and the swaths axis simultaneously (Figure 4.25). To avoid classifying every single peak as a LIM, the algorithm needs to have a bounding dimension on each axis. This signifies that the peak has to be unique over a dimension reflecting the available resolution in the 3 dimensions. The next examples illustrate this idea: considering only a small number of intensity samples along the axis being analyzed, small oscillations in intensity values can be considered an intensity peak as there is no other higher peaks to compare it with; considering a large number of intensity samples, a desired peak (LIMs) could be bypassed because another higher intensity peak was found in the sampled area, and the algorithm would fail to detect it. Figure 4.26 shows a target detection (i) and noise (ii) where the algorithm would fail and classify noise as a LIM if the search was executed through a smaller number of samples or classify targets as noise if using a larger number of samples. Analyzing the intensity time series (B) the 3 targets are clearly seen as intensity peaks, but if the search window is enlarged to a size that covers all targets, the algorithm would have to decide between them, and classify only one as a LIM. In the angular intensity plot (C), noise (ii),

that may be a side lobe, appears similar to the target (i), the intensity peak is just smaller. If the search window is shortened to the size of 1x beam width the algorithm would also classify the noise as a LIM. As the LIM must be unique over the tri-axial length scales that define the size of the cube, the size of the cube box needs to be defined before the cube box is used. These dimensions are automatically chosen to reflect the achievable angular and range resolution of the sonar as described in Chapter 2. The automatic dimensions are the most effective ones when executing water column detecting, but the user can decide on other dimensions depending on the purpose of the search (an example would be to use a larger window to detect only larger objects on a set of several sizes of objects) (see section 4.2.4.2). However, it should be kept in mind that smaller windows will capture noise and larger windows will miss detect smaller intensity objects close to higher intensity ones. Although the user can override it, the automatic calculation is preferred, avoiding unrealistic dimensions with respect to the system being used.
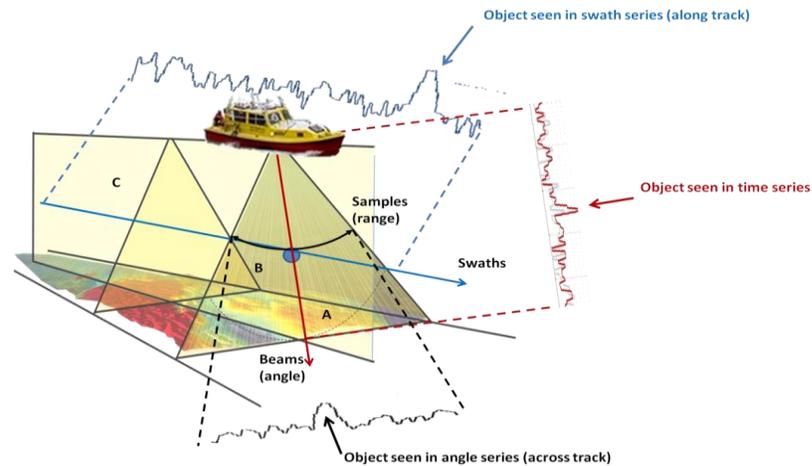
Figure 4.25 - 3D Image showing the 3 axis, and 3 intensity series associated with object detection

In each axis (swaths, beams - angle, samples - time) the correspondent intensity series is illustrated, and the object detection is always a simultaneous peak intensity at each of these axis.
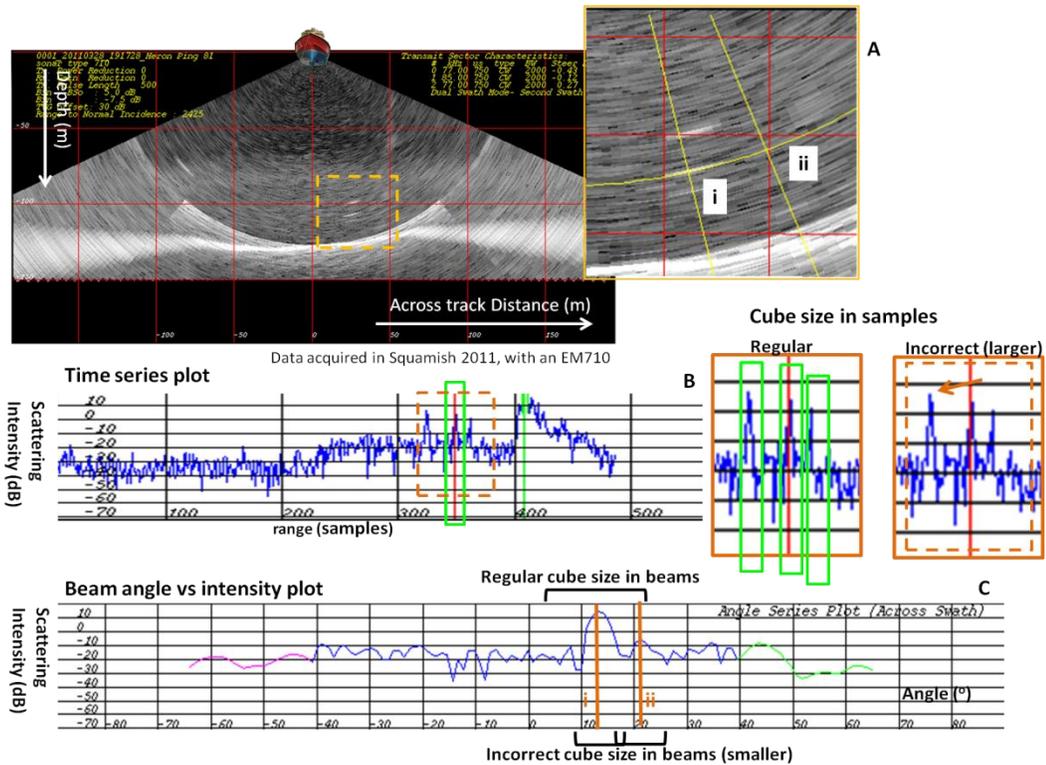
Figure 4.26 - Cube size reflects MBES imaging geometry to accomplish correct LIM classification

A - shows a target being detected (i) and noise (ii). B shows target (i) and compares the cube size in samples, detecting all LIMs when using acceptable size and detecting only one LIM when using an incorrect size (larger), rejecting the other LIMS that have lower intensity. C shows target (i) and noise (ii) and compares cube size in beams detecting noise when using an incorrect size (smaller) and rejecting noise when using the acceptable size. (Note that values need -30dB offset applied)

This cube is defined using swaths, beams and samples number as its axis. Figure 4.28 illustrates the cube axis and usage. A shows the axes being used, B the cube concept and C shows the planes defined by the axes in the cube. D shows what is actually used, the 3 planes centered on the sample being examined. E shows examples of intensity plots on each plane and F illustrates how those intensity plots relate back to each axes. Finally G illustrates how the search is done, moving the cube through each sample on each beam

of each swath. The cube is merely the concept used as the true final shape defined by the size of each plane is actually is not a cube as it is defined using multibeam geometry and all its sides may be different, it gets more like a polar parallelepiped shape as shown in Figure 4.29.

The algorithm compares samples intensity values in three planes only, similar sample, similar swath and similar beam angle creating a 3D planar search, simplifying the cube as the changes appear mainly in these directions and not obliquely (Sections 2.3 and 2.4). This concept means that two objects may be detected in the same cube size area if they do not lay in the same planar axis (Figure 4.27) as their side lobes intensities will not be mixed with the other object detected intensity. This assumption relies on the fact that Mills-Cross beams seem to suppress most side lobes in all directions except the two planes defined by the transmitting and receiving arrays (Figure 2.2), along track (swaths) and across track (beams).
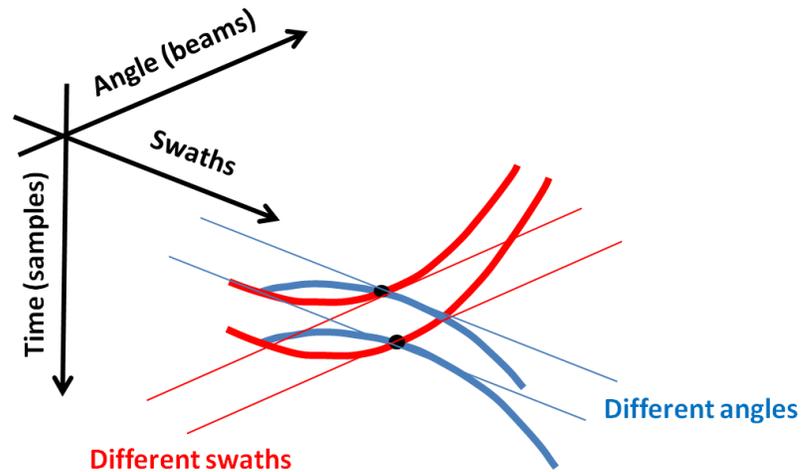
Figure 4.27 - Two Objects in different 3D planes but same cube size area

Object A and object B are detected in different swaths and different beam angles with their side lobe effects not interfering with the other object.

105

A

Beams

Swaths

Samples

B

C

3D Cube

The 3D Cube is defined using beams, samples and swaths.

Only the planes of each axis are used, as the side lobes appear on these planes.

Only the simultaneous peaks in all 3 axis are classified as detections.

D

E

F

Beams

Beams

All swaths

All beams

All samples

G
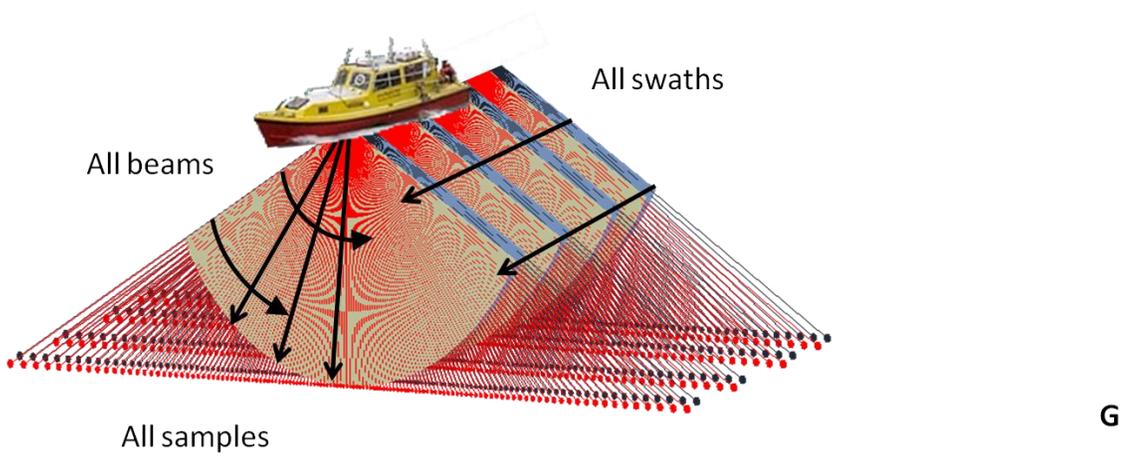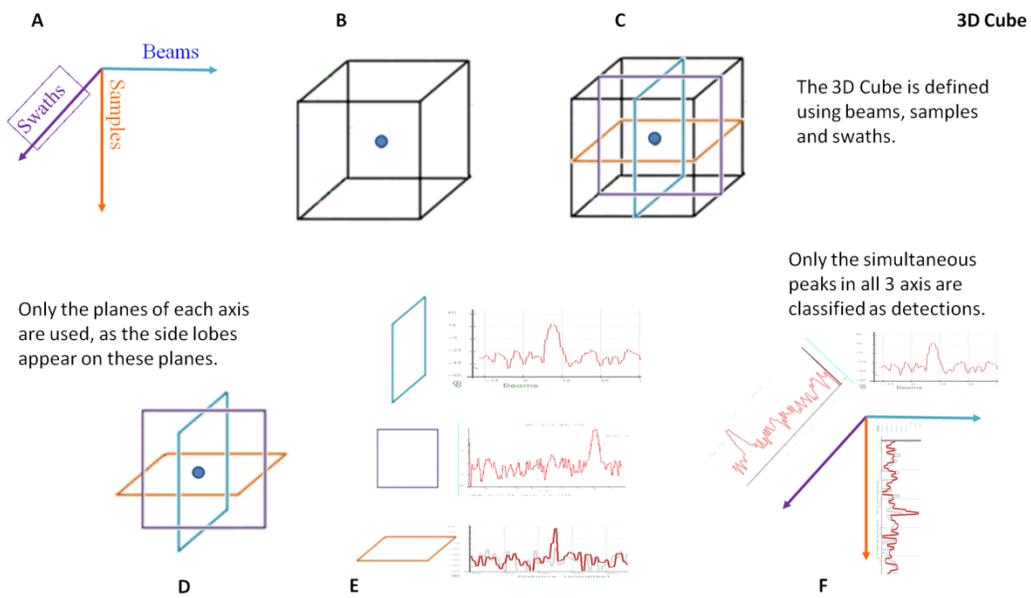
Figure 4.28 - An image showing the cube, it's axis, size, and usage through the water column data

3D Cube will be used through all the water column data, checking all the intensity values above the threshold. All swaths, all beams, all samples will be checked

106
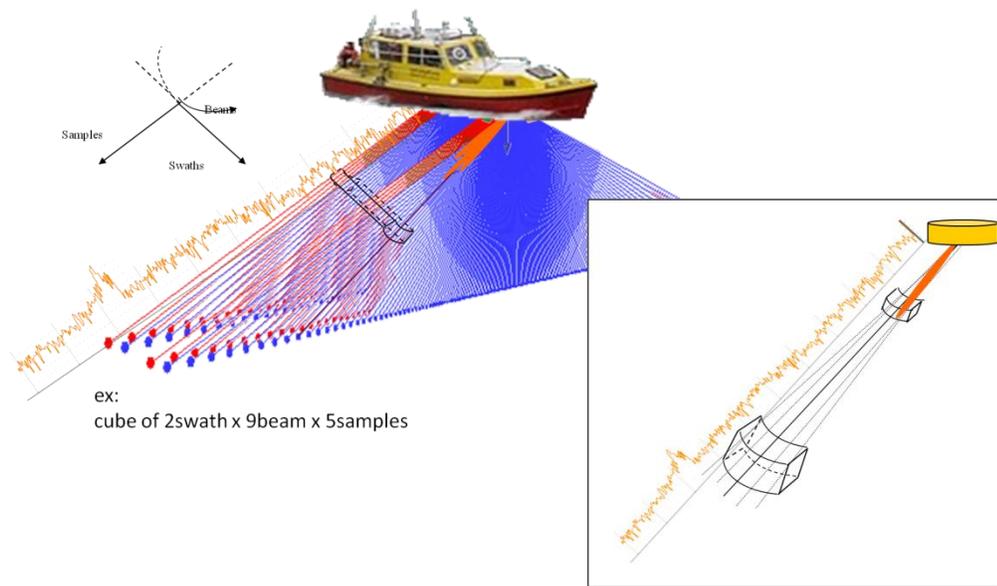
Figure 4.29 - Figure showing the true shape of the cubic box

The cube is not really a cube, because it is defined using MBES imaging geometry

4.2.4.1   3D Cube box size

To define the Cube box size the algorithm needs to know the effective transmitter and receiver beam widths. As the only way to calculate it is to analyze the data, the algorithm does a full search on the search area when it starts, and checks all the relevant multibeam parameters (system used, number of swaths per ping, number of sectors used through all data, frequencies used, sound speed, Tx beam width, Rc beam width, Tx Array size, Rc Array size, range resolution, vessel average speed, ping rate, wave length at each sector, MSR at each sector, start and stop beam at each sector, time of transmit at each swath). Once all the parameters are loaded, the algorithm creates a replica of the beam pattern for each transmitting and receiving beam angle, at each known frequency

(as will be explained in next section). Then the algorithm compares each sample with the threshold, and once a sample is found whose intensity is above the threshold it re-checks all system parameters and calculates the size of the cube and verifies if it is a LIM. The size in samples is defined as 2 times the range resolution (using pulse length/bandwidth). In the beams axis, the algorithm uses the system receiver array size, the beam steering angle, the shading function, and the noise level to calculate the effective beam width (above noise level). The size is defined as 2x the effective beam width. This size is then converted to beams using the beam spacing at the sample being analyzed. As to the swath axis, the spacing depends on the transmitter effective main lobe beam width and shot spacing. Consequently the survey platform, ping rate, and swath tilt angle have an influence on this also. So, the effective transmitter beam width is calculated in degrees using the system transmitter array size, the shading function, transmitter tilt angle, and range of the sample being analyzed. The size is converted to swaths using detection range, vessel speed and pulse rate and multiplied by 2 to get the cube size in swaths. All this calculation process is intentionally done only for the same swath, using the same frequency, inside a ping (1st swath vs next/previous 1st swath). If the user forces a single swath approach (Section 4.2.6) the algorithm will start comparing different swaths in this process (1st swath vs next/previous 2nd swath in a dual swath system). This automated approach seems to solve the problem and define the most appropriate size values for the cube box.

The use of this cubic box concept brings some advantages and disadvantages to the algorithm detection method.

The first advantage to be mentioned is the fact that it allows the control of LIM spacing and number of LIMs. As mentioned before, the algorithm classifies as LIM all intensity peaks that are the highest peak inside the cube size area, looking at the three axes. The minimum LIM spacing in each axis is half the size of the cube in that axis (Figure 4.30), and increasing the size of the cube can diminish the number of detections. The cube size is supposed to reflect the minimum resolvable capability of the sonar. If there are two targets closer than half the cube, in the same axis, it should not be possible to identify them any way.
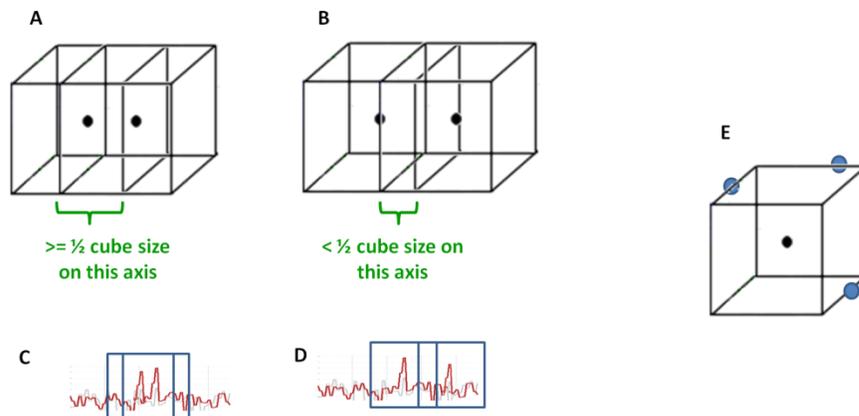
Figure 4.30 - Figure showing that the cube size defines the minimum detection spacing

A) shows two adjacent cubes with spaced more than ½ cube size. This situation leads is then shown in C) where only one LIM is classified (the highest peak). B) shows two adjacent cubes spaced less than ½ cube size, leading to D) where both peaks are classified as LIMs. E) illustrates that only new LIMs outside the cube area will be allowed.

109

The second advantage is that this cube technique has an effect of bringing together close peaks while searching for LIMs, concentrating the result in a single LIM. This side effect makes the algorithm mark large homogeneous objects (whose intensity peaks do not oscillate up and down along the same axis) as a single LIM. Still analyzing the fact that a LIM is the highest peak inside the cube area, if the algorithm finds two peaks inside the same cube space, it automatically discards one. When the second one is analyzed, if another highest one is found inside its cube space, it will also be discarded. In the end, if several 'peak cubes' are overlapped, only the highest peak of all will be marked as a LIM. Figure 4.31 shows the neighbour detection side-effect that allows this. As an example, a large steel bar sitting horizontally in the water column would be detected several times, but as it is homogeneous enough, the algorithm would only mark it once or at intervals reflecting the cube size spacing along the bar. Another example is a school of fish, if it is homogenous, it is marked once (Figure 4.32). Although the algorithm is using only 3D planar detection, this effect still applies for large objects while their intensity value decreases homogenously from one point.
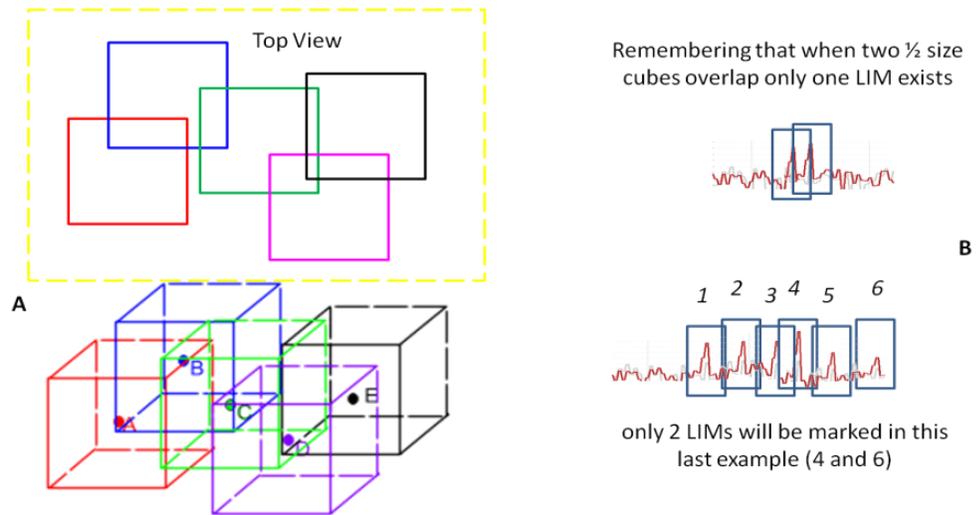
Figure 4.31 - Figure showing cube dispersion and neighbour detection side effect

A) Imagining cubes of ½ the size of the ones used, we can say that 2 cubes cannot overlap in order to have 2 LIMs(and that if 2 cubes overlap, only one LIM will exist). This brings us to a point where we can understand the idea of contamination in large homogeneous objects. If several peak cubes overlap, only the highest intensity one will be classified as a LIM. All others will be excluded by the highest peak neighbour. B) shows the same concept seen only in one axis through an intensity plot.
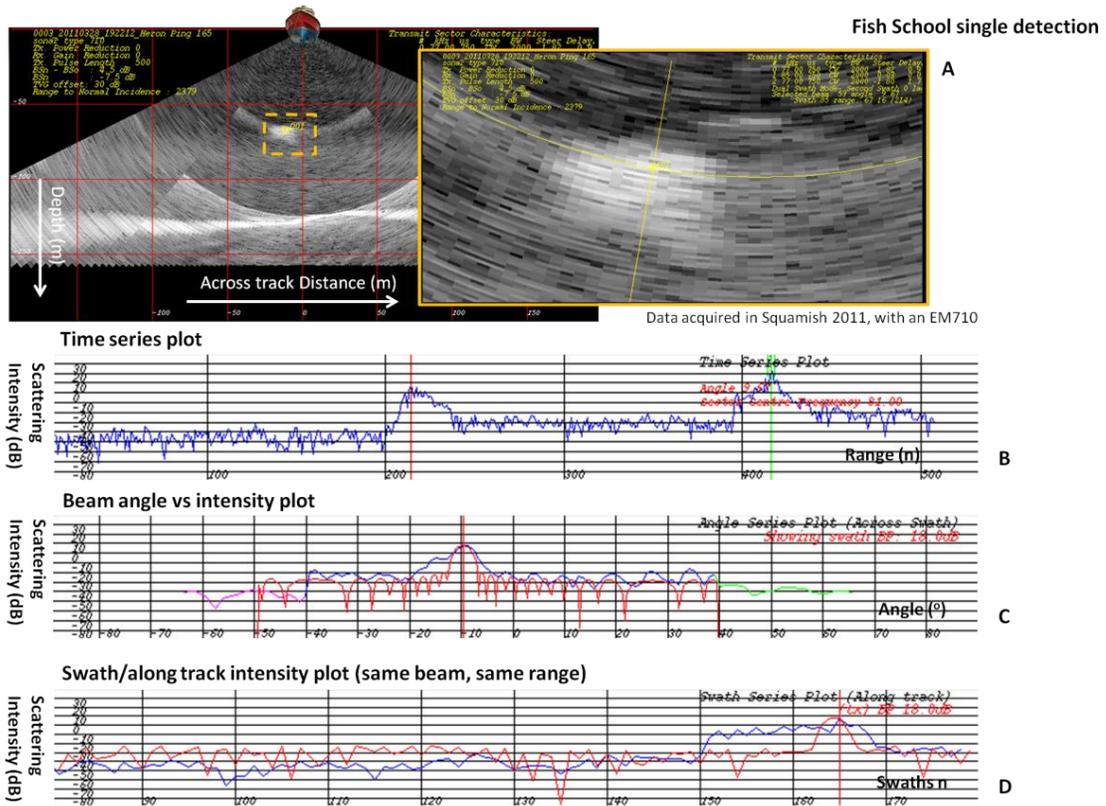
Figure 4.32 - Figure showing a school of fish being detected once

(A) shows water column image of the fish school, and one detection only. (B) shows time series intensity plot, (C, D) show across and along track intensity plots. The homogeneity of the fish school is visible in all plots with a relatively flat intensity line defining the fish school. Red line is predicted scattering field of a point target at that location. (Note that values need -30dB offset applied)
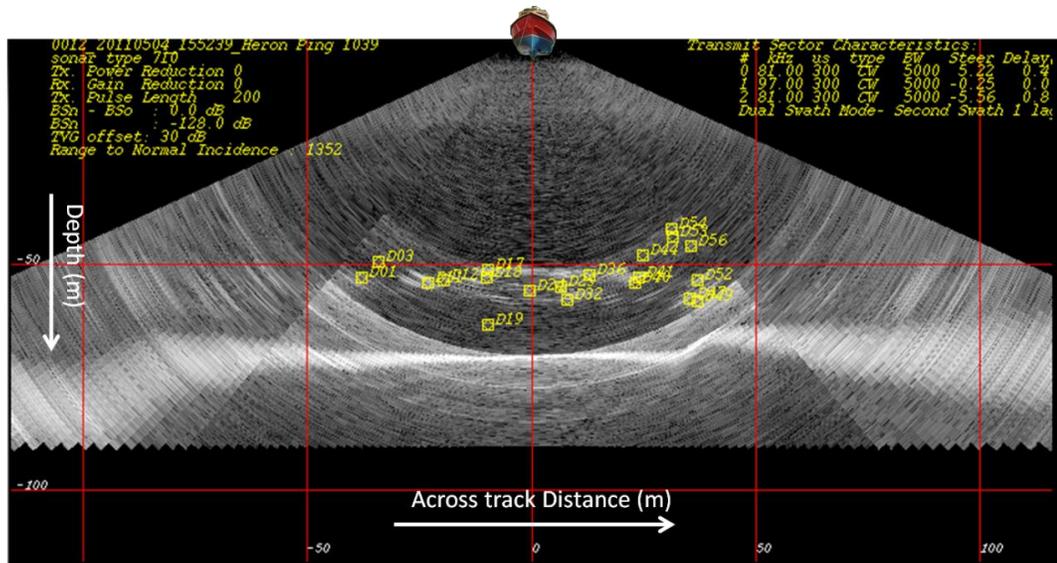
Data acquired in Squamish 2011, with an EM710

Figure 4.33 - Example of a patchy fish school

The big disadvantage actually corresponds to the last advantage as well. First of all, the side effect of bringing together close peaks only works in homogeneous objects. If the target loses homogeneity in a distance large enough (depending on the search box size) a second detection will be picked up. An example of this can be a patchy school fish, as shown in Figure 4.33. But also, this side effect might not be what we want. It makes the algorithm work very well when trying to detect small objects, with respect to the beam width and band width (with a wider spacing between two of them than the beam width and band width). It also eliminates the over population of detections, but it eliminates the possibility of detecting and marking the lateral extent of big homogeneous objects, because it will only get the "brightest" spot, the LIM. The way it is defined now, this phase of the algorithm does not make structural detections, meaning it does not mark the whole structure. As an example, a mast of a ship wreck would probably be marked only

113

once or at spacing of half the cube size (depending on its homogeneity), and there is no guarantee it would be on the shallowest part of it (Figure 4.34) at that is not necessarily the brightest echo within ½ cube spacing. In this 2D example image, we can see part of the steel bars being detected and the side lobe ghosts defining the shape of the bar. Although the steel bars are not seen at its full extent, the algorithm only marks each bar at one single point in each swath as they are sufficiently homogenous (depends on the size of the cube). However, they are detected and marked along the other swaths as well and it is possible to build a 3D image with the detections drawing the oil platform in 3D, as will be shown later, with all marks being spaced at a distance greater than the cube size. Not marking homogeneous objects along their full extent may seem a big disadvantage however, Some small changes to this 3D cube approach could fix this problem and even guarantee the shallowest point is marked.
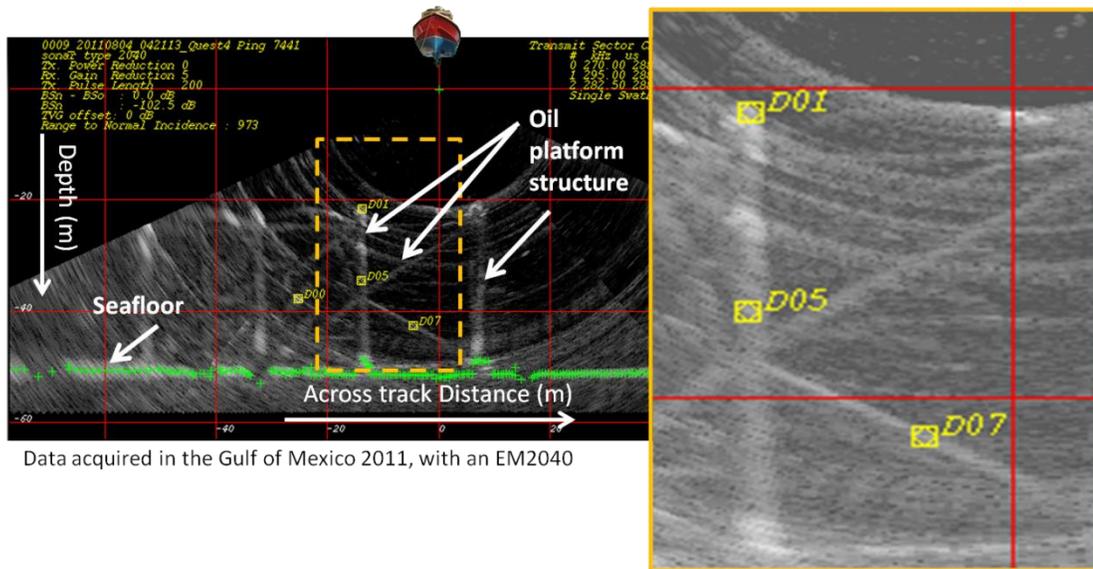
Figure 4.34 - Figure showing structural detection

Sample of an EM2040 water column image over a sunken oil platform consisting of multiple connected spars. Note that only one object detection exists for each steel bar.

4.2.5 Check for beam pattern (3D pattern search) (step 5)

Having found a LIM, classified by the 3D cube search, other tests need to be used to actually certify it is a response to an actual object at that location and not just some random/systematic noise (that would not exhibit the characteristic arc/hyperbolae), (Figure 2.16)(Figure 2.17). This step uses the calculated range resolution and effective beam widths (transmission and reception) to search for the characteristic beam pattern (BP) that is seen for single suspended points in the water column as explained in Chapter 2. As side lobes are sometimes masked by background noise, this step searches only for the main lobe beam width coverage.

The beam pattern changes with each system, and even with the changing receiver and transmitter steering and pulse length within a single system, and thus will create a uniquely characteristic detection pattern along the water column. As these patterns are examined in beam/swath units, they will also change with some user defined variables such as vessel speed, ping tilt angle, swath coverage. In this step the algorithm creates a replica of the detection image pattern, calculating the characteristic common range arc and hyperbolic echo for the specific LIM being analyzed, at the beam steering angle, swath tilt angle and range used. Then uses this replica as a match filter to verify the LIM has the expected characteristics of a detected object in the water column, classifying it as a detection when it does. If a LIM does not match the scattering pattern match filter, this LIM is discarded.

4.2.5.1 Beam pattern replication

In the range axis the pattern depends only on the pulse length. The algorithm checks if the parameters being used are the same as the ones detected in the beginning and corrects range resolution if they have changed. Then range resolution is compared with sampling size and the time series replica along range is created to match the range resolution. At this point, Kongsberg's water column sampling always matches range resolution which makes range resolution beam pattern almost irrelevant to object detection. However, the algorithm is still coded to recalculate it according to the sampling size being used, granting its use even if the water column sampling method changes.

The beam patterns along and across track are replicated using the synthetic beam patterns already calculated (if the system parameters are the same), as mentioned in the previous section. The beam patterns for each beam were created taking into account the array length, the sound speed, frequency, beam steering angle (or transmission tilt angle) and shading function (Equation 4.1, Figure 4.35). The array is considered to have m elements, depending on the array size, separated at a specific distance d (never coarser than 1/2 the wave length of the higher frequency – the standard value used is 1/2 the wave length, as smaller values define m number too large for the computer to execute calculations in an acceptable time frame). As the beam pattern of each beam, at the transducer, does not change during the survey, considering the system parameters stay constant, the system initially detects all different frequencies being used at different sectors and swaths, and creates a single beam pattern, ranging from -89 to 89 degrees, for each beam steering angle (or transmission tilt angle) spaced 0.3 degrees at each frequency

116

(again smaller values will increase the number of iterations and increase processing time).

$$\bar{V} = \sum_{n=1}^{m} \left(A_n \cos\left(\omega t + \emptyset_m + \theta_{delay}\right) \right)$$

A_n is the voltage response including shading

$\omega = 2\pi f, \quad$ where f is the frequency

$\emptyset_m = \dfrac{2\pi m d}{\lambda} \sin \alpha, \quad$ where α is $90 - $ the steered angle of the array

m is the number of elements composing the array

d is the distance separating each element

$\theta_{delay} = \dfrac{2\pi d}{\lambda} \sin \beta, \quad$ where β is the BP angle

Equation 4.1 - Beam Pattern equation
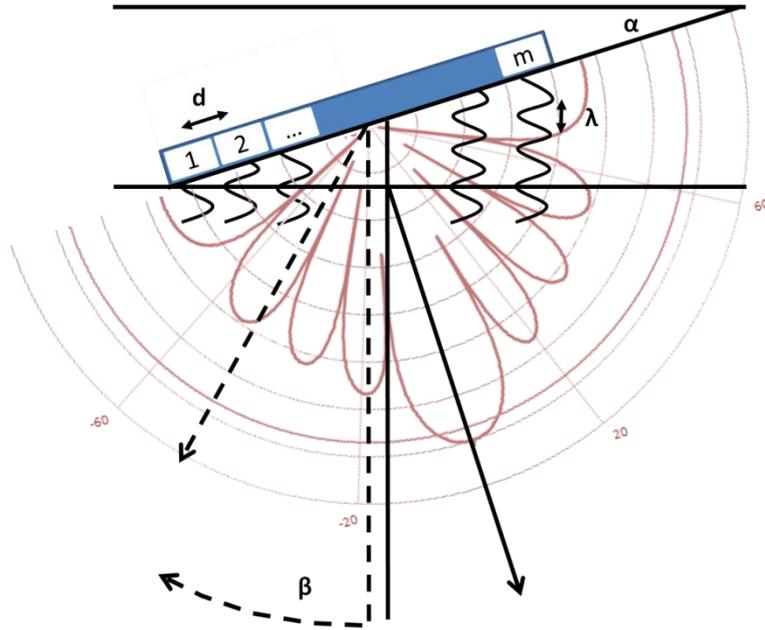
Figure 4.35 - Beam Pattern calculation illustrated

The sound speed used is the one detected initially for each frequency. Although this value clearly influences the beam pattern shape, its influence is minimal before the first null is reached. Sound speed changes are neglected and the same sound speed is used through all the survey, unless it changes more than 20m/s where all the beam pattern calculations have to be performed again. Figure 4.36 compares the expected beam pattern calculated using different sound speeds to show they do not differ much for low changes in sound speed. In this example, the expected pattern is calculated for a LIM. The main lobe closely replicates the observed angle pattern indicating good agreement for a point scatterer at that location.

118
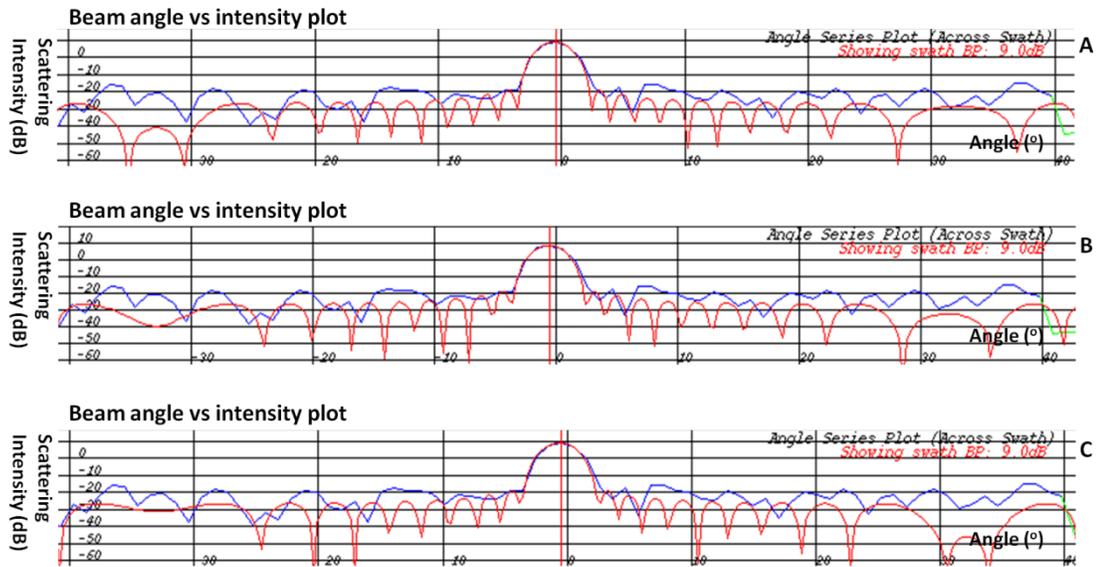
Figure 4.36 - Comparing beam pattern for different sound speed values

White line shows observed echo angle series, green shows modeled echo angle series. A) shows beam pattern (in green) calculated using 1480m/s sound speed. In B) 1500m/s sound speed was used, and in C) 1520m/s was used. Note that although the beam pattern shape clearly changes, the main lobe change is minimal for 20m/s differences.

The shading function used to reduce side lobes was Dolph-Chebishev. As the correct shading function used by Kongsberg is unknown (not documented), several tests were run and Dolph-Chebishev shading functions clearly best approximates the pattern seen in water column data as seen in Figure 4.37, as with Dolph-Chebishev's shading function side lobe supression is the same through all beam angles.. Note that the effective calculated beam pattern approaches the beam pattern shown by the water column data, with special relevance to the main lobe beam width seen at -3°, and side lobe supression. In the predicted beam pattern a mismatch is seen as beam angle increases. However, to have the exact match the correct side lobe shading function used in KM systems would

have to be known. Although, if system parameters are not changed, beam pattern does

not change during the survey for each beam at the transducer, it does change differently

for the transmission and receiving beams along the water column. Considering this, the

creation of the effective beam pattern replica for the transmitting swath and the receiver

beams was created separately.
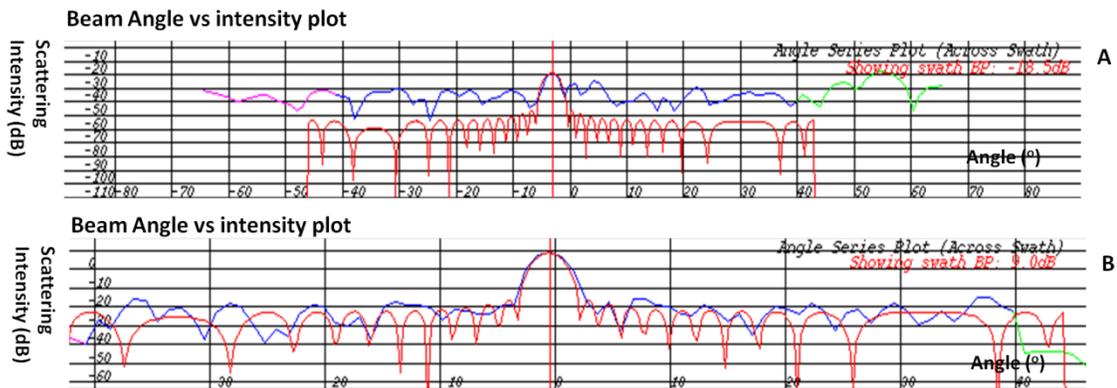
Figure 4.37 - Comparing Dolph-Chebichev shaded composite beam pattern with water column data
Effective (composite) beam pattern is shown in red, superimposed on a weak echo (A) so that it lies
below the water column data, and a strong echo (B) to verify it matches side lobe supression.

The receiver beam pattern was calculated from the minimum detected beam angle

to the maximum detected beam angle using 0.1 degrees spacing. Then combining all

beam patterns for each single beam angle, a final effective beam pattern was created that

replicates the received across-swath pattern detected in the water column data. Figure

4.38 shows both beam patterns example. A) illustrates how the effective beam pattern is

calculated. B) shows the calculated beam pattern for the selected beam only, that depends

on the system parameters and on beam steering angle. C) shows the effective beam

pattern at the selected beam angle when combining the contribution from all the receiver beams. Figure 4.37 shown before compares data already with the replicated effective beam pattern. At this point the algorithm has stored an effective beam pattern for any beam angle (spaced 0.1 degrees), that can be used as a match filter, as it does not depend on any other factor.

The transmitted beam pattern is calculated the same way at the beginning. It is calculated from the minimum detected transmitting sector tilt angle to the maximum detected transmitting tilt angle using 0.1 degrees spacing (typically no more than $\pm10^{o}$). The transmitted beam pattern actually depends on depth, vessel speed and ping rate. Knowing these characteristics the effective beam pattern can only be calculated when the LIM relative position (beams, samples, swaths) in the water column is known. Figure 4.38 illustrates how the effective transmit beam pattern is calculated. The method of calculation is similar to the one used for the effective receiver beam pattern, but the angle at which each beam detects the same object has to be calculated using the vessel speed and ping rate. The algorithm calculates for each transmitting swath in the water column slot being used (Figure 4.39), the distance (Ds) at which the swath is from the swath that detected the LIM using vessel speed and time of transmission. Then it calculates the range (R2) from each swath to the LIM. Using the calculated values the angle (θ) between the main lobe boresite of each swath and the LIM is calculated. Knowing this angles the beam patterns of each swath are combined to create the effective along track transmit beam pattern about the LIM.
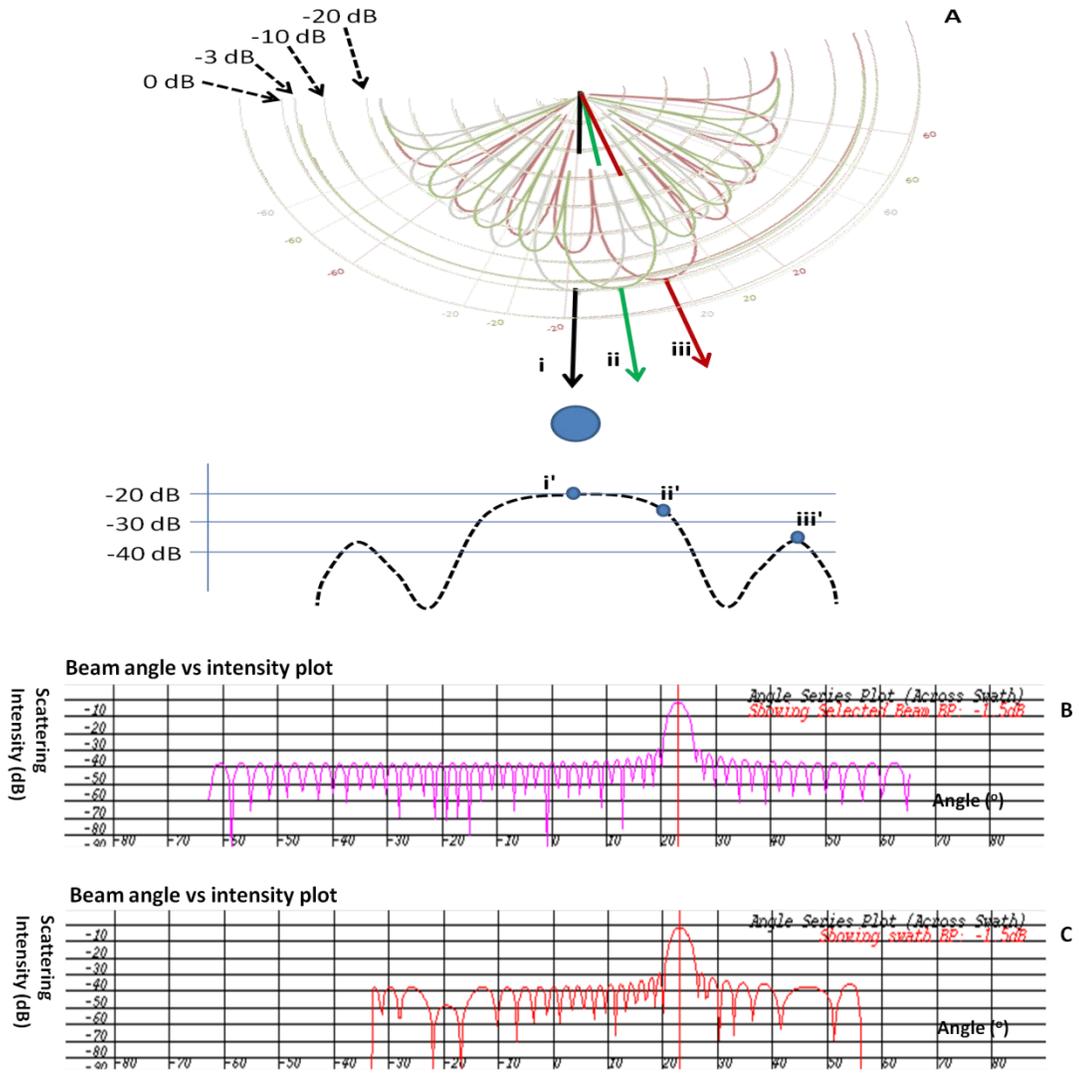
Figure 4.38 - Calculating the effective beam pattern

A) illustrates how the beam pattern is calculated. Each beam across the swath will receive a specific backscattered intensity from the target at the angle the target is for that beam depending the own beam pattern. Beams i) ii) and iii) received intensity is projected to a plot as i' ii' iii' for better understanding. For each beam angle a composite of all beams, beam pattern detections across the swath is calculated. The result is presented in C) for a specific angle, where the specific beam at that angle would present the beam pattern shown in B).
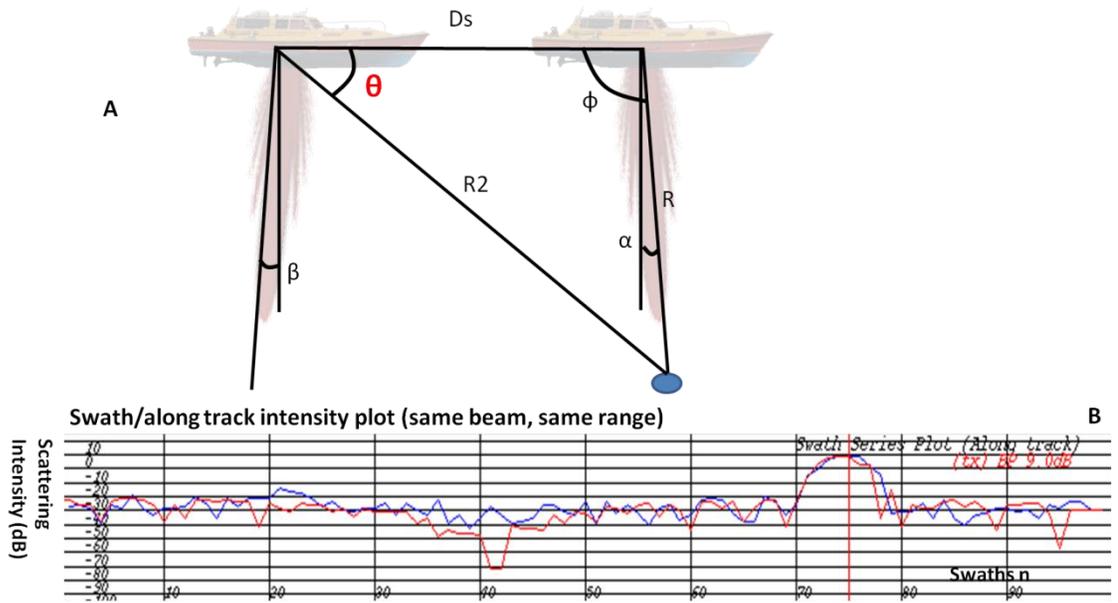
Figure 4.39 - Calculating the effective transmit beam pattern

A) illustrates the calculations to find the angle θ at which each other tx beam in the contiguous swath is detecting the same object. This calculation is executed for each tx beam at each receiving angle and the calculated scattered intensity (according to each tx beam's beam pattern) will be added to the beam pattern of the beam detecting the object at the swath where the object is detected. B) shows a plot where the tx beam pattern (red) was superimposed on the water column data (blue).

4.2.5.2 Pattern match filter

Having the effective beam pattern for transmitting and receiving beams the effective beam widths are analyzed by matching the predicted beam pattern with the observed data. The effective beam pattern peak is set at the LIM and the differences between the intensities along the effective beam pattern and the water column data around the LIM are calculated. To compare the effective beam widths only, the match filter is only run until the noise level or the first null is reached, considering the noise

123

level the mean peaks calculated at step 3 (threshold calculation). For every LIM if the beam pattern differences show the effective beam width is too narrow in the data, the LIM is excluded. Otherwise it is considered an object detected. Figure 4.40 illustrates the match filter procedures. The predicted effective beam pattern is aligned to the main lobe of the LIM detection. The algorithm then compares each side of the main lobe separately. Calculates the differences from the data to the beam pattern for each beam, from the peak to the first null or until the noise level is reached (reaching the effective beam width). The algorithm checks if the differences mean a narrower or broader scattering pattern by checking their signal and then all differences (squared) are added together and divided by the number of beams analyzed. The square root of the result will have to be smaller than N (the number of beams analyzed) multiplied by 2dB, allowing a total of 2dB difference per beam (an easy decision method to exclude noise). This means the algorithm will only exclude LIMs whose scattering observed pattern is narrower than the calculated effective one. This decision is taken because the projected scattering pattern of large objects will clearly be larger than the effective beam width as can be seen in Figure 4.41, while no object can be detected without its projected scattering pattern showing at least the beam width.

Strictly, other factors should be considered for the effective beam pattern calculation, such as heave and roll at each ping and sound speed. At this point, as the sidelobes rarely are clearly visible above noise levels, this simplified pattern match filter does not consider side lobes and tests the match only on the effective main lobe beam width using a simple decision procedure for validation.

124

For the focus of this thesis, the emphasis has been on correctly calculating the correct shape for the expected scattering pattern due to a point target which is small with respect to the sonar resolution. Only a simplified matching criteria ("at least as large as") is implemented so far. There are, however, many potential extra classifying criteria that can be gained from examining the mismatch. For example, how much larger than the minimum resolvable dimension is the object.
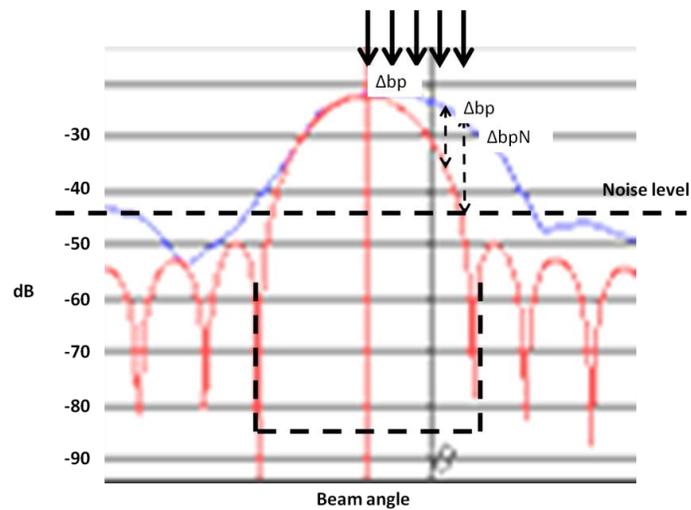
$$\Sigma\ (\Delta bp1, \Delta bp2, \Delta bp3 \dots \Delta bpN)^2/N < N*2dB$$

Figure 4.40 - Match filter decision

Blue line shows observed angular scattering pattern. Red line shows predicted angular scattering pattern.

Data acquired in Squamish 2011, with an EM710
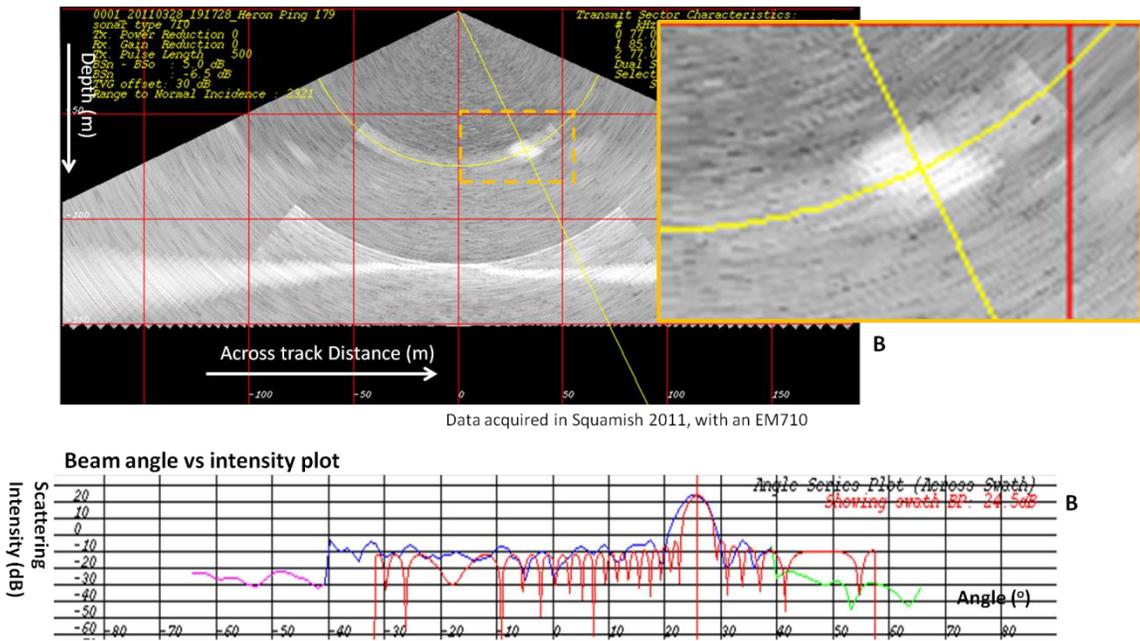
Figure 4.41 - Fish school wide scattering pattern

(Note that values need -30dB offset applied)

Finally, the range resolution and transmitter and receiver beam pattern match filters (main lobe beam width) are independently optional (by default the system applies all, but the user can block the use of each one independently), as the user might have the need to find detections that do not have one or any of this beam pattern effects. The most important example would be noise as will be described in Chapter 6.

4.2.6　Check different frequencies (swaths)

Multibeam systems nowadays use dual swath, using different frequencies for each swath. Multi swath systems were introduced to increase along track coverage, but create some problems when comparing detections from different swath frequencies. Knowing that different frequencies have different source levels, different attenuations, different reflectivity values, and even different side lobes for similar objects, all previous tests were run only for similar frequencies, avoiding the comparisons with different scales. This last step on automatic detection brings back the concept of one survey line and one system by actually comparing detections in different frequencies and choosing between them. The algorithm checks through all detections found for neighbour detections, including all frequencies. Using the same 3D cube size from step 4, the algorithm checks if in the vicinity of each detection there is another detection of a different frequency (similar frequencies were excluded already). If the algorithm finds 2 detections inside the same cube space, it compares each frequency and intensity value, to decide which one to keep, excluding the weakest one (Figure 4.42), leaving only one detection per search box as desired.
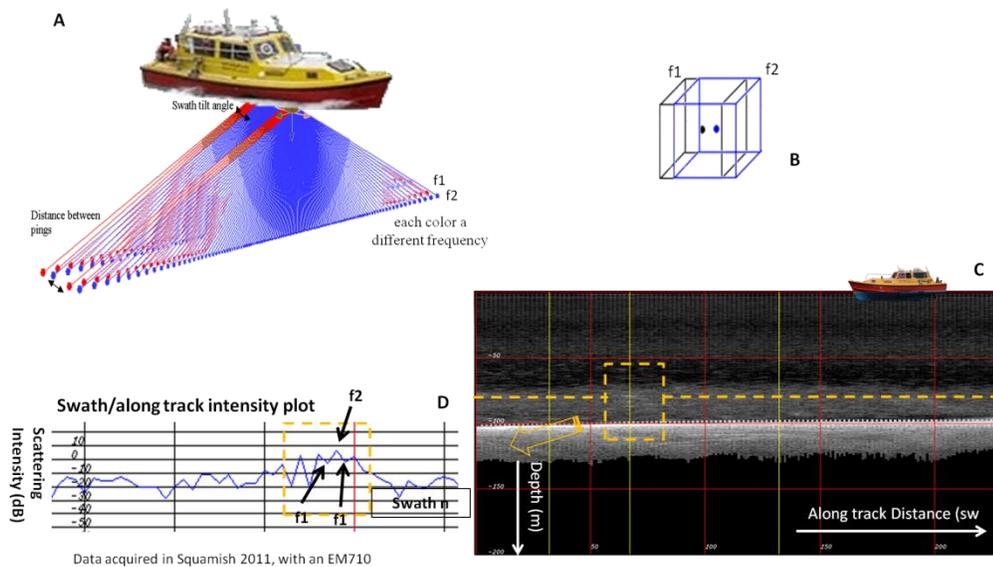
Figure 4.42 - Figure showing dual swath and neighbour elimination

(A) MBES uses dual swath to increase along track coverage, (B) When 2 detections fall inside a 3Dcube area, one has to be deleted, (C)(D) show targets being detected by 2 different frequencies Note the alternate decrease and increase in intensity between the two frequencies. As f2 is lower, it is rejected. (Note that values need -30dB offset applied)

The algorithm is only prepared to work with multi swath systems up to 5 different swaths (which may one day not be enough, but for now there are only dual swath systems). Finally, if the user is confident that the frequency differences are being correctly fixed, this whole process can be overridden and consider the system as a single swath system from the beginning.

4.2.7   Lock on desired target geometries

Lastly, having all the detections marked, the algorithm starts to search for the desired target clusters. The algorithm uses a 3D geometric match filter to find the targets. All the detections are now classified and stored in a list. All the algorithm needs to do is to try and match each target's geometric filter with the detections.

This step is optional, as the user might be interested in simply finding all the detections and not just specific targets. In this case, the target shape file is not needed.

4.2.7.1 Target definition and creation

Targets are defined in a specific format target shape file. The user can define one or more specific targets that are intended to be found in this separate format file (as many targets as are needed). The target shape is defined assuming each target is composed of several pieces. This way each target will have several pieces and each piece will be separated from the next piece by a certain distance and a specific angle. The user needs to describe the known spatial relationship between each piece in the file in order for the algorithm to be able to create a 3D geometric filter. The way it is presented to the algorithm, each target is composed of a group of pieces, and each piece has its size and will be separated from the next one by a specific distance and vertical and horizontal angle (Figure 4.43). The user can also provide a tolerance value for each distance and angle, in case the distance and angle are not accurate enough, or for cases where currents and sea floor steepness may be an issue (Figure 4.44). The last piece composing the target has a distance to the sea floor option. This allows the use of single piece targets,

and also eliminates possible fake targets floating around as it narrows the search. As it was said, it is an option, and the user may not use it when looking for floating targets.
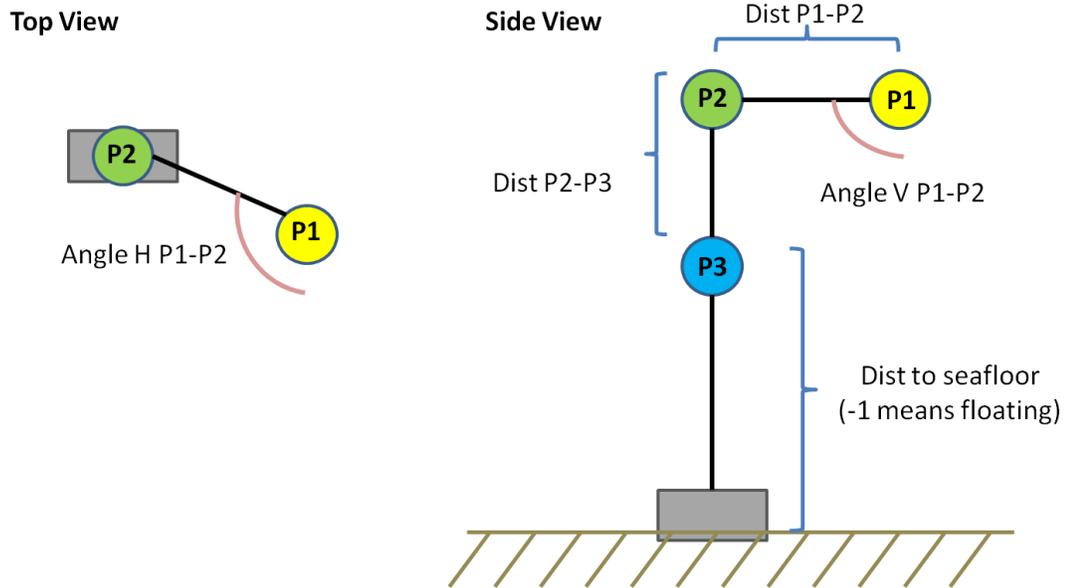
Figure 4.43 - Target shape, flat sea floor

The angles are supposed to be used to search for complex rigid structures, and not to account for tides or currents
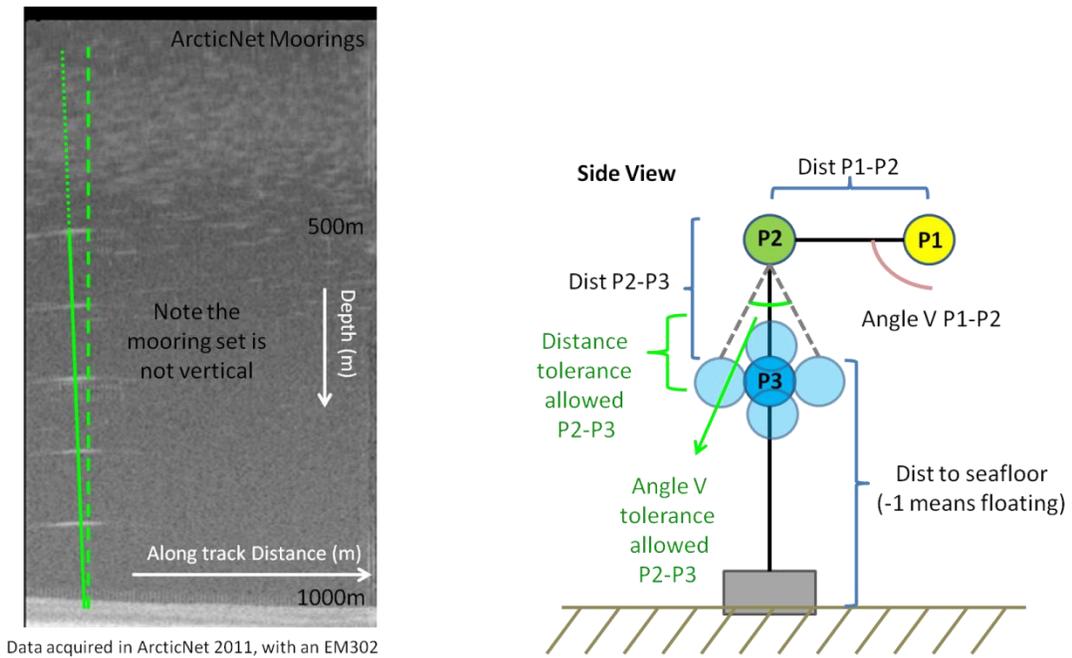
Figure 4.44 - Target definition, tolerance value

Angles are assumed vertical when looking for moorings.

4.2.7.2 Search for targets (3D geometric filter)

Having the target's shape file, the algorithm reads the file and creates a 3D geometric filter for each target, according to the target's shape and size definitions. Then using this geometric filter, a run through all the detections is done using this filter on each detection to check if the target shape is found. The algorithm finds one detection, considers it the first piece and then searches for the next piece at the given angles and distance and corresponding tolerance values. The angles were supposed to be used to search for complex rigid structures. As the horizontal angle does not have a reference direction, the algorithm would search around 360° horizontally for the first piece, narrowing the search for the next pieces (the next angles will already have a reference defined by the first-

second piece detection). Although this idea was planned when building the algorithm, and as the main purpose of this thesis was to use it to search for Squamish targets which are vertically aligned, the angle calculations are not implemented in the code, only searching for vertical targets. However it must be mentioned that even without the calculations introduced the search pattern is implemented using angles (the vertical situation is always considered for simplification).

When a target is successfully matched, each detection composing the target cluster is marked as a target component (Figure 4.45). The algorithm identifies each specific target from the list that was given in the targets format file and names the detection accordingly for future use (Figure 4.46). All detections that are not marked as targets can be excluded in the end. It is also an option for the user to decide.
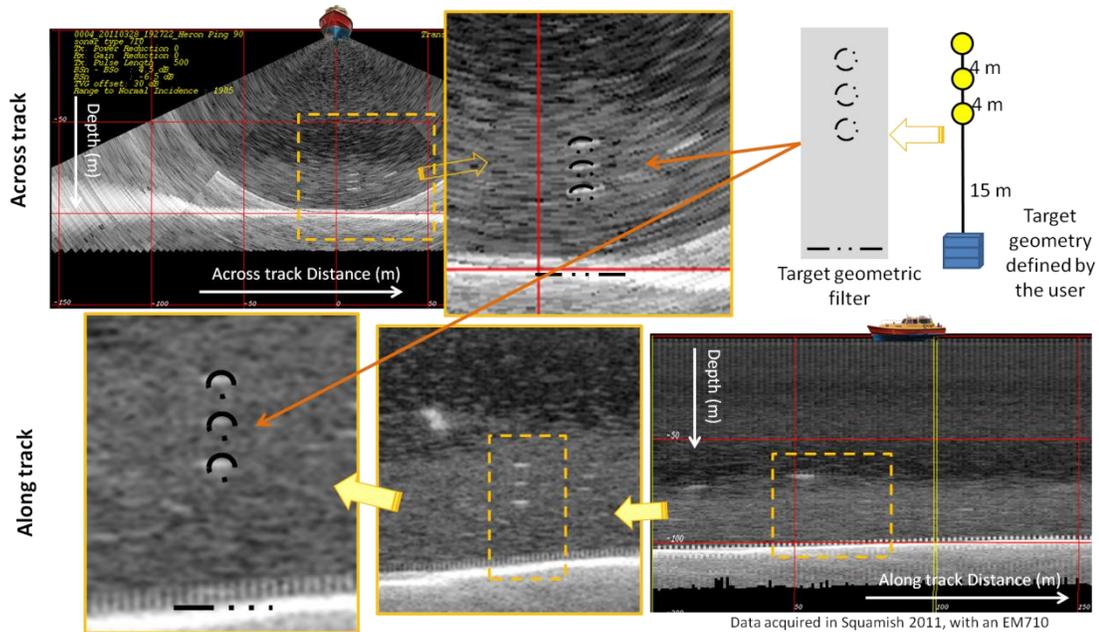
Figure 4.45 - Figure showing 3D geometric filter

The geometry is replicated in a filter and used to find targets among all the LIMs

132
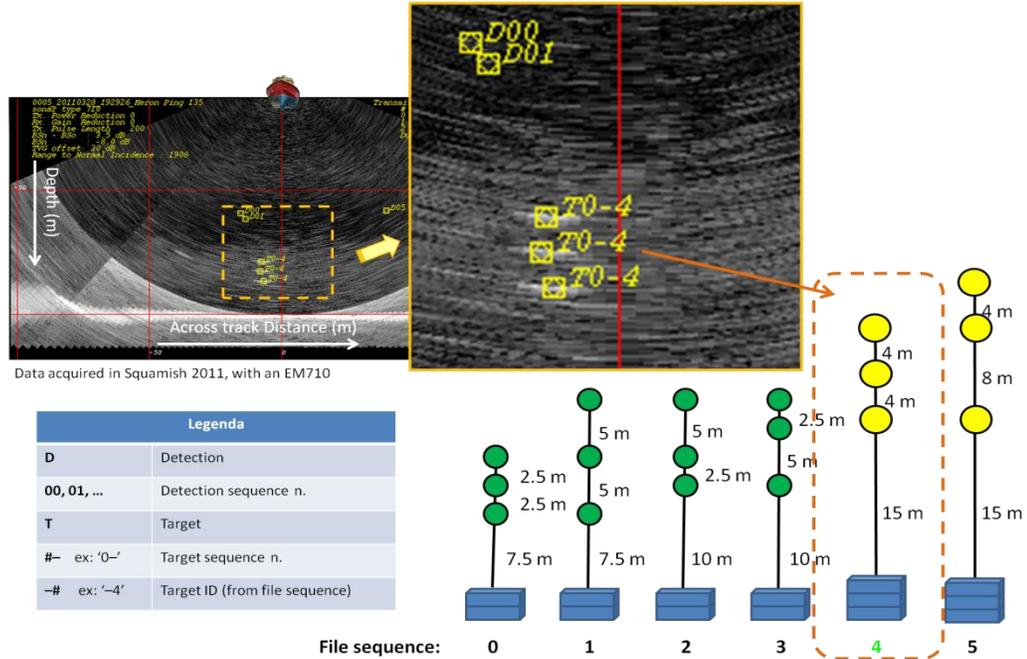
Figure 4.46 - Figure showing targets name structure

4.2.8   Geo referencing targets

The final results, either the detections and/or the targets list, will allow the computer to use the bathymetric MBES characteristics, using sonar location, beam depression and azimuth angles, detection range and sound speed to calculate the position of the object (each piece) and subsequently by using several survey lines separated in time (usually several days), calculate its movement if required. This calculation can be done using sound speed and raytracing the beam to the target position for more accuracy (Figure 4.47).

133
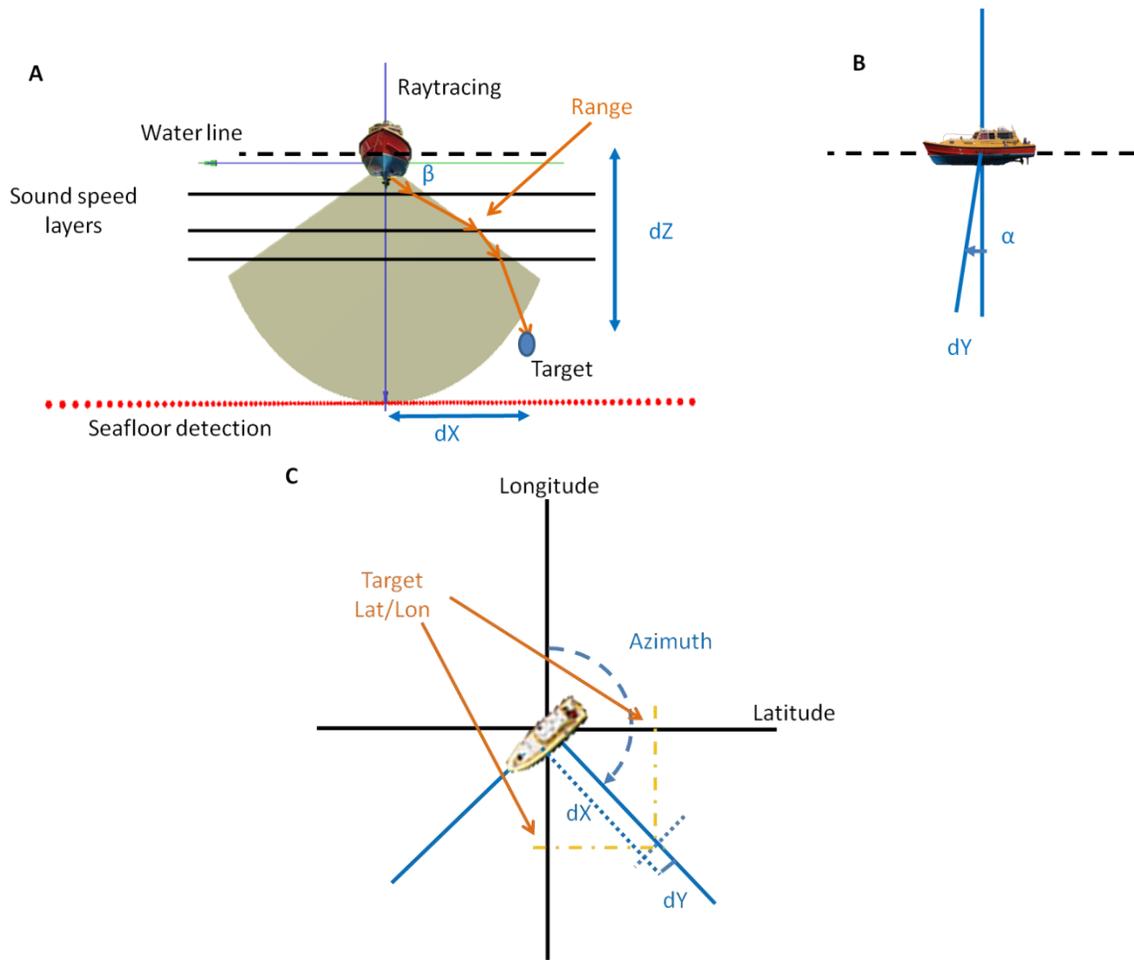
Figure 4.47 – Raytracing to get target position

Raytracing is done using: A - target's beam angle β, range and swath, to find across track distance (dX) and depth (dZ). B – swath angle α, along track distance (dY) is calculated. C – Horizontal position, uses beam azimuth to calculate Latitude and Longitude

4.2.9 Storing results

The final results are stored in the targets file which contains a list of all the detections, both manually and automatically identified. This list carries all the information needed for future analysis, for each detection (Figure 4.48). Values like ping number, time of detection, beam number, sample number, range, depth, latitude, longitude, are stored in this list. The only differences between detections and targets in this list are the label and an identification tag, with targets marked with a 'T' and 'hunted' and detections marked with a 'D' and 'detected'. Both the geo referencing and storage are done using an already built routine in OMG code (Jonathan Beaudoin, 2011 unpublished).

Figure 4.48 – A list of targets as it comes from OMG subroutine, showing target IDs

5. Results and Analysis

This algorithm was tested on 3 specific sets of data. (Squamish Project, ArcticNet moorings, sunken oil platform). The prime aim of the tests were to verify that the algorithm could robustly detect objects in the water column under various scales and MBES geometries. For the case of the Squamish project, once the detection capability had been demonstrated, the tool was used to track a set of targets over a period of a month to demonstrate the practical utility of the tool for tracking targets (Chapter 6).

In the first half of this chapter, the application of the algorithm is presented for the main thesis objective (Squamish targets). As mentioned in Chapter 1 however, the algorithm was deliberately designed to detect any desired object in the water column so that it could be used for other purposes. In the second half of this chapter, other applications are demonstrated to illustrate the flexibility of the developed algorithm and the improvements that were achieved for other uses.

The algorithm was tested using Squamish data regarding target detection, fish detection, and gas plumes detection. Using the ArcticNet data some tests were done on object detection, target detection, gas plumes, and noise detection, And as an extension of this project the algorithm was also tested to see how it would behave when detecting elongate man-made structures, such as a sunken oil platform, using data acquired in the Gulf of Mexico.

5.1 Separating objects from noise

To demonstrate the combined use of steps 4 and 5, recognizing LIMs and separating real targets from interference, an example is presented using the Amundsen EM302 data with both buoys and interference in Figure 5.1 and Figure 5.2.

Both the buoys and interference will generate LIM's. But the scattering pattern in range, beams and swaths of the real targets should match that predicted form (Chapter 2). In contrast the noise, derived from a singular (in time) electrical acoustic event will not necessarily share the range characteristics (being time independent of MBES pulse length). Nor will it necessarily share the expected elevation and pattern across swath. And it should not show up in previous and post swaths. Thus the pattern match filter (step 5) should identify a separate real object (matching the effective beam pattern) and noise (not matching the beam pattern).

Figure 5.1 shows the algorithm executed without the use of step 5, meaning the pattern match filter was not used and all LIM's were marked as objects in the water column. Both real objects and noise show up as objects detected.

Figure 5.2 shows the same swath, but this time step 5 was applied and the noise was excluded by the use of the pattern match filter, only the real objects are classified as detections.

Figure 5.1 - Figure showing detections done without pattern match (no step 5)

The vertical line of targets on port side are a real mooring chain. The arc of targets on the right is a

burst of interference.

Figure 5.2 - Figure showing same detections done with pattern match (using step 5)

5.2 Showing noise when blocking step 5

Blocking the use of step 5 (3D pattern match filter) the algorithm classifies as detections everything that is a peak in intensity. This will allow random/systematic acoustic noise to be picked up as a detection. As acoustic noise is actually not a physical feature, it is not a detection, it cannot be expected to have the expected object scattering pattern associated with it. Acoustic noise is just a peak in intensity caused by some acoustic interference. When noise is present in one swath, it will be in a completely different position on the previous and next swaths (unless it is carefully synchronized). This excludes the possibility of having any interference from the transmitter beam along track. By blocking the algorithm step that searches for this pattern, noise will appear as a regular detection (Figure 5.3) (Figure 5.19). As a term of comparison we can look at the intensity plots in Figure 5.4 and check that although in the time series (A) and across swath (B) the noise scattering pattern does match the expected beam pattern, along swath (C) the main lobe beam width is much narrower than the expected beam pattern, and the side lobes are not present either.
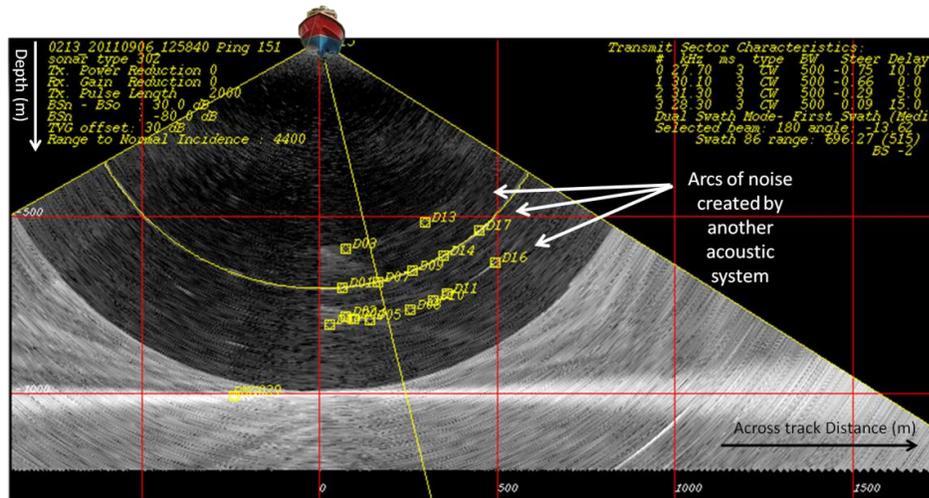
Data acquired in ArctiNet 2011, with an EM302

Figure 5.3 - Figure showing noise arcs
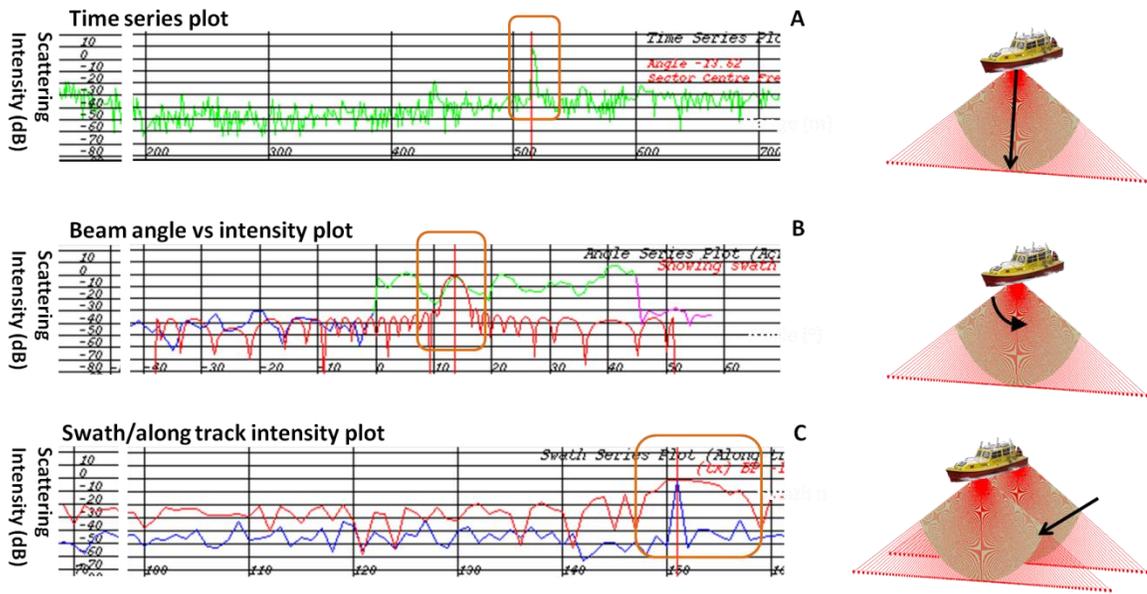
Figure 5.4 - Figure showing intensity plots of noise

Note that noise appears to present the beam pattern characteristics in samples (A) and beams (B) axis, but the main lobe beam width is not present in swaths axis - along track (C). Along track noise is defined only by one swath (other swaths never picked up the noise because it existed only on one swath, when it was detected. (Note that values need -30dB offset applied)

140

5.3 Separating target clusters from other targets

Herein the utility of the target geometric filter is demonstrated. Figure 5.5 illustrates a range of objects successfully detected in the EM710 data from Squamish. As can be seen, solitary large fish-like scatterers and the DSL are present as well as the 3 target cluster. Using knowledge of target spacing and elevation above seafloor, the vertically aligned 3 object is successfully identified.
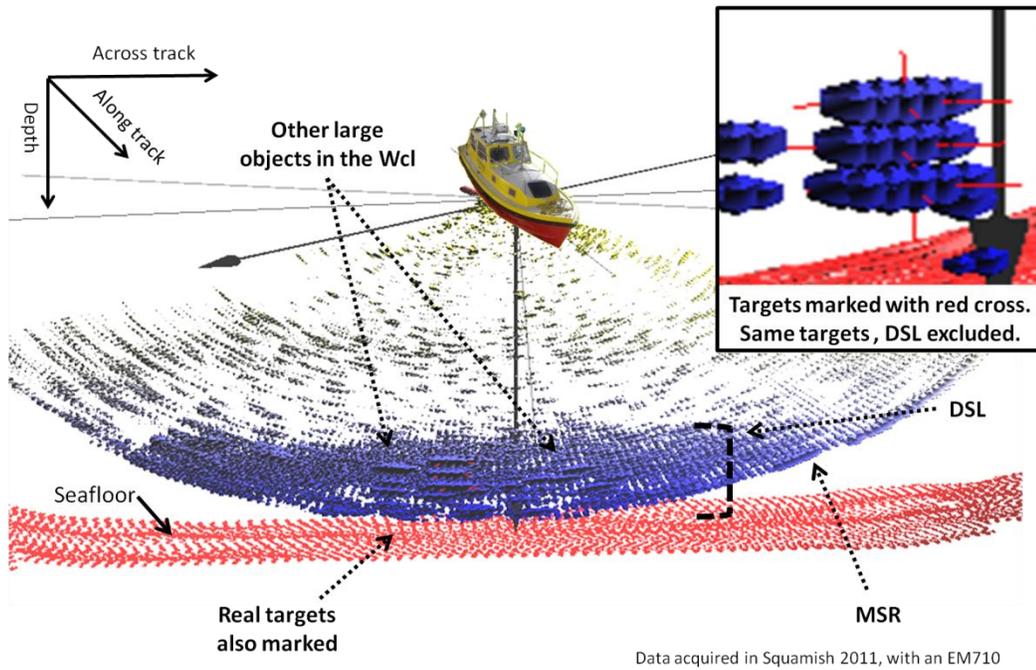
Figure 5.5 - 3D Figure showing targets

The result of applying the target geometric filter when looking for targets is easier understood when comparing Figure 5.6A with the Figure 5.6B. Both figures correspond to the same swath, the same data, but on A) the target geometric filter was not applied, as opposed to B) where this step was used.
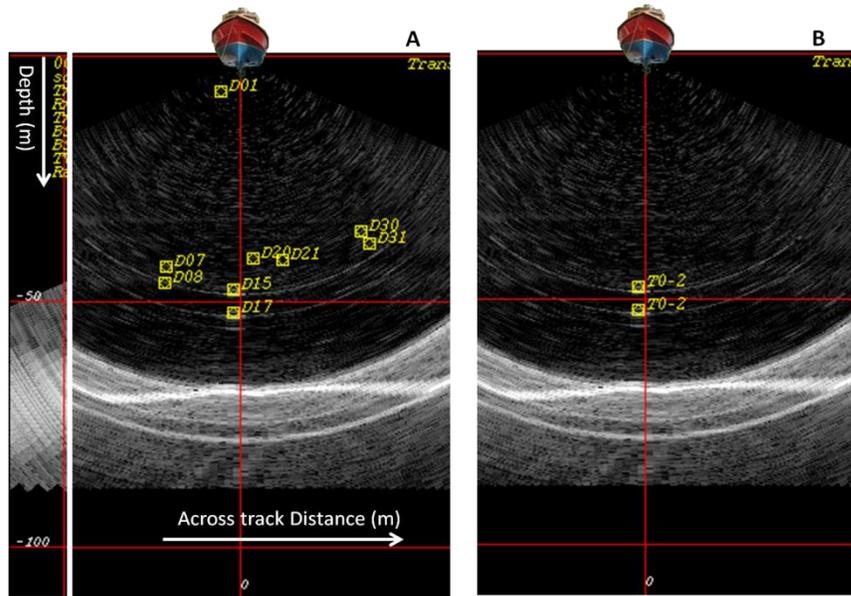
Data acquired in Squamish 2011, with an EM710

Figure 5.6 - Figure showing detections with (B) and without (A) the application of step 7

Note that in B targets are marked. Remaining detections were deleted. Only 2 of the 3 targets are marked as this is only one swath. The 3rd target is in a post swath.

Figure 5.7 shows the importance of using the optional distance to the seafloor value. When this value is not used, several other appropriately spaced clusters detection may actually match the target's geometric shape. The figure gives a 2D view of a target being marked in a gas plume several meters above the sea floor, as well as a 3D view of several vertically separated targets being marked in a gas plume.

Still testing step 7, Figure 5.8 shows the special labeling of each target. Each piece of the target is detected separately and each one is labeled with the letter 'T', a sequential number, followed by the number that identifies the target. This last number, '0' for Figure 5.8 (A) identifies the target position in the target's shapes formatted file Figure 5.8 (B), starting with 0 for the first target. This was shown previously when explaining step 7

142

(section 4.2.7.2). All targets were detected and labeled accordingly as shown in Figure 5.9. Some target clusters appear marked only with two targets, as the image only shows one swath. The other target is marked in a post or previous swath.
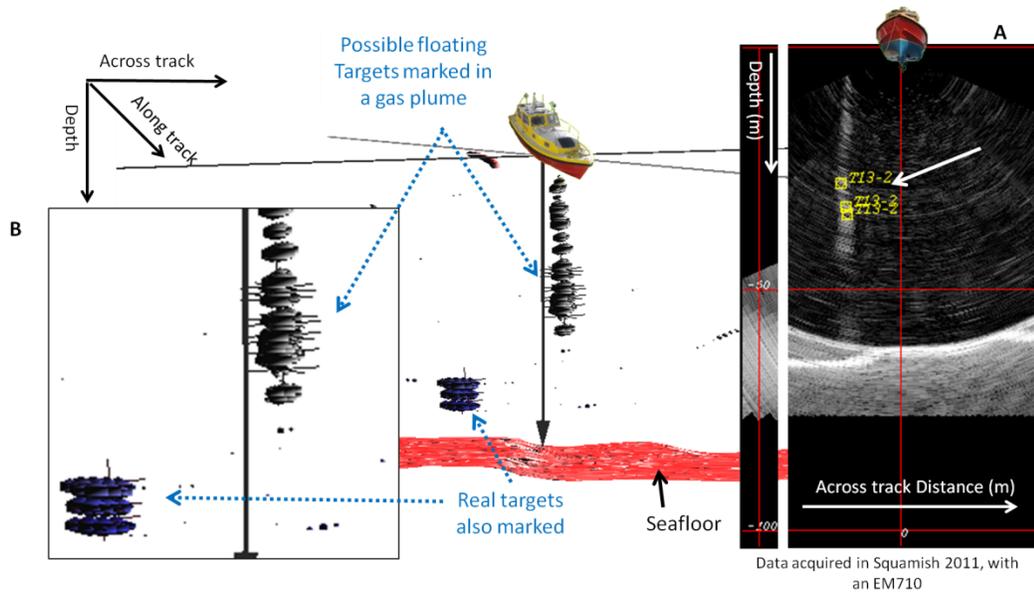
Figure 5.7 – Step 7 - floating option, targets detected but also gas plumes detected as a target.
Figure illustrates the use of the depth off seafloor option. Without this option targets can be found anywhere in the water column. A) Note that the geometry of the target is exactly the same as the one of target 2, but as a depth off seabed was not given and the algorithm marks the target wherever it is found in the water column. B) shows a similar situation in 3D where both the real targets and fake targets in a gas plume were marked.
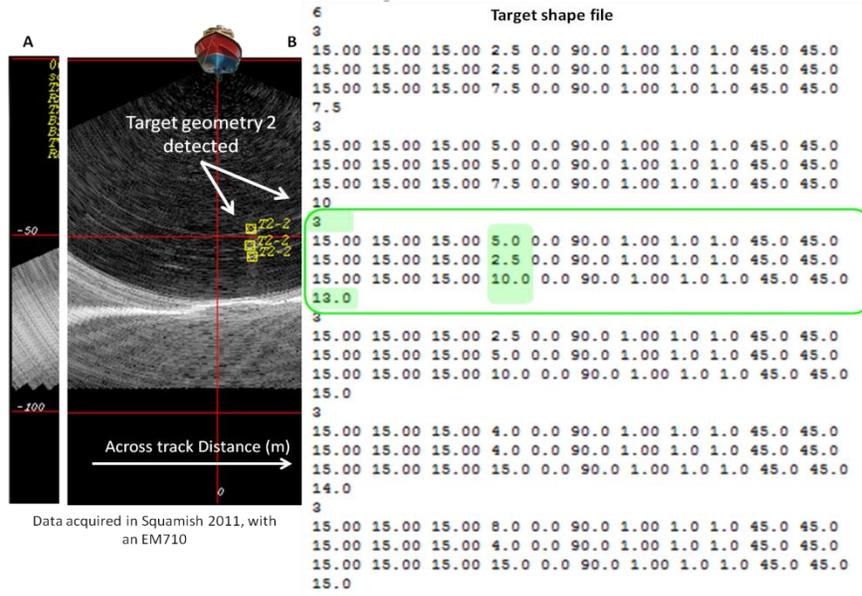
Figure 5.8 - Target labeling (file dependency) - target 2

In (A) target 2 is shown in the water column, (B) shows the target file and the geometry used. The number of pieces, distances separating each piece and distance to seafloor values are highlighted
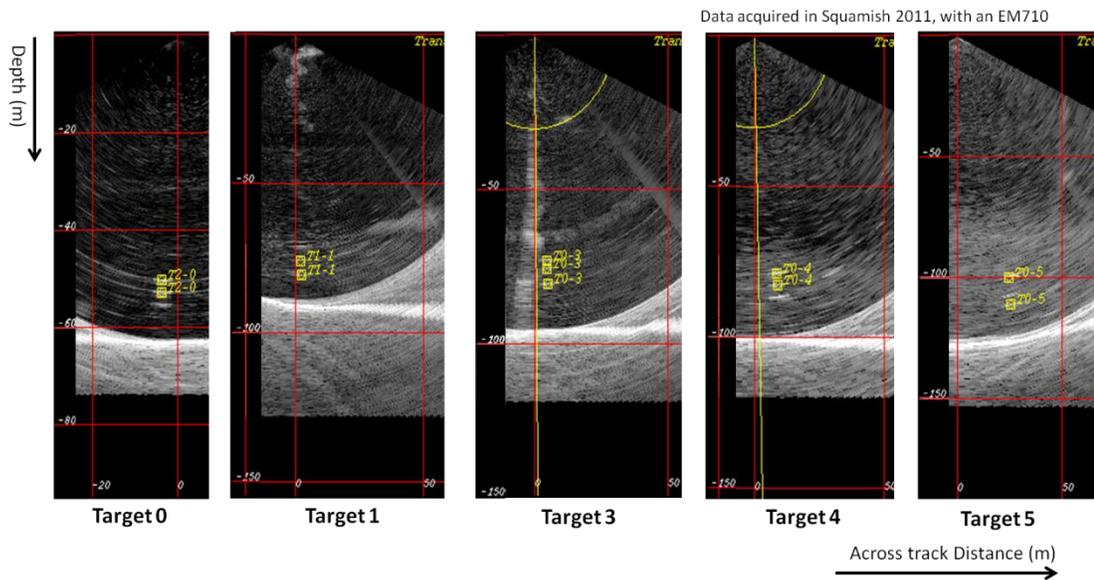
Figure 5.9 – Target labeling (file dependency) - remaining targets used

Note some targets have only 2 pieces marked because the 3rd one is in a different swath.

5.4 Use of object detection for examining fish and fish school geometry

As all features are detected, fish schools, and even isolated fish can also be detected. Figure 5.10 is an example of EM710 data showing both a fish school and an isolated fish (or small fish school with respect to the sonar resolution) moving along several swaths. Figure 5.11 shows the isolated fish time series (B) and the beam angle (C) intensity plots, while Figure 5.12 shows the same information for the fish school. Figure 5.13 shows along track intensity plots for both the isolated fish and fish school for comparison.

The fish's imaging pattern is seen across the swath as shown by the side lobes, and it can also be seen in the intensity plot (Figure 5.11C). The beam pattern of a small isolated fish should be similar to the theoretical single point detection in the water column, and this one closely resembles it. The main lobe beam width effect is always present across swath and it matches the effective calculated beam pattern (red) and is shown in the same plot. As to the side lobes, they are mixed with water column noise but still present.

Fish schools commonly imaged in Squamish usually appear as a single detection, because they appear as a large homogeneous object without interspaced bright point scatterers. This effect was explained in step 4, section 4.2.4.2. Figure 5.10 and Figure 5.12 show this effect, as the isolated fish merges into the fish school, it's echo disappears as it becomes part of the large homogeneous object that the fish school is. The common range arc can be seen more clearly in a fish school because the object is larger in the range axis as shown in Figure 5.10. The effect of main lobe beam width can be pointed out in Figure 5.12C but this time the scattering width shown by the data (blue) is much

145

larger than the calculated effective beam width (red). This effect is seen every time the object is larger than the effective beam width. The object itself will always scatter intensity values close to the peak intensity of the beam pattern. This is easily explained by the boresite of several beams hitting the object. The decay in intensity appears, reflecting the object's actual angular width, when the object is hit by the main lobe of the beam, but no longer it's boresite as explained in Chapter 2. This explains why, small objects, with respect to effective beam width, (like isolated fish) appear with a similar beam width to the one calculated in step 5 (beam pattern match filter). Opposing this, large objects, like fish schools, will show an angular scattering width larger than the calculated one. This was the main reason to have the match filter process (step 5) rejecting LIMs only when the beam pattern is smaller than the calculated effective beam pattern, as was shown earlier with noise (Section 5.1). Analyzing the side lobes of the fish school, they usually are also shown clearly in both water column image and intensity plot (Figure 5.12C), as their intensity is above the water column noise values.
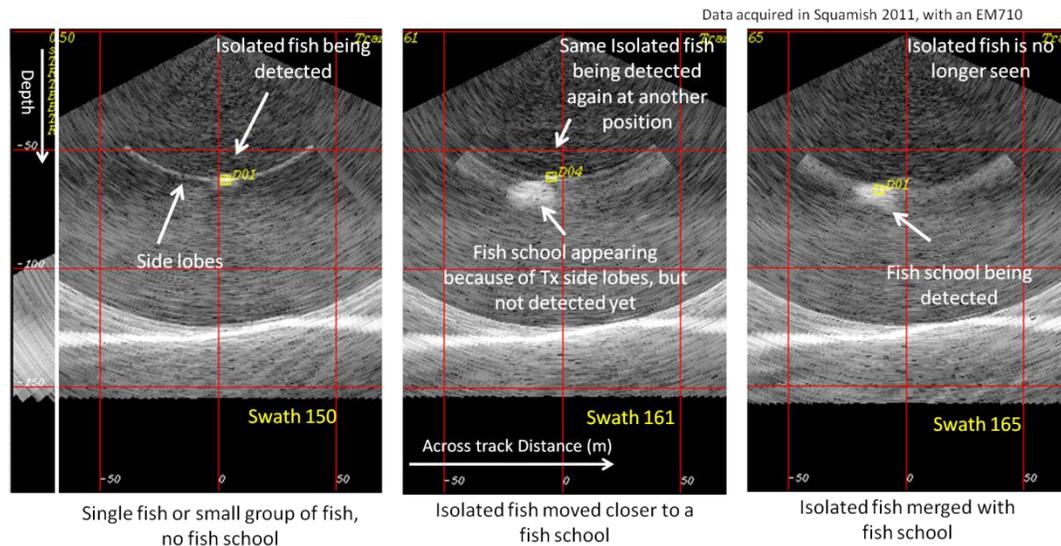
Figure 5.10 - Figure showing isolated fish merging with fish school

The echo called 'isolated fish' was followed for several swaths moving in the direction of the fish school, disappearing once mixed with the fish school, to reappear again later, leaving the fish school.

Along track, the main lobe beam width detection pattern is also present for both cases. Figure 5.13A shows the water column along track image where the side lobes of the fish school are clearly present showing the hyperbolic echo effect. B) and C) show the along track plots for the isolated fish and the fish school. The same comparison used across track for the main lobe beam width is applied here along track. Now the beam patterns of both objects are larger than the calculated effective beam pattern in step 5. But they still show differently. The fish school has what can be called a constant intensity pattern along track defining its peak, showing the large along track extent object it is. The isolated fish shows the intensity increasing from swath 140 to the peak in swath 150, clearly not matching the calculated effective beam pattern. A sudden drop is seen after

147

the peak, due to the change in frequency (which alternates every other value due to the dual swath geometry), and as can be seen along track (observed data) the frequency used at this specific swath has always lower intensity values. Besides that, after the peak, the beam pattern decays at a rate nearly matching the calculated effective beam pattern. The beam pattern seen for this "isolated fish" shows that it may actually be a small fish school with different size fishes rather than an isolated fish, or simply that it was moving in the same direction as the vessel making the aft beam pattern stretch and showing the expected beam pattern forward as the fish changed direction to meet the fish school.

Figure 5.14 and Figure 5.15 show a small object with respect to multibeam imaging geometry, possibly a single fish whose intensity plots show a close match of its scattering pattern and the calculated effective beam pattern.
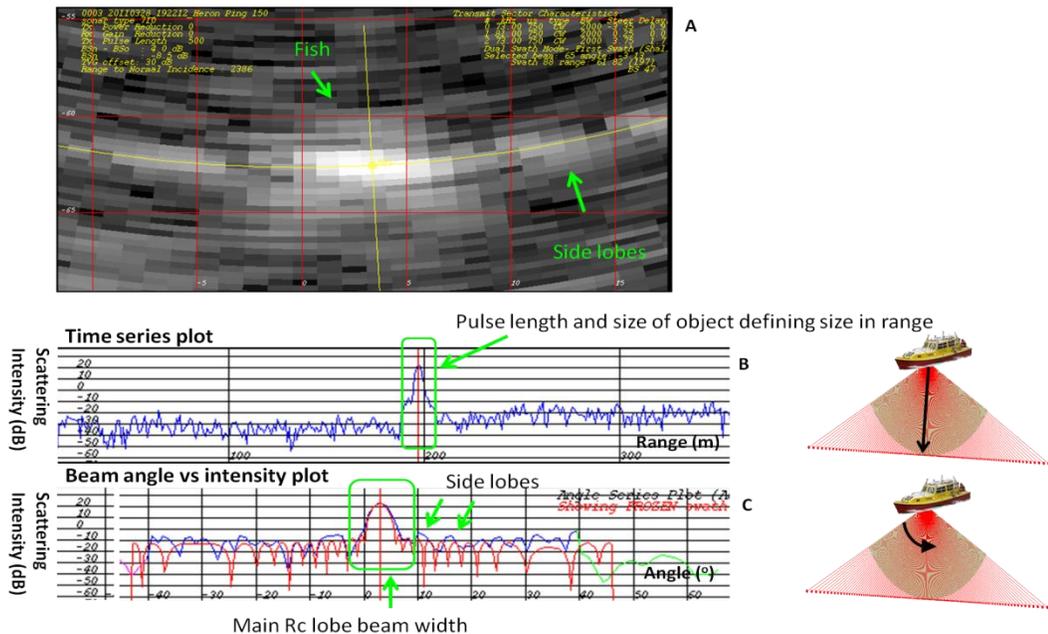
Figure 5.11 - Isolated fish Rc main lobe beam width

Note that the isolated fish is much smaller in range than the fish school. (Note that values need -30dB offset applied)

148
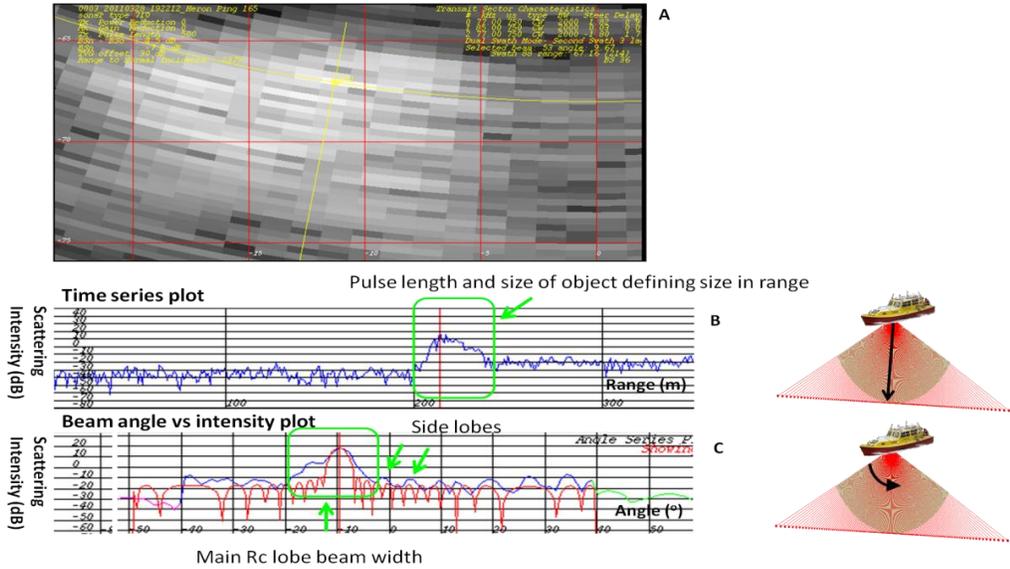
Figure 5.12 - Fish school fish Rc main lobe beam width

Note that the fish school has a wider dimension (range) and angular width (across track size) than the isolated fish. (Note that values need -30dB offset applied)
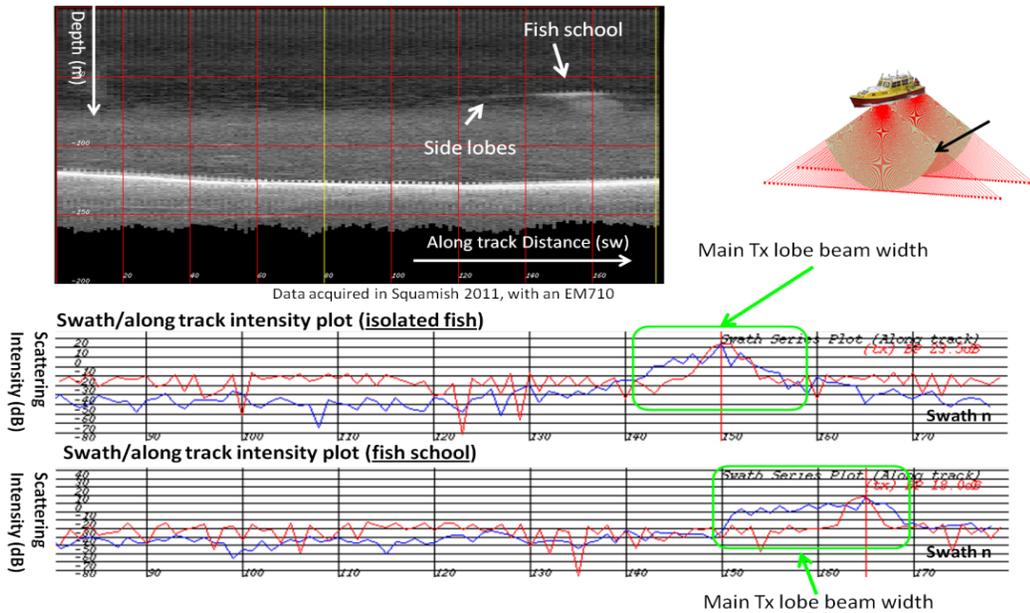
Figure 5.13 - Isolated fish and Fish school Tx main lobe beam width

Note that the fish school is much larger in swaths (along track size) than the isolated fish. (Note that values need -30dB offset applied)

Data acquired in Squamish 2011, with an EM710
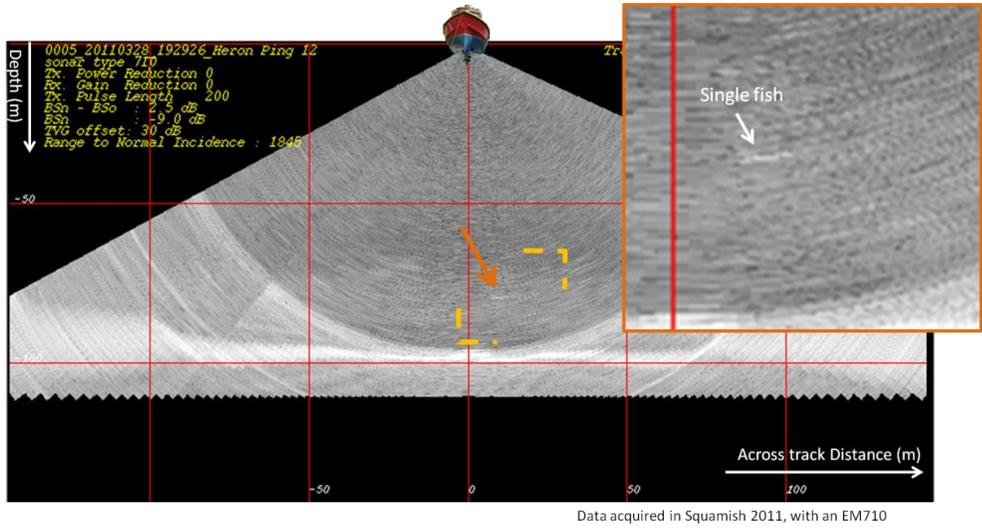
Figure 5.14 - Single fish detection in the water column 2D image

Note the size and backscatter can easily be confused with water column background noise.
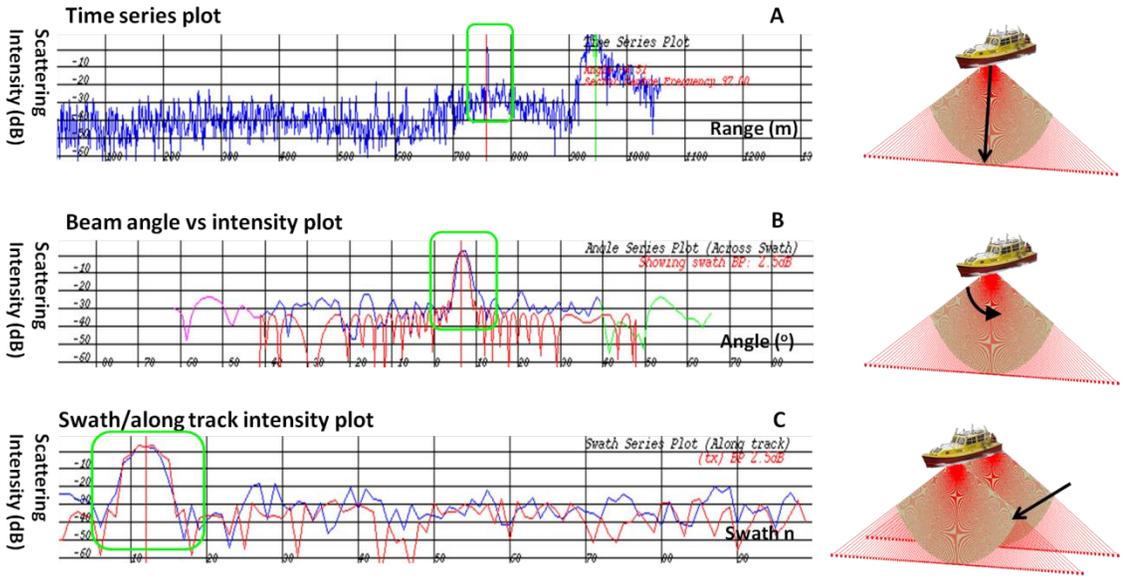
Figure 5.15 - Single fish beam pattern shown in intensity plots

Plot A shows the fish being detected by only 1 sample (equivalent to 1 pulse length), plot B shows the Rc main lobe beam width (knowing beam spacing), and plot C shows Tx main lobe beam width (using speed to know shot (ping) spacing). (Note that values need -30dB offset applied)

150

5.5 Use of algorithm to identify gas plumes

Another feature that is captured when using this algorithm is gas plumes. Gas plumes, with a variable density of bubbles frequently appear in the water column image for the Squamish data. As gas bubbles are effectively objects moving at low speed, the object imaging pattern can still be applied to those bubbles. Using the algorithm on Squamish data, revealed the existence of some gas plumes as can be seen in Figure 5.16. Each one of the bubble groups (that fall inside the 3D cube area – step 4) that were detected (above threshold match pattern) shows the main beam width effect across swath in the water column image and in the intensity plots as well (Figure 5.17). As the object is large in the range axis, it does not appear as a peak in A), it shows as a group of peaks revealing the detection of several objects rather than a single one. Plot B shows the match between the water column data (blue) that shows the gas plume and the calculated effective beam pattern (red) – step 5. Along track (plot C) the main lobe beam width is still present. Because the backscattered intensity is so low, the side lobe effect is not seen as it gets mixed with the noise (Figure 5.16 C). Note also that the number of detections for a gas plume, depends on the number of bubble groups (inside the 3D cube area – step 4) detected but also on its spacing (or homogeneity) (Figure 5.16 B). Sectors can also be a problem when detecting gas plumes. As said before, detecting targets across sectors seems to be a near impossible task. If sectors are transmitted with the same tilt angle, gas plumes can be shown across sectors. Otherwise they just seem to vanish in the sector boundary. This shows the problem of sectors not matching as it was explained before (Section 2.5, Figure 4.2). Note, however, that the algorithm will still mark the gas plumes

in their correct position and they will line up in a 3D image, assuming they are still

detected on different sectors.
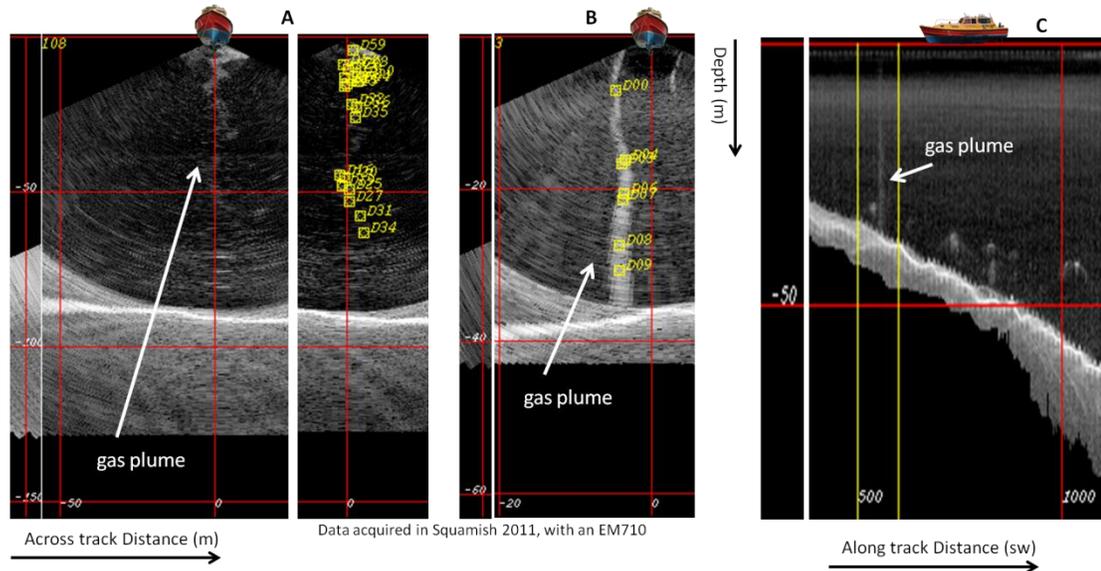
Figure 5.16 - Figure showing some gas plume examples

In (A) a gas plume is shown at the left, and the same gas plume is show at the right but showing the

detections found. In (B) a much more homogeneous gas plume is detected. (C) shows a gas plume

seen along track.
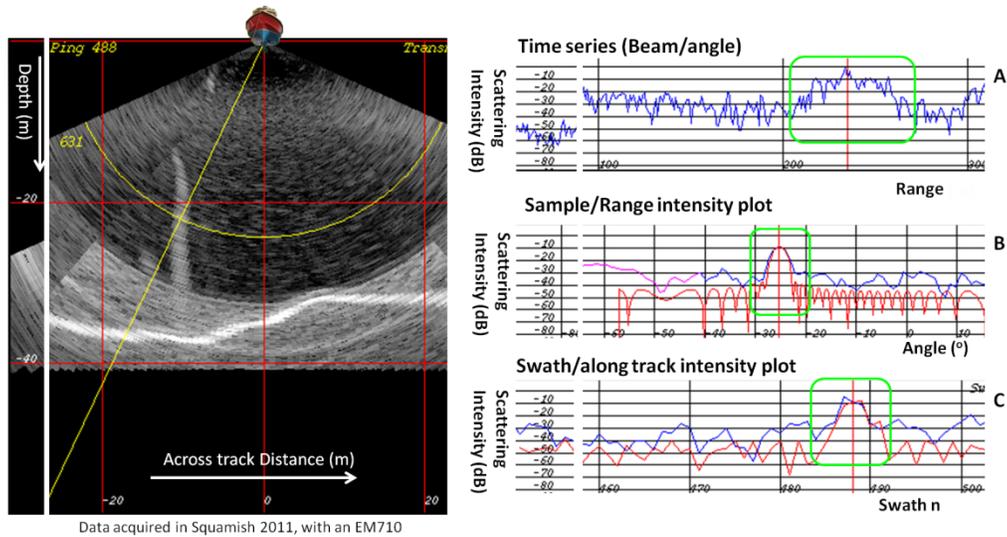
Figure 5.17 - Figure showing intensity plots of a detected gas plume.

Note that the gas plume shows the expected beam pattern in the 3 axis, Tx and Rc beam width in plot B and C, and a pattern larger than the pulse length in plot A. (Note that values need -30dB offset applied)

5.6 Use of algorithm to detect oceanographic moorings

A specific purpose for the use of this algorithm could be the detection of oceanographic moorings. Actually, this search was already being done manually in the ArcticNet program. An operator would sit and analyze every swath of a survey line, searching carefully in the water column image for echoes that would resemble the shape of the desired mooring. A oceanographic mooring is something similar to the targets we used in Squamish. The oceanographer mounts several equipments attached to buoys that will be tied to a strong cable and moored in a specific position where the scientific research will take place. Figure 5.18 shows an example of one buoy with oceanographic equipment. Usually this buoy/scientific equipment set is large and will produce a good

153

echo in the water column making it easier to detect by the operator. As it is a physical object, its scattering pattern should show exactly as expected, pulse length, main lobe, including detection effects and side lobes (if above noise) in transmission and receiving beams. The algorithm identifies each buoy as an object and if the distance between each buoy is known the mooring set can be treated as a target and easily found in the water column image. Figure 5.19 shows a 3D image of a mooring set being detected while looking for it in the ArcticNet program. Those moorings were placed in the Beaufort Sea, and their position roughly recorded. There was no acoustic location system working, nor any surface location buoy. In order to locate them, a MBES survey was used analyzing the water column images to locate them, and safely retrieve them.

Figure 5.18 – An example of an oceanographic buoy
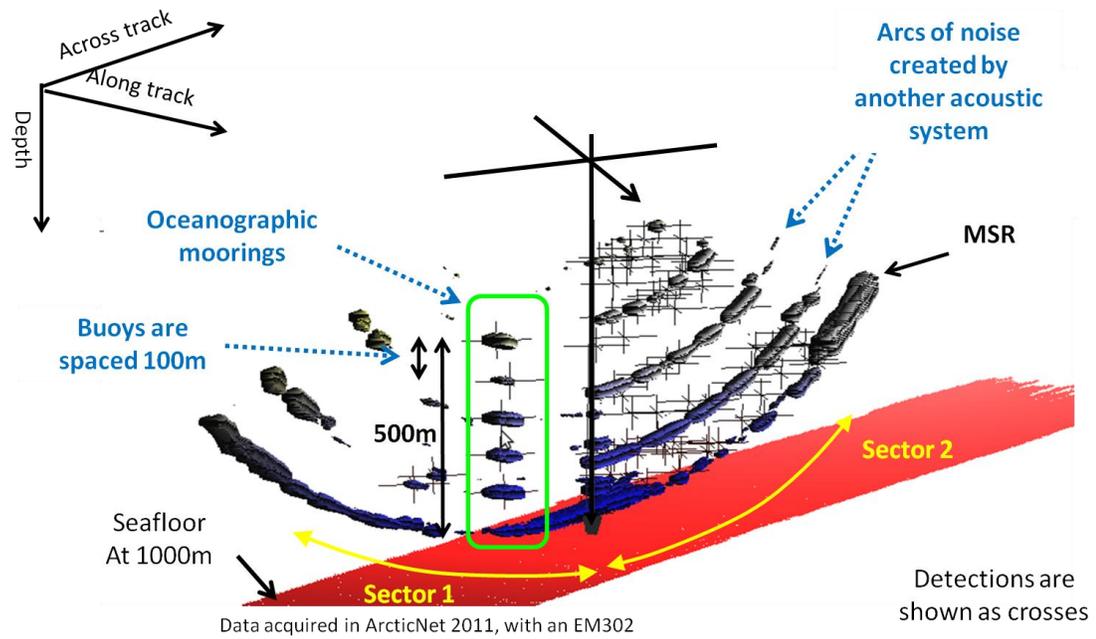
Figure 5.19 - 3D Figure showing mooring detection and presence of noise interfeerence

The scattering pattern is present for every buoy as expected and the main feature to point out is that the mooring set was detected along several swaths (Figure 5.20). This means that each buoy's intensity peak was detected in different positions along track. This effect is probably the result of deep sea currents in the area. The complete mooring set is about 500m in total length, having the buoys separated by about 100m, which makes it easy to understand that the buoys can be pushed by the currents.

Also note the size of the buoy's scattering field across track is about 50m at 70m range and 180m at 860m range.
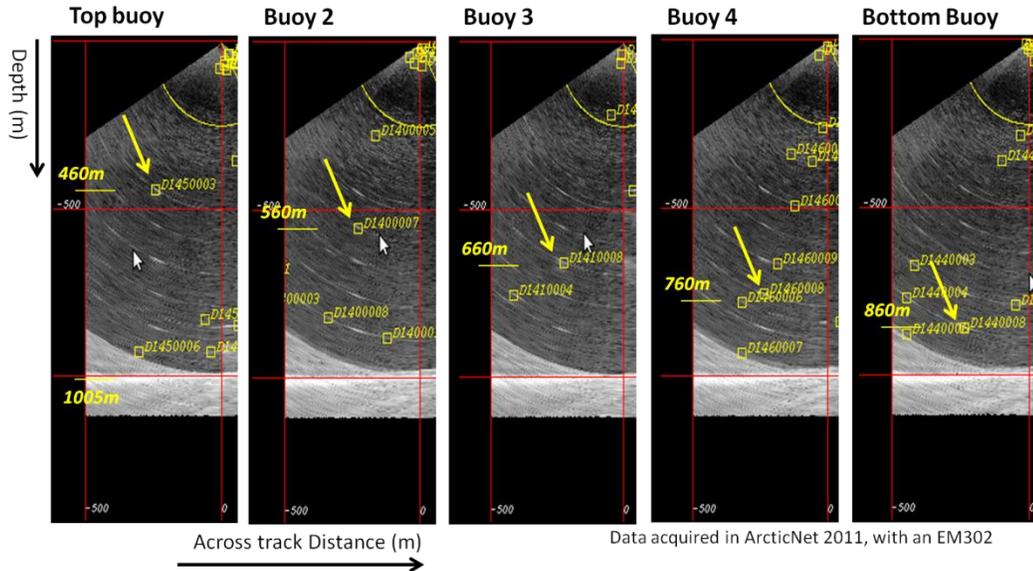
Figure 5.20 – Oceanographic buoys being detected along several swaths

5.7 Algorithm performance on spar-like man made objects

Some tests were also done to see how the algorithm would work when searching for elongate man made structures. As explained before, the algorithm searches for LIMs discarding all neighbour peaks so that only one peak is marked for large objects in the water column. This limits its use when detecting structures. The algorithm actually found every structure piece in the water column, but the number of detections that are found on each structure depend on the data homogeneity as explained in Section 4.2.4.2. An example of a sunken oil platform was given in Figure 4.34.

Spar-like man made structures usually have high scattering characteristics, making side lobes easily appear above background noise. This would make the detection algorithm identify and mark the object in several places along the side lobes if step 5 is

156

not applied. Applying step 5 makes the algorithm mark as an object only the correct echoes excluding the side lobes. However the problem of how often the object is marked along its elongate size still remains. Another issue with man made structures like these is that they may be oblique. This fact will make the side lobes appear over and above the structure complicating the 2D visualization by the human operator. The algorithm will actually mark the structure where it is, although it is hard to understand it visually when looking at the data. But adding all the points in 3D will show the expected structure shape.

Although the algorithm needs changes to better detect structures, another test was done to see the results in a 3D view. As the structure is complex, the search area was limited to one steel bar only. The results are shown in Figure 5.21, and it seems to mark the structure well enough to be perceptible. Although the results are good, the algorithm should be modified in the future for the purpose of detecting man made structures. Including a backtrace of all identified LIMs would help the algorithm identify and mark man made structures at a specified spacing.

Along track
Across track
Depth
Search area limits across track
A
Depth (m)
Along track Distance (m)
Steel bar detected over several swaths
Detections are shown as crosses
Seafloor line
MSR
Data acquired in Gulf of Mexico 2011, with an EM2040
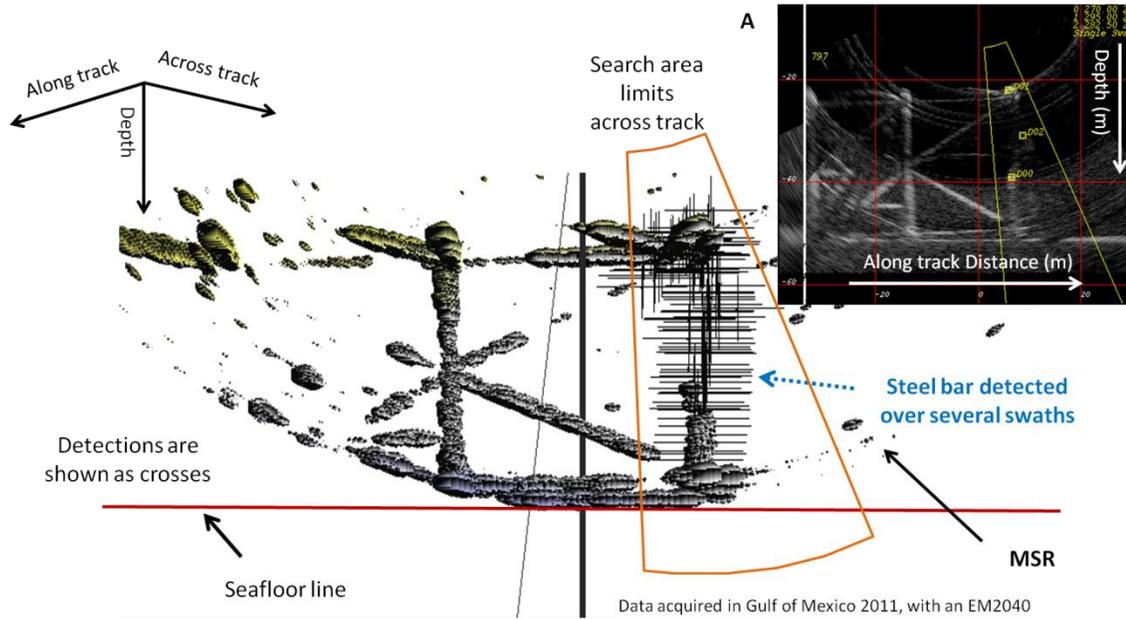
Figure 5.21 - Detecting a sunken oil platform

Figure A shows a 2D view of the sunken platform and the search area delimited by yellow lines trying to detect only the vertical steel post..

6. Howe Sound case study
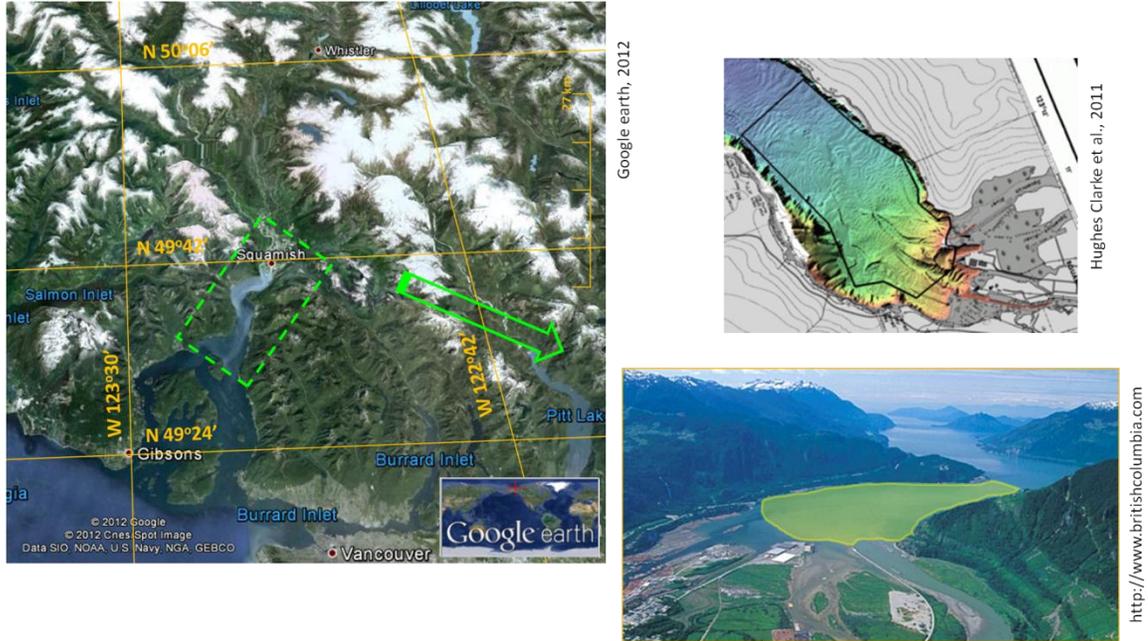
Figure 6.1 - Squamish location and survey area

The survey area was located in the Squamish river pro delta.

As mentioned, this research started with the necessity to track targets in the Squamish Project (Howe Sound, British Columbia) (Figure 6.1, Hughes Clarke et al, 2011, Hughes Clarke et al, 2012), using a Kongsberg EM710 system, so this was the main case study.

The aim of the target component of the Squamish project was to observe whether there was bulk displacement of sediment, rather than progressive movement through current induced bedload sediment transport. The idea for this project came from Paull et al. (2010) who used seabed targets to monitor bulk displacement in a submarine canyon.

They originally had attempted to put current measuring devices on the floor of Monterey canyon to monitor what they assumed would be predominantly bedload and suspended load sediment transport. Those instruments were periodically destroyed and thus they suspected bulk displacement.

A concrete block is too heavy to be moved through conventional bedload transport under any conceivable current (up to at least 10m/s, well above recorded). However, should the seafloor, on which the block is lying move as a solid mass (a landlslide) the block would float along on the surface of the displaced sediment unit (Figure 6.2).

The approach of Paull et al. (2010) was to have concrete blocks with an embedded acoustic transponder for tracking. They did indeed detect displacements but ultimately (after several months) lost the block and associated acoustic instrumentation. The instrumentation was worth about US$20,000 and thus would be prohibitive for the Squamish program.

In Squamish another approach was used, involving a mooring system to place small heavy targets on the sea floor and monitor their displacement by tracking the buoys suspended above them. The mooring system would still have the weight needed for the research purposes and the suspended targets would not only allow the tracking of the targets without the use of expensive instrumentation, but also allow the basal mooring to be tracked even after they are buried.

The targets geometry was explained in Section 3.2, and their placement along three different channels was also shown. The area was surveyed several times and all lines were analyzed using this algorithm. The targets could be located over time and a better view of what happened can be imagined. Figure 6.3 shows the initial location of all targets.
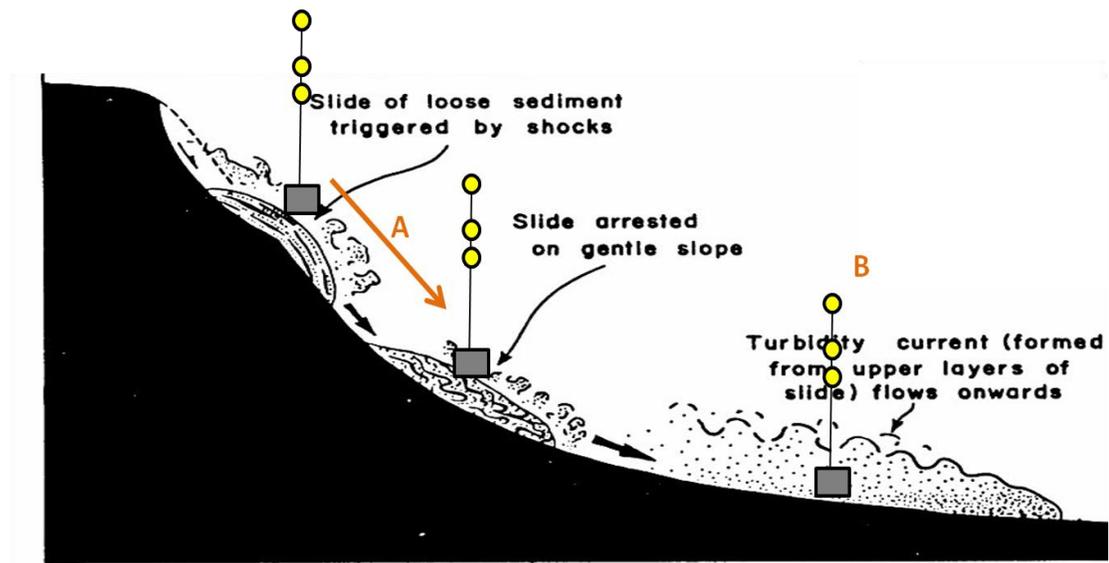
Figure 6.2 – Target movement with sediment displacement

As the underwater landslide occurs, the targets will sit passively (A) on the top of the moving sediment, and their movement will help understand the landslide characteristics. A target that lies only within turbidity current activity (B) shouldn't move. (Edited from Hughes Clarke 2011b)
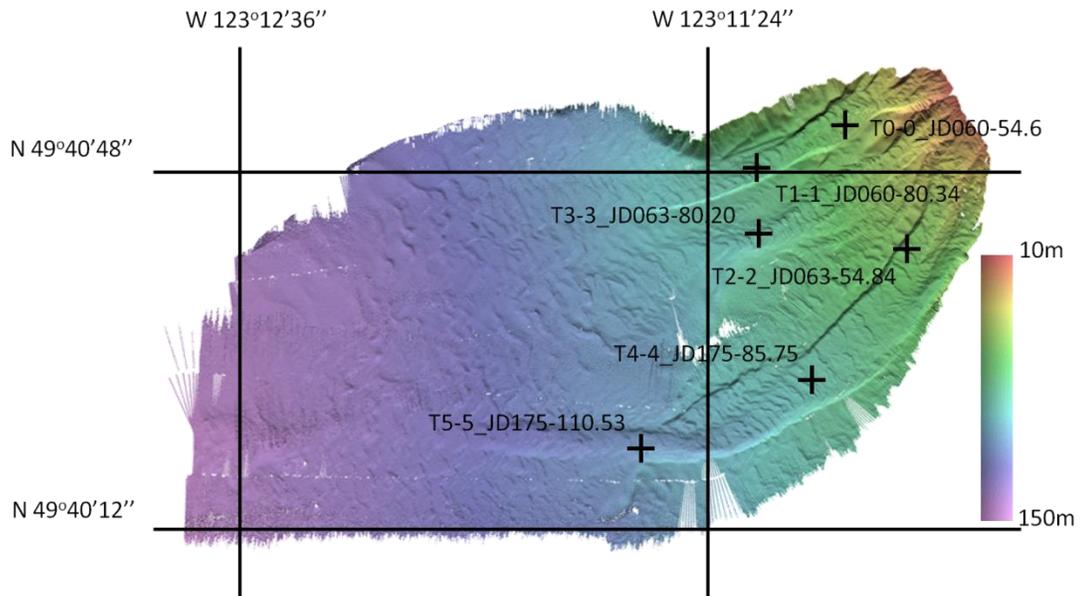
Figure 6.3 - Initial target locations in all 3 actual channels at various distances down slope. The aim was to see if the transport mechanism changed with depth/slope. Targets are labeled using the software notation. The day of the year was added after 'JD' followed by the depth at which the buoy was detected.

The following figures and graphics illustrate the use of the target tracking algorithm on the 6 blocks deployed in the Squamish pro-delta channels (as described earlier). The one complication that needs to be described here is that it is clear that the blocks at the base of the suspended targets were progressively buried in the channel floors (even while still being laterally displaced). This complicated the step 7 where a known distance off the seafloor is assumed. The algorithm was adapted to actually monitor the remaining elevation between the lowest suspended target and the current sediment water interface.

The example shown here is about target 0, which was placed at a depth = 54.60 in March 1st 2011 (Figure 6.3), and in June 24th 2011 it was detected away from the initial

162

position at a depth = 68.48 (Figure 6.4). In a quick analysis we can say the target moved 145m in 115 days. Looking at the results presented in Figure 6.4 and Figure 6.5 we can see that two large discrete events must have happened between the surveys on days 137 and 138 and between days 161 and 164. Between those events no gradual displacement was recorded. Slight variations in position (±2m) can easily be explained by minor current displacement of the upper buoy. Finally, target 0 couldn't be detected after day 181 meaning a large scale event may have happened that either moved the target away from the survey lines or buried it. Analyzing Figure 6.6 we also notice almost all targets were partially buried during the time period from day 60 to day 181. Target 0 actually got reexposed at the sediment water interface again on day 164. Finally targets 0 and 1 both disappeared on days 181 and 137 respectively not to be detected again although monitored up to the end of the survey (day 234).

A plot with the total movement of each target, from day 60 to day 181 is presented in Figure 6.7. And a map with each target's initial location and location at day 181 is presented in Figure 6.8 for completeness.
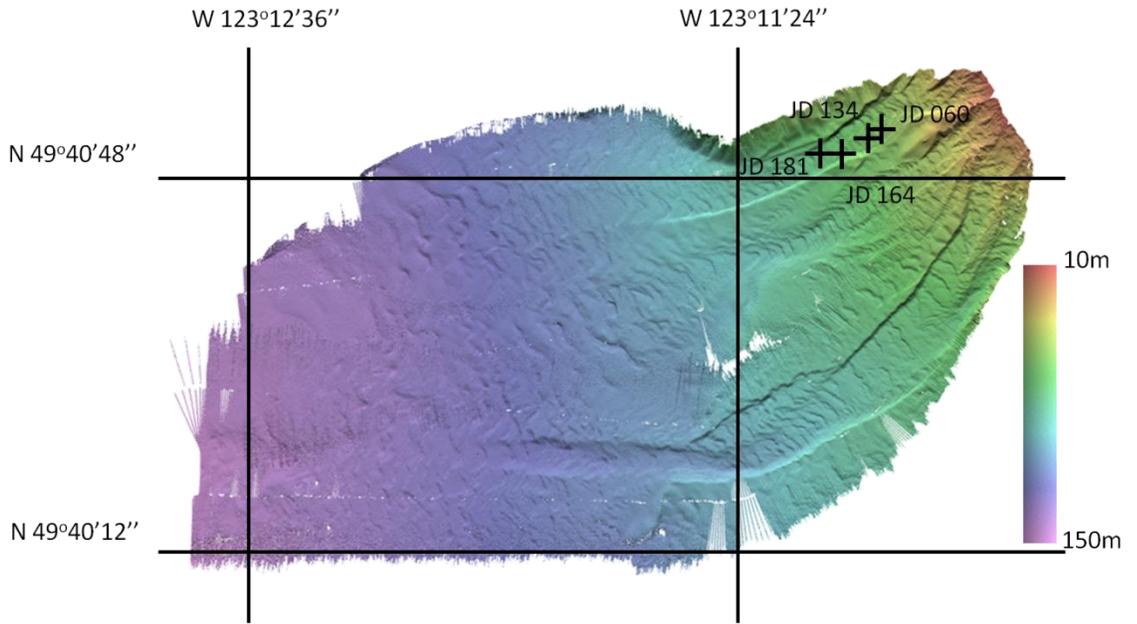
Figure 6.4 Target 0 movement map, showing progressive displacement along the north channel axis.
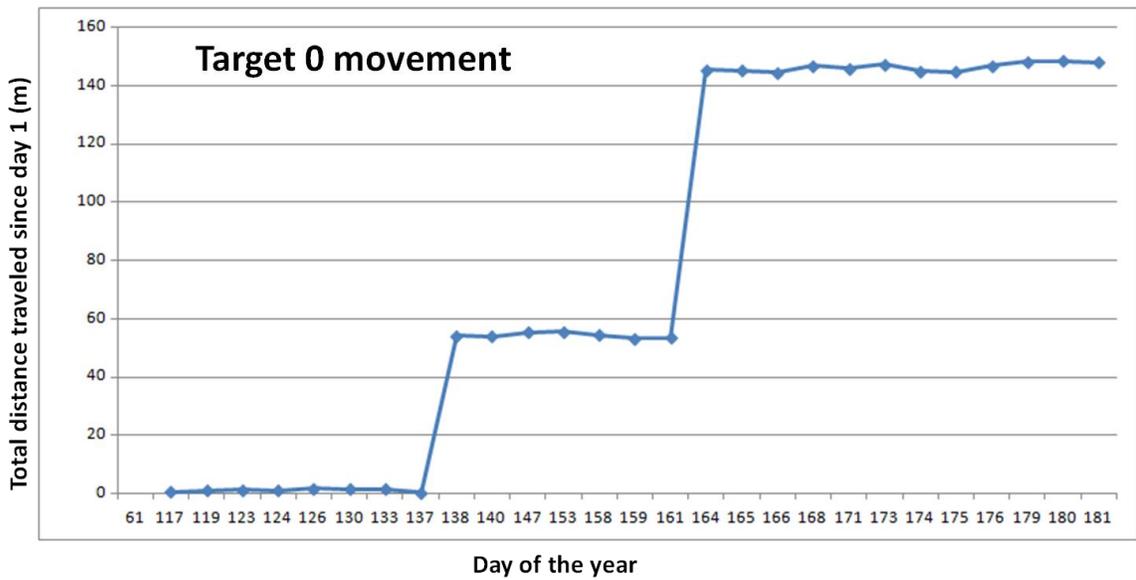
Figure 6.5 - Target 0 registered movement from begining of survey (day 60)
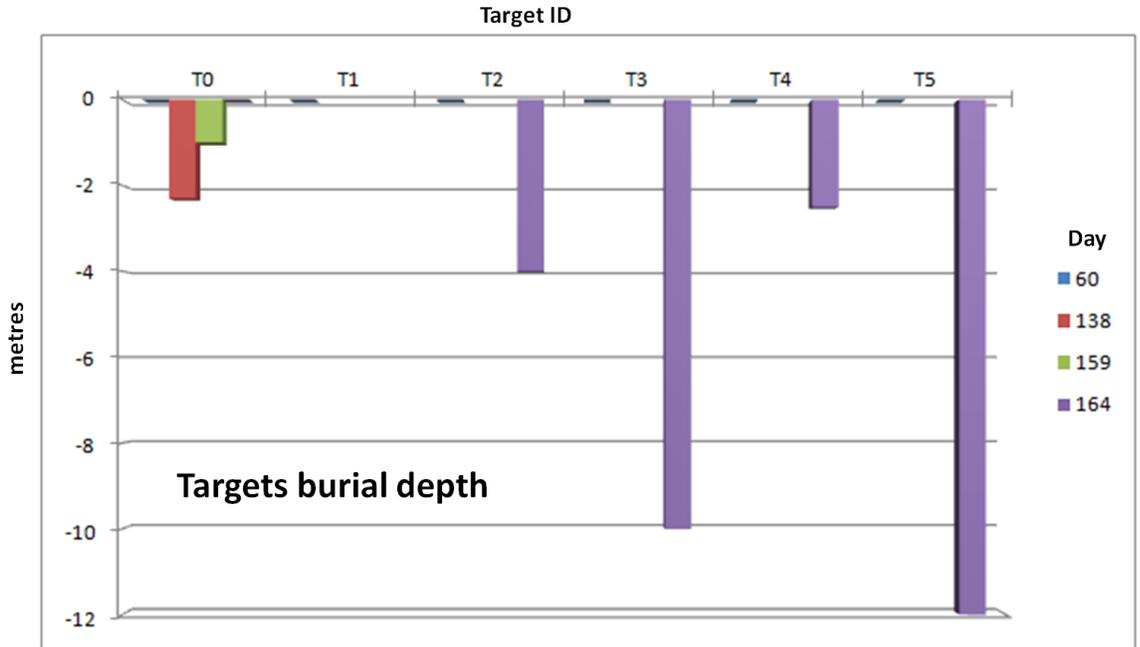
Figure 6.6 - Distance at which each target base was buried during part of the survey period (day 60 to day 181)
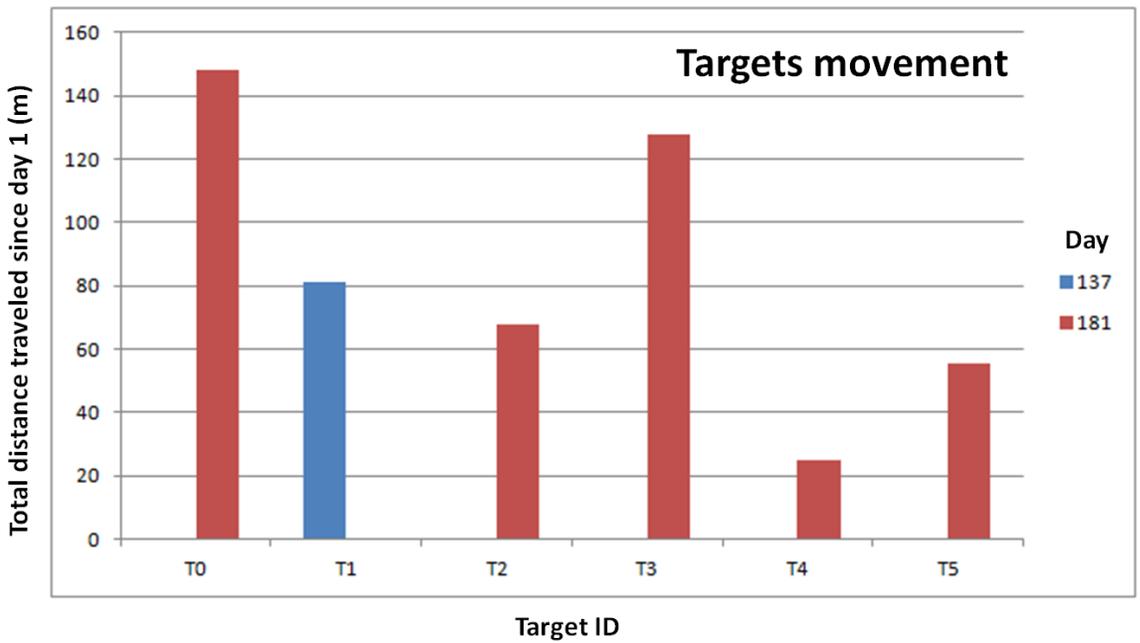
Figure 6.7 - Total distance traveled by each target from day 60 to day 181

165
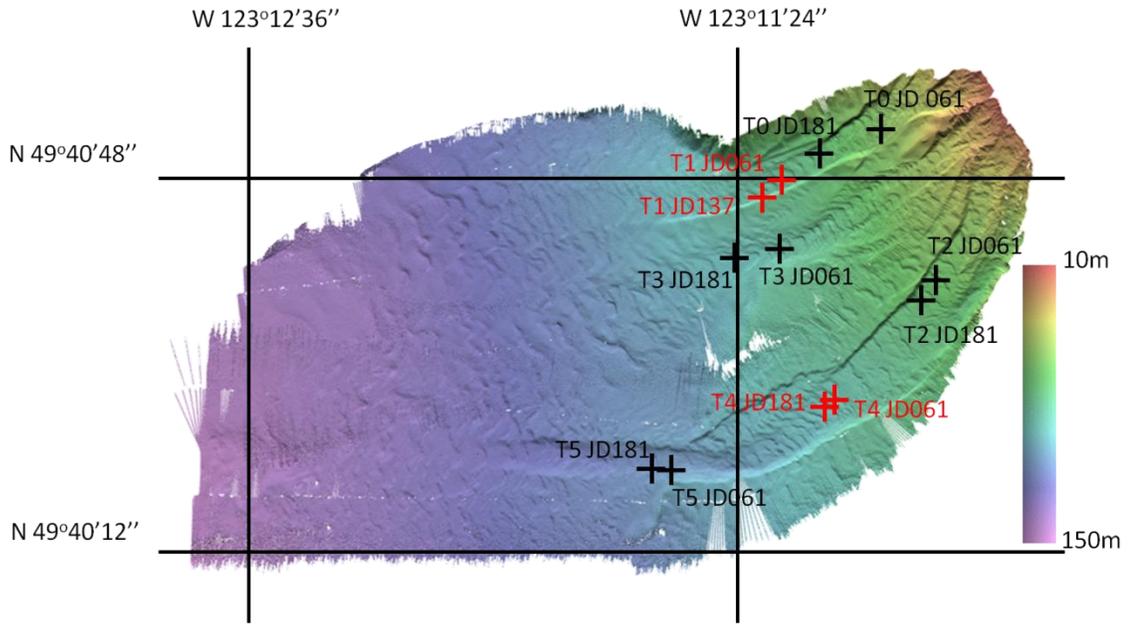
Figure 6.8 - Target initial position and position at day 181

All the analysis done in Squamish using the algorithm was verified manually by a human operator. In all the lines analyzed by the algorithm the target was always found if it was present, with one exception. This exception actually proved the algorithm was working properly. The failure is explained by the fact that the target base was buried, changing the target cluster geometry. With the target geometry being different, the algorithm could not find it. Once this fact was accounted for in the targets shape file the problem was fixed.

All the lines where the target was not found were verified carefully by an experienced operator. And all the results returned by the algorithm were verified to check if they were correct. From the results obtained it was found that in specific situations the algorithm may return fake results for target locations. This situation was verified

166

sporadically, whenever specific detections were found with exactly the same geometry as the one defining the targets. The distance to the seafloor option removes most of these cases, but some still remain. In this case it only happened with gas plumes that show a large amount of vertically aligned detections. Identifying the gas plumes and excluding targets at the same location could fix this problem.

Some comparison tests were done with manual search for targets by a human operator. An example of one 45 min survey line is used to illustrate the improvement achieved with the use of this tool. The line, surveyed with an EM710, is 4.2NM long, and covers an area with depths ranging from 20m to 160m. A trained human operator takes about 40min to search the survey line carefully and identify every target within it and still the positioning needs to be done. The algorithm does the same in 3min, locating and positioning every desired target giving the result in a list. It needs 1 extra minute every time the survey parameters change (acquisition mode) as it needs to do some new pre-calculations for the beam pattern. In addition to this it was found that the algorithm can detect faint targets in the background noise that are commonly missed by the operator, as they are not clearly visible. Also from the results, it was seen that the operator can easily miss the exact position of the targets, marking them erroneously while analyzing the 3D volume.

The brief analysis presented herein clearly illustrates the utility of this tool. Not only does it require less time, but it also does not need the use of an operator. It is possible to simply set the parameters and run the algorithm on all survey lines. It is now being used as part of the active research program looking at landslide mechanisms in Squamish.

7. Conclusions

The aim of this thesis was to create an algorithm to locate specific target geometries (clusters of objects) in the water column data and position them accurately. The intention is to use Bathymetric MBES high resolution and accurate positioning characteristics to locate and position specific objects. The purpose of this algorithm is to reduce the time consuming manual task of looking for specific objects in the mid water range. This new algorithm should be developed and integrated as a new toolkit in the OMG software. In the end the algorithm is to be used in the Squamish project to monitor the displacement of targets used to follow the development of river delta landslides. Potential future uses include oceanographic mooring detection and better discrimination of submerged man made spar like objects.

7.1 Summary

Detecting objects in the water column usually implies a tiresome manual task that is very susceptible to errors. The trained operator has to run through each swath of all survey lines searching for a specific known pattern until the object is found so that it can then be positioned. If tracking for the object movement or when searching for objects in unknown positions the amount of work needed grows to large proportions. Using the algorithm the user will now only need to define the geometry of the targets and feed the algorithm with the survey lines that can contain those targets.

To search for detections the algorithm needs to be aware of the imaging scattering pattern around a single suspended point in the water column. This scattering pattern, that

characterizes water column detections, is dependent on several factors, the most important ones being the pulse length, and effective transmission and receiver beam widths. The algorithm calculates these values, and searches all local intensity maxima's (LIM's) for the targets using a pattern match filter to verify the existence of the expected scattering pattern. Then a 3D geometric filter is used to specifically search for each desired target cluster, using the target geometry defined by the user. Finally, using another toolkit from OMG software, a list of all targets found is output stating their position and the survey line in which they were found.

Using this detection algorithm, specific objects can effectively be detected and accurately positioned in a 3D reference frame just by running the algorithm over the whole survey.

There is a large improvement in time as was expected, and the user is not involved in the search process anymore, saving time and human resources in the scientific research. Also, comparing the algorithm reliability with manual search reliability, there were several cases where the algorithm detected the targets where a human would probably have not found them. Examples of those are targets mixed with fish, noise and gas plumes. A closer look to the water column image, and the target position actually confirms the existence of a target.

The algorithm still needs improvement as some mistracking may occur in some situations. Occasionally, false targets are reported, as the bottom part of gas plumes may be classified as targets if the detections match the target cluster geometry. Also, if the background noise increases, the user may need to define a lower threshold multiplier as the automatic calculated values may be too high for the target's scattering intensity. No

other mistracking was detected and the targets were detected every time the algorithm was run on a line that contains targets. As all the tests were done with targets being detected in the central sector, there is no data about target detection to say the algorithm is fully reliable in the outer sectors. However, the algorithm accomplishes regular object detection in the outer sectors (gas plumes, fish schools).

7.2 Limitations and Future Work

With the development of the algorithm some limitations were found and as the algorithm was tested other limitations were registered. Water column data imposes some limitations to target detection, the minimum slant range (MSR) limit and the sector boundary gap in data were explained and the algorithm only searches for targets above the MSR and in sectors separately.

As to the algorithm itself, some limitations must be pointed out. Not knowing exactly what side lobe suppression was used, limits the replication of the beam's beam pattern and therefore limits the correct use the pattern match filter. This is most critical for correct side lobe location and prediction. In practice, usually only the main lobe shape is compared. Although just using LIM detection seems to produce very good results, some false detections are still found (for example other system's noise interference), requiring the extra step of using a pattern match filter. The pattern match filter used tries to replicate the beam pattern in a simplistic way and matches only the main lobe beam width.

Another limitation is the use of planes in the 3D cube search for LIMs. Higher intensity LIM's belonging to the same object may actually lie within the remaining area of the cube and the full 3D cube search could produce better results if accounting for that also. This improvement would be at the expense of greater processing time.

Still analyzing the 3D cube search, the effect of bringing together similar LIM's does not allow the algorithm to mark large homogeneous structures all along the structure, detecting one single LIM in the highest peak intensity as explained before. Although large structures are still detected, the algorithm may not mark the structure with detections spaced at the expected distance of half the cube size. When large groups of intensities have their peaks above the threshold (large structures) the algorithm will mark only the highest peaks on each group defined between troughs of intensities.

Knowing this limitations, and even though it produced very good results when looking for targets in the Squamish Project some improvements may be done in the developed algorithm.

- Add the capacity of using a top intensity limit also when searching for targets. If the user knows exactly which intensity response to expect from the targets, a top intensity limit could be used to exclude higher intensity objects and speed up the detection process.

- Improve the geographic search area definition, allowing the use of just swaths of a line in an area.

- Recognize the correct side lobe suppression and modify the 3D Pattern Match filter to also match the side lobes.

- Improve the 3D Target Geometric Match Filter to also use angles when searching for specific targets.

- Add a new calculation method to the algorithm, allowing the calculation of the position of the targets more accurately, as the algorithm may suggest the target lies between beams rather than exactly on one.

Despite the fact that initially the development of a method to track targets in the mid water range was solely aimed for the Squamish Project, new capabilities arose as the results from the tests were being analyzed. Using the same approach to water column detection, new strategies can be studied to:

- Automatically position gas plumes as well as possibly characterize their density and direction.

- Accomplish man made structure detection, like ships and ship masts that usually are mistracked by traditional bottom detection algorithms.

- Achieve automatic systematic noise detection and design characterization methods.

7.3 Recommendations

More tests should be performed. Using other data sets and other systems would help understand how the algorithm behaves in different situations.

Although the algorithm allows the user to define most boundary values (3D cube size, threshold value, etc…) default values should be used always. This capacity was included mostly for testing purposes.

Correct settings should be used for surveys where the main purpose is to detect mid water targets. Equiangular beam coverage, and most appropriate acquisition mode depending on the ratio between target backscatter and background noise.

Optimizing weak volume scatterers may require longer pulse lengths than would be the default for bottom mapping.

Bibliography

Beaudoin J., (2011). "*Water column targets OMG routines*", Unpublished

Calise, L., Knutsen, T., (2012). "*Multifrequency target strength of northern krill (*Meganyctiphanes norvegica*) swimming horizontally*", ICES Journal of Marine Science, 69: 119–130.

Conti, S., Demera, D., Brierleyb, A., (2005). "*Broad-bandwidth, sound scattering, and absorption from krill (Meganyctiphanes norvegica), mysids (Praunus flexuosus and Neomysis integer), and shrimp (Crangon crangon)*", ICES Journal of Marine Science 62, Pag. 956-965.

C&C Technologies, (2011). "*World DGNSS C-NAV 3050*", C&C Technologies Inc., Lafayette, USA.

Everson, I, (2000). "*Krill: Biology, Ecology and Fisheries*", Blackwell Science Ltd, USA

Gallaudet, T., de Moustiera, C., (2003). "*High-frequency volume and boundary acoustic backscatter fluctuations in shallow water*", Journal of the Acoustical Society of America, Vol. 114, No. 2, August 2003. pp. 707-725.

Gardner, J.V. , Malik, M.A., Walker, S., (2009). "*Plume 1400 Meters High Discovered at the Seafloor off the Northern California Margin*", EOS Transactions, American Geophysical Union, v. 90, 1p. Journal Article.

Gerlotto, F., Fréon, P., Soria, (1999). "*From two dimensions to three: the use of multibeam sonar for a new approach in fisheries acoustics*", Can. J. Fish. Aquat. Sci. 56: 6–12.

Hughes Clarke, J. E. (2006). "*Applications of multibeam water column imaging for hydrographic survey*". Hydrographic Journal, (120), 3-14.

Hughes Clarke, J.E., Lamplugh, M., Czotter, K., (2006a). "*Multibeam Water Column Imaging : Improved Wreck Least-Depth Determination*", Canadian Hydrographic Conference 2006, Halifax.

Hughes Clarke, J.E., Brucker, S, Czotter, K., (2006b). "*Improved Definition of Wreck Superstructure using Multibeam Water Column Imaging*", Lighthouse, Journal of the Canadian Hydrographic Association, Edition No. 68.

Hughes Clarke, J.E. (2011a). "*Lecture notes of Imaging and Mapping II*", Department of Geodesy and Geomatics Engineering, University of New Brunswick, Fredericton, N.B., Canada.

Hughes Clarke, J.E. (2011b). "*Lecture notes of Marine Geology*", Department of Geodesy and Geomatics Engineering, University of New Brunswick, Fredericton, N.B., Canada.

Hughes Clarke, J.E., Brucker, S., Muggah, J., Church, I., Cartwright, D., (2011). "*The Squamish Delta Repetitive Survey Program: A simultaneous investigation of prodeltaic sedimentation and integrated system accuracy*" , U.S. Hydrographic Conference 2011.

Hughes Clarke, J.E., S. Brucker, J. Muggah, I. Church, D. Cartwright, P. Kuus, T. Hamilton, D. Pratomo and B. Eisan, (2012a), "*The Squamish ProDelta: Monitoring Active Landslides and TurbidityCurrents*", Canadian Hydrographic Conference 2012, Proceedings, 15pp.

Hughes Clarke, J.E., S. Brucker, J. Muggah, T. Hamilton, D. Cartwright, I. Church and P. Kuus, (2012b), "*Temporal progression and spatial extent of mass wasting events on the Squamish prodelta slope*", Landslides and Engineered Slopes: Protecting Society through Improved Understanding - Eberhardt et al. (eds) , Taylor and Francis Group, ISBN 978-0-415-62123-6, p.1091-1096..

Jones, C.D., (2003), "*Water-column measurements of hydrothermal vent flow and particulate concentration using multibeam sonar*", Journal of the Acoustical Society of America 114, 2300–2301.

Kongsberg Maritime – Simrad, (2006). "*Simrad MS70 – Scientific multibeam sonar system*", Kongsberg Maritime AS - Simrad, Horten Norway.

Kongsberg Maritime – Simrad, (2006). "*EK60 Scientific sounder with multiple frequency operation*", Kongsberg Maritime AS - Simrad, Horten Norway.

Kongsberg Maritime, (2006). "*EM3002 Multibeam echo sounder*", Kongsberg Maritime AS, Horten Norway.

Kongsberg Maritime, (2006). "*EM302 30 Khz Multibeam echo sounder*", Kongsberg Maritime AS, Horten Norway.

Kongsberg Maritime, (2006). "*Simrad ME70 - Scientific multibeam echo sounder system*", Kongsberg Maritime AS, Horten Norway.

Kongsberg Maritime – Simrad, (2009). "*Simrad SX90*", Kongsberg Maritime AS - Simrad, Horten Norway.

Kongsberg Maritime, (2009). "*The hydrographic product family Sound in water reveals the secrets of the deep blue*", Kongsberg Maritime AS, Horten Norway.

Kongsberg Maritime – Simrad, (2011)., "*Simrad scientific systems dedicated to fishery research*", Kongsberg Maritime AS - Simrad, Horten Norway.

Kongsberg Maritime – Simrad, (2011). "*EK60, Scientific echo sounder*", Kongsberg Maritime AS - Simrad, Horten Norway.

Kongsberg Maritime, (2011). "*EM710 Multibeam echo sounder*", Kongsberg Maritime AS, Horten Norway.

Kongsberg Maritime, 2011, "*EM Series Multibeam echo sounders Datagram formats*", Kongsberg Maritime AS, Horten Norway

Kongsberg Maritime, (2012). "*EM2040 Multibeam echo sounder*", Kongsberg Maritime AS, Horten Norway.

Mayer, L.A., Hughes Clarke, J.E., Dijkstra, S. (1997). "*Multibeam sonar: applications in fisheries research*", In Changing Oceans and Changing Fisheries: Environmental Data for Research Management, pp. 79–92. Ed. by G. W. Boehlert, and J. D. Schumacher. NOAA Special Publication NOAA-TM-NMFS-SWFSC.

Paull, C.K., Ussler. W., Caress, D.W., Lundsten, E., Covault, J.A., Maier, K.L., Xu, J. & Augenstein, S., (2010). "*Origins of large crescent-shaped bedforms within the axial channel of Monterey Canyon, offshore California*" Geosphere 6(6): 755–774.

Robertis, A., (2002). "*Small-scale spatial distribution of the euphausiid Euphausia pacifica and overlap with planktivorous fishes*", Journal of Plankton Research, Vol 24, Number 11, pag. 1207-1220.

Van der Werf, A. (2010). "*Mast tracking capabilities of EM3002D using water column imaging*", M.Sc.Eng. thesis, Department of Geodesy and Geomatics Engineering, University of New Brunswick, Fredericton, NB, Canada.

Weber, T., Bradley, D., Culver, R. L., Lyons, A., (2003). "*Inferring the vertical turbulent diffusion coefficient from backscatter measurements with a multibeam sonar*", Journal of the Acoustical Society of America, Vol 114, Issue 4, pp. 2300.

Weber, T., Beaudoin, J., Shedd, B., Malik, Mashkoor A., Jerram, Kevin, Rice, Glen A., Mayer, L.A., (2011). "*Detecting and mapping gas seeps with a deepwater multibeam echosounder*", Subsea and Arctic Leak Detection Symposium, Houston, TX, USA, 8-9 November. Conference Abstract

Appendix A

Although the main aim of the thesis was just to develop the algorithm to locate the targets, the best way to test it would be to have a visual guidance using water column images. Also, it was not practical to have the algorithm developed and tested without having it integrated with other tools to work with multibeam data. Fulfilling these necessities, the algorithm was integrated with the OMG software that has a diverse variety of tools to work with multibeam data, including water column imaging tools. This appendix describes in detail the software design and implementation.

OMG software 'swathed' has a toolkit window where water column images of single swaths are displayed in the polar plot format that are easier to understand at human eyes, as the reference axis are shown in meters. This same water column display tool, also displays intensity plots for a selected beam, and a selected range. In this same tool there is an option to read a target file list, that is associated with each survey line and contains target coordinates, and display the targets in the water column image (Beaudoin, J., 2011 unpublished). These targets can be manually identified in this same water column tool display. Figure A. 1 shows the main window of this tool (WaterColumn analysis toolkit). This water column tool, has several other features including a list of important values about the data being displayed (Figure A. 1) and the capacity to show an along track view of the water column at nadir (Figure A. 2). Swathed itself has several tools that help reading the data and understanding the data (Figure A. 2). Nothing was changed in Swathed, but the WaterColumn Analysis toolkit needed some changes to integrate a tool to search for the targets. The changes were minimal on this subject, only with the introduction of a button 'Target Hunt' that starts the target detection tool (Figure

A. 1). But while using the Target Detection tool other necessities arose and some more changes were done. As part of this thesis development the WaterColumn Analysis toolkit now also features a new along track intensity plot, added to the along beam and across range ones that existed already. This new plot is activated pressing 'p' while the cursor is on top of the lower plot area, and replaces the across range plot. Another improvement is an expansion of the information text that was shown. The tool now shows the beam number and angle being analyzed, and also swath number, range and sample number (Figure A. 1). A handy help menu was also added, showing some of the shortcuts to activate the new features. The help menu is activated by pressing 'h' in the main window. Also, all plots are now visible in white when 'n' is pressed. Both these feature are shown in Figure A. 3. Integrated with the target detection tool, the WaterColumn Analysis tool also shows now the expected beam pattern, across and along track, for the selected swath/beam/range as was shown previously. The implementation also allows the user to freeze the beam pattern and navigate through the date for comparison purposes. Finally a major change was introduced with the Target Detection tool. While using the tool it is possible to show in the main display of the WaterColumn Analysis toolkit the search area being used (Figure A. 5).

The algorithm was coded to use OMG software to get water column data from multibeam specific format files. And also the final geo referencing is done using OMG software built in tools. Final results are stored in the existing target list that is associated with each water column survey line also using already built in tools. Although the object detection tool was integrated in the OMG software, it was developed independently in its core code. It was decided this way to maintain the code tight enough so that any code

bugs would be restricted to a known place. The only link to the OMG code is the input data and the output data. Two new tools were created 'Target detection toolbox' and 'targethunt' using 6 new files. The files 'c_wcpick.c' 'c_wcpick.h' contain the algorithm itself. A small widget box was created to integrate the algorithm with the water column display tool from 'swathed' using 'c_wcl_toolbox.c' and 'c_wcl_toolbox.h' files. These files contain the code to create a widget tool that allows some user definable variables to be changed to adjust the algorithm. It is using this widget that the user decides how to use the algorithm when using the 'swathed' water column display tool.

Data acquired in Squamish 2011, with an EM710
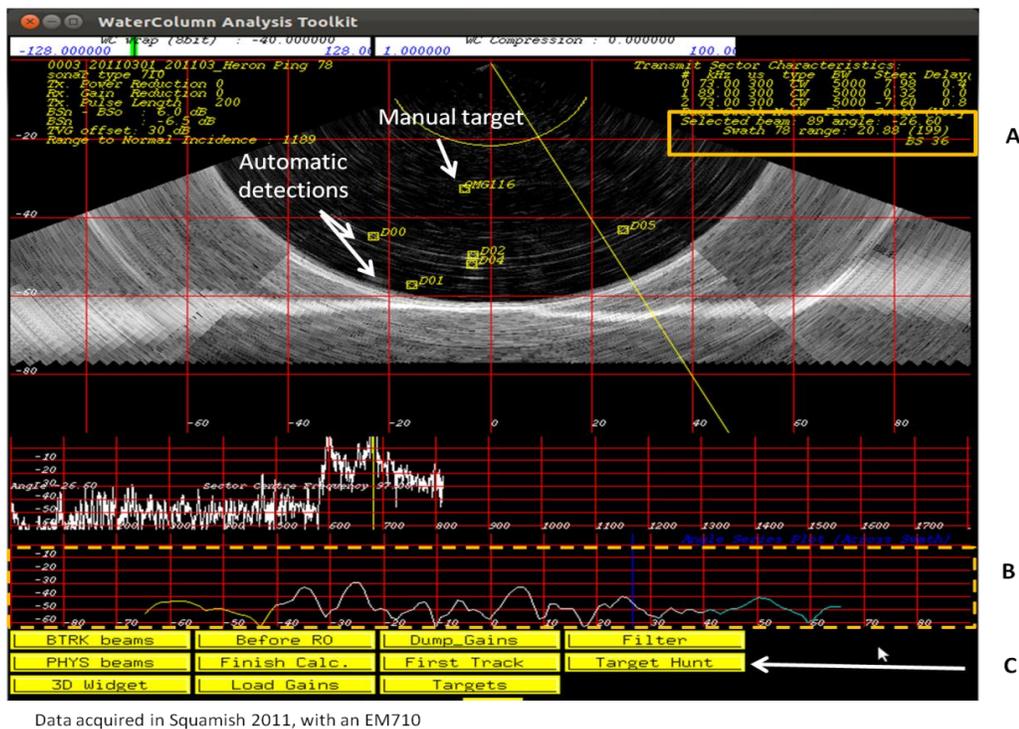
Figure A. 1 - Figure showing swathed water column image

OMG WaterColumn tool displays multiple information, allowing a careful analysis of the water column data. It also allows the user to mark targets manually. A – Now also shows values about the data being analyzed with beam and range yellow markers, B – The bottom plot changes between across range and along track intensity plots, C – a new button 'Target Hunt' activates the Target Detection Tool

Finally, when the algorithm was tested, and to work as a stand-alone tool to read files without needing the use of 'swathed', the new tool 'targethunt' was created using 'targethunt.c' and 'targethunt.h' files. This new tool skips all visual process and simply applies the algorithm to the desired survey lines, looking for detections or targets or both. The user has all the algorithm options available in this tool, as all the variables that can be changed can be changed using this tool. It is more powerful than the 'Target detection toolbox'' tool.

Data acquired in Squamish 2011, with an EM710
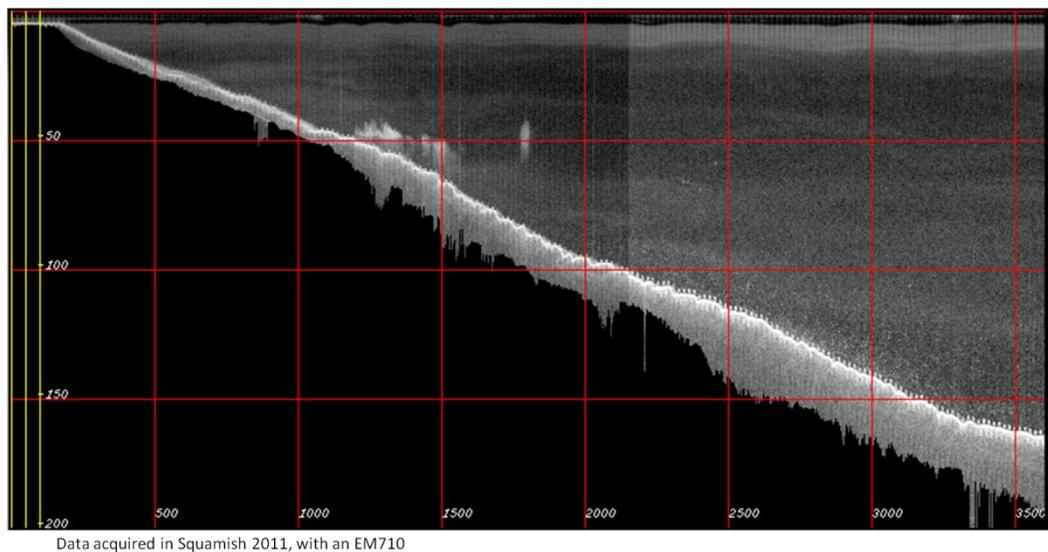
Figure A. 2 - Figure showing along track view

OMG's WaterColumn tool displays also an along track profile view of the water column at nadir.
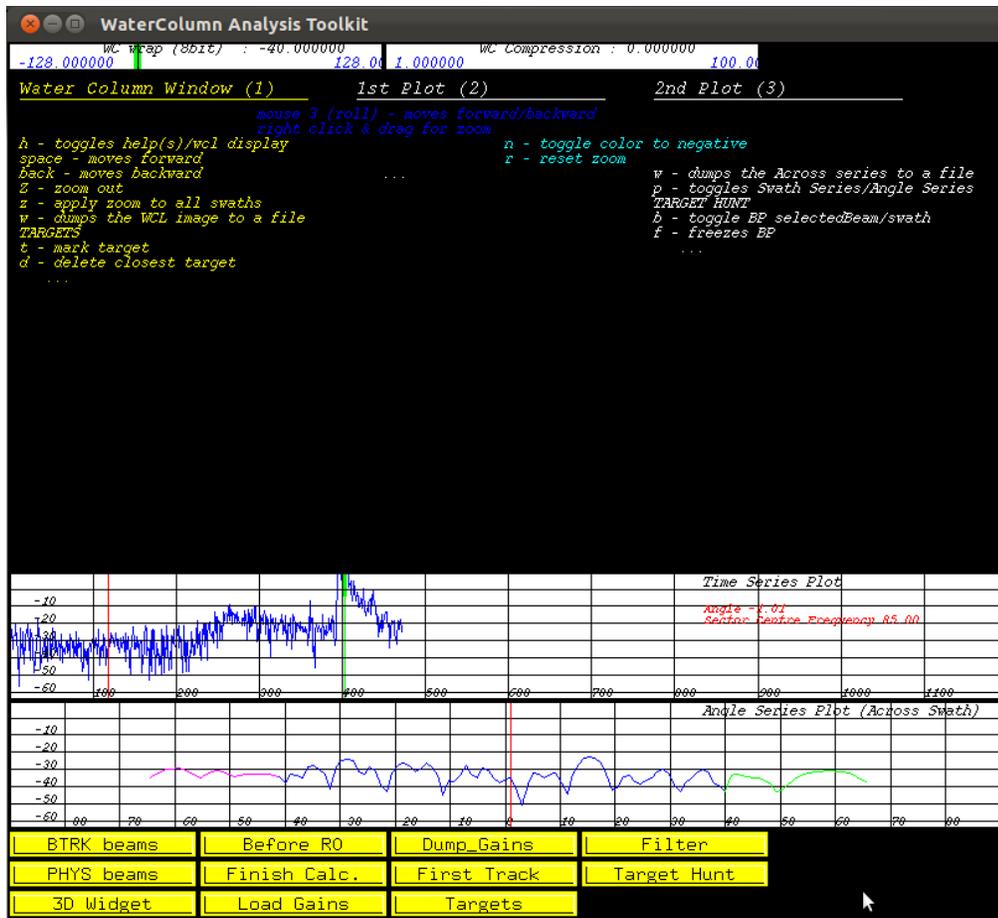
Figure A. 3 - Swathed help menu and white plots

The 'Target detection toolbox'' tool reads the water column data directly from water column structure being used by 'swathed' and stores the detections/targets in the same target file being used by 'swathed'. As to the 'targethunt' tool, it reads the water column data directly from the OMG format water column file, using OMG built in functions, into OMG specific structures. The results are also stored in the OMG target list file. Both tools use OMG structures so that it becomes an integrated tool and easily adapted to any future changes.

Each tool has its options and a quick preview of it will be shown here.

1.1 - Target detection toolbox

'Target detection toolbox' is the name used for the widget available in the 'swathed' water column display tool (it should not be confused with the file that contains the algorithm). The name comes from water column pick tool. The widget is shown in Figure A. 4 and will appear when the button 'targethunt' is pressed in the water column display tool.

This widget is composed of several buttons, several slide bars and two information areas. The slide bars give the user some liberty to change specific algorithm variables. It allows the user to adjust the algorithm variables and find the best way to use it in a pre analysis to the water column data. At the left, the user can change the variables that change the way the algorithm works: decide on a fixed threshold value, for example. At the right, the user decides the search area size, where to search for the targets: can decide the minimum/maximum sample, minimum and maximum beam, minimum/maximum swath to define the search area and also sectors to use. The 'Show search area' button enables the search area to be shown in the WaterColumn Analysis toolkit display (Figure A. 5).
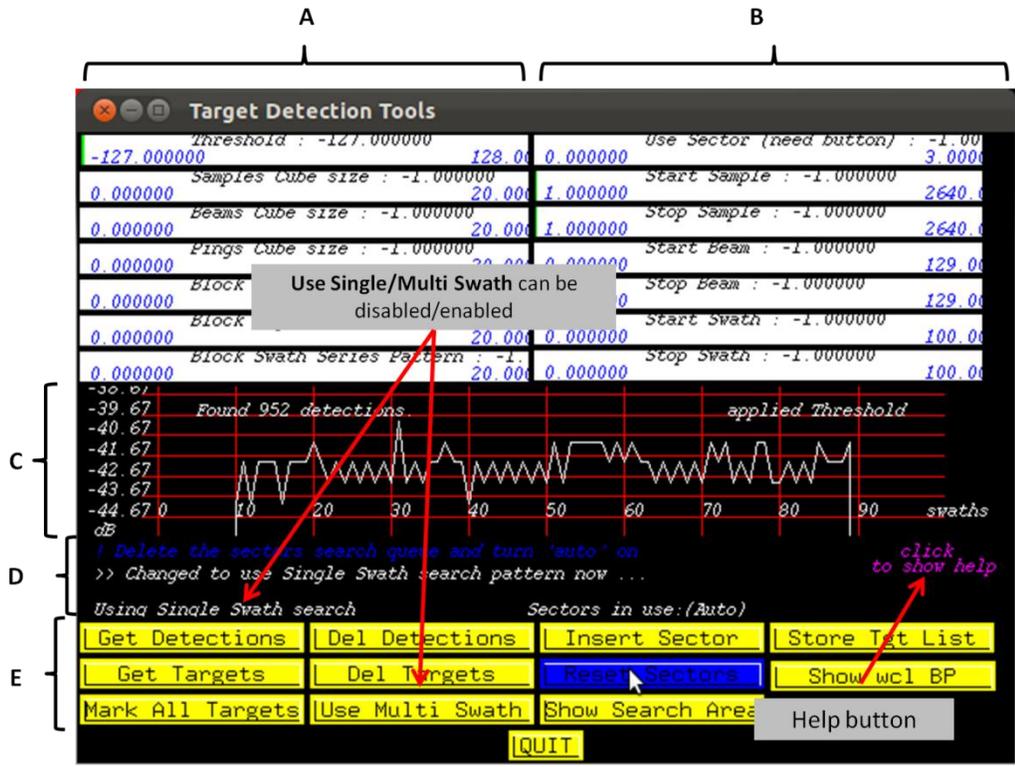
Figure A. 4 - Figure showing Target detection toolbox widget

A - Left side is used to define Threshold and to control the size of the search box used. B - Right side is used to define the search area, C - Area displays the results and the mean Threshold value used in each swath. Also shows the help when selected., D - Area shows pointed action (blue), last action (white) and also has a status line (lower white line), E - Buttons area has some action buttons to Get and Del Targets or Detections, store the target list and some control buttons: the use of Multi swath search, selecting sectors to use, show search area in water column tool.
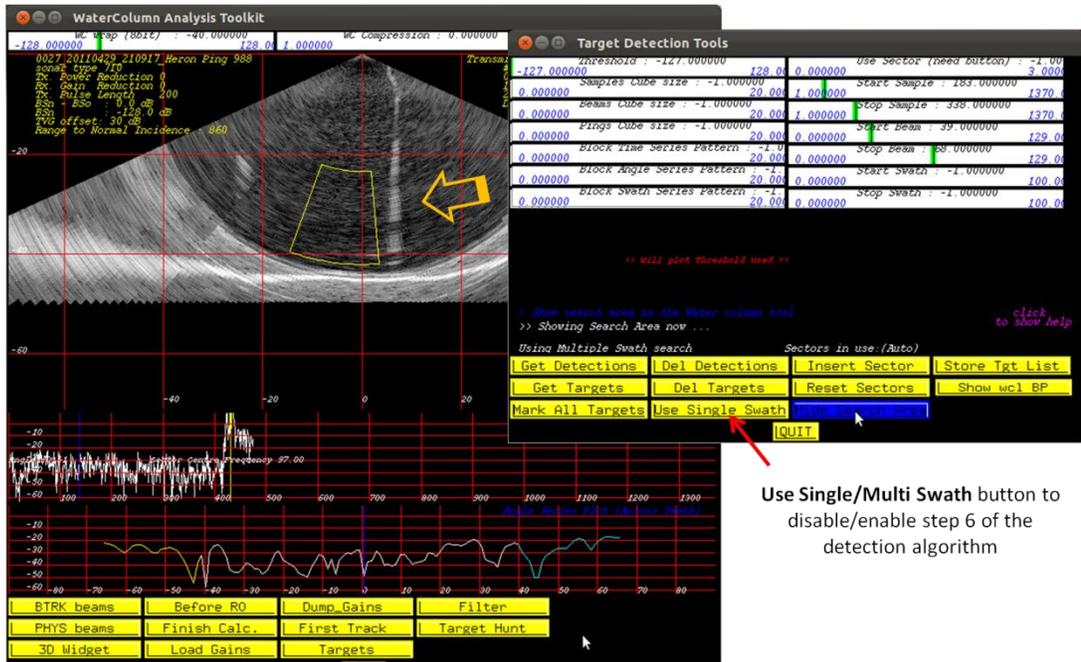
Data acquired in Squamish 2011, with an EM710

Figure A. 5 - Figure showing wcpick search area definition
The values that are defined in the Target Detection tool are passed to the WaterColumn tool and displayed in the water column polar plot. Only beams and range are displayed in this view.

Some buttons also allow the user to adjust some variables and decide on the way the algorithm works: multi-swath or single swath for example. There are 2 clean buttons, one for targets and one for detections, that clean all the targets/detections from the list. And the remaining buttons run the algorithm once all variables are defined: get targets, get detections. There is also a button available to mark the targets from the detections in the list. The algorithm does not do any detection here, only step 7 is executed.

Finally, the two information areas are used to show what is happening with the tool. The top one shows the results of applying the algorithm, and also has a small help link at the right bottom corner. When the algorithm is finished it displays the count of detections

or targets and shows a plot of the threshold average values used in each swath. The bottom one shows which button is being pointed to and gives a small hint on what it does.

1.2 - Targethunt

'targethunt' was the name chosen for the stand alone tool that uses this thesis's algorithm. This stand alone tool is supposed to be used to search for targets/detections in any survey lines that have water column data. This tool is intended for operating application of the new algorithm to the Squamish dataset (results included in Chapter 6). The tool has a 'help' option and a 'usage' option that explain what the tool does and how it works. The 'usage' option displays all the possible options to use the tool as shown in Figure A. 6.

The only thing the tool needs to operate is the file(s) in which to search for targets, and the targets file if the user wants to look for targets.

The most important options to point out are that the user can decide to search the targets in 1 or multiple files, or even just by giving the coordinates of the area where to search. Also, there are options to detect specific targets or just all detections, or both.

The user can use single swath mode, disabling step 6 (Section 4.2.6) or multi swath (default). Also the user can decide to disable step 5 (Section 4.2.5) for any specific purposes. All options available are shown in (Table A.1).

```
:| targetHunt - hunt for targets in the WCL data!

USAGE: targetHunt (options) -infile inputfile
- - - - - - - - - - - - - - - - - - - - - - - - - - - - -
---------- Mandatory ----------
-infile aaa aaa >> the input filenames


--------- Help ---------
-h >> shows the help text
-v >> sets the verbose flag on
-w >> sets the workflow flag on (default is ON)
-s >> activates silent mode (no workflow, no verbose, no debug)
-noinfo >> does not print software info in the output
---------- Options ----------
-shapefile aaa >> the input target shape file for the selected files
-setThresh # >> use static threshold of #
-dynThreshLayerX # >> use dynamic threshold depth layer multiplier of # (multiplied by pulse length)
-dynThresh # >> use dynamic threshold #diff multiplier (default = 1)
-amplOffset # >> used an X_LogOffset of # in acquisition (default = 0)
-cubeSamples # >> use 3D cubic box with size # in samples
-cubeBeams # >> use 3D cubic box with size # in beams
-cubeSwaths # >> use 3D cubic box with size # in swaths
-blockPlPat >> block time series pattern search
-blockAngPat >> block Angular series pattern search
-blockSwPat >> block Swath series pattern search
-shadeNIL >> use no shading function
-shadeLinear >> use Linear shading function
-shadeCos >> use Cos shading function
-shadeCos >> use Cos squared shading function
-shadeDolph # >> use Dolph Chebishev shading function with # side lobe supression
        system uses dolph chebishev by default
-minsamples # >> search only after sample number #
-maxsamples # >> search only before sample number #
-minRange # >> search only after # m range
-maxRange # >> search only before # m range
-minbeams # >> search only after beam number #
-maxbeams # >> search only before beam number #
-minswaths # >> search only after swath number # (NEEDS TO BE INSIDE THE SURVEY LINE)
-maxswaths # >> search only before swath number # (NEEDS TO BE INSIDE THE SURVEY LINE)
-insideArea ##.##.## ##.##.## ##.##.## ##.##.## >> search only inside area          specified by min/max (Lat Lon) ##.##.## deg.min.sec
-insideAreaD #.## #.## #.## #.## >> search only inside area          specified by min/max (Lat Lon) #.## dec degrees
-sector # >> search only in 1 sector, #
-useSectors n # # # >> search in n sectors specified next with #
-force1Swath >> dont use multiple swath search technique
-detect >> dont use target hunt (only detection)
-keepdetections >> keep detections after target hunt
-slotSize # >> define wcl data slot size
-printOnly >> will print list and exit, doesn't even open the wcl file
-print >> will print list in the end
-pause >> pause after processing each file
-output >> will print an output ascii list
--------- Dumping data control ---------
-dumpThresh >> dump all threshold values to file (uses all swaths by default)
-dumpThreshCmp >> dump dynThreshold and StaticThreshold values to file (uses all swaths by default)
-dumpSamples >> dump sample values to file (uses all data by default)
-dumpSw ## >> dump wcl swath ## only
(dump controls can be combined)

i460d $
```

Figure A. 6 - Figure showing the usage of targethunt

Option	Arguments	Description
-h		Shows the help text, and usage.
-v		Enables verbose output.
-w		Enables workflow output.
-s		Disables all output except the result in the end.
-noinfo		Blocks the program from writing header info on output files.
-infile	*aaa aaa*	Defines which '*aaa aaa*' .merged files to use in the search (even when using '*-insideArea*' *option*, files must be given here) (.merged needs to be included)
-output		Prints and output ascii list with all the targets
-insideArea	##.##.## ##.##.## ##.##.## ##.##.##	Uses two pairs (min/max) of coordinates (lat/lon in deg.min.sec)
-insideAreaD	##.### ##.### ##.### ##.###	Uses two pairs (min/max) of coordinates (lat/lon in decimal degrees)
-shapefile	*aaa*	Defines a specific target geometry file (otherwise uses the .tgShape in the same directory as the merged file)
-setThresh	##	Sets the threshold to the fixed value ##
-dynThresh	##	Sets the dynamic threshold multiplier to the value ##
-wclLayer	##	Sets the threshold depth layers to the value ##
-boxSizeSamples	##	Defines samples the size of the 3D Cube box to ## samples (should always prefer automatic, its included only for tests)
-boxSizeBeam	##	Defines beams the size of the 3D Cube box to ## beams (should always prefer automatic, its included only for tests)
-boxSizeSwath	##	Defines swaths the size of the 3D Cube box to ## swaths

		(should always prefer automatic, its included only for tests)
-samplesPat	*##*	Defines samples the size of the Pattern match box to ## samples (should always prefer automatic, its included only for tests)
-BeamsPat	*##*	Defines beams the size of the Pattern match box to ## beams (should always prefer automatic, its included only for tests)
-swathsPat	*##*	Defines swaths the size of the Pattern match box to ## swaths (should always prefer automatic, its included only for tests)
-minsamples	*##*	Defines the minimum samples for the search area definition
-maxsamples	*##*	Defines the maximum samples for the search area definition
-minRange	*##*	Defines the minimum range for the search area definition
-maxRange	*##*	Defines the maximum range for the search area definition
-minbeams	*##*	Defines the minimum beam for the search area definition
-maxbeams	*##*	Defines the maximum beam for the search area definition
-minAngle	*##*	Defines the minimum beam angle for the search area definition
-maxAngle	*##*	Defines the maximum beam angle for the search area definition
-minswaths	*##*	Defines the minimum swath for the search area definition
-maxswaths	*##*	Defines the maximum swath for the search area definition
- sector	*##*	Defines a singular sector to be used in the search area definition
-useSectors	*n # # # #*	Defines the use of '*n*' sectors in to be used in the search area definition (sectors are introduced next '# # # #')
-force1Swath		Disables the use of step 6 of the Algorithm (check multiswath)
-noPattern		Disables the use of step 5 of the Algorithm (3D Pattern match)

-detect	Disables the use of step 7 of the Algorithm (3D Target Geometric Filter)
-keepdetections	Disables the removal of detected Objects/LIMs after step 7 (target search). Allows the user to keep all detected objects in the list together with the hunted targets.
-slotSize	Defines the size of water column image slots to use when computing. May help speeding up the algorithm in very slow computers. Slot size always needs to be larger than 3x the size (in swaths) of the 3D cubic box.
-printOnly	Blocks every action of the program, it will ONLY print the list of targets attached to the .merged file
-print	Prints to the terminal the complete list of targets attached to the .merged file
-pause	Enables pausing after each file search is complete

Table A.1- Target Hunt Options

While the tool is working, and as the algorithm operates, some messages will be displayed showing that the algorithm is working, and which file is being analyzed (Figure A. 7). The amount of output to the terminal display can be controlled with options '–v', '–w' and '–s'. In the end the final output is just a message informing the user how many targets were found. The user can also ask for a list of targets in the output (Figure A. 7).

Figure A. 7 - The output of targethunt tool

Figure A. 8 - The list output of targethunt tool

Curriculum Vitae

Candidate's full name: Carlos Rubrio Videira Marques

Universities attended:

- Naval Academy

Almada, Portugal

B.Sc. in Naval Military Sciences, 1998

- New University of Lisbon

Caparica, Portugal

BEng. in Computers Engineering, 2004

- Portuguese Hidrographic Institute

Lisbon, Portugal

Graduated in extension Hydrography Course Cat. A (IHO), 2007

Conference Presentations

Carlos Rubrio Marques, John E. Hughes Clarke, 2012, Automatic Mid-Water Target Tracking using Multibeam Water Column , Proceedings of the Canadian Hydrographic Conference, Niagara Falls 2012